

Reports

---

9-1-1978

## A Storm Surge Model Study: Volume II A Finite Element Storm Surge Analysis and its Application to a Bay-Ocean System

H. S. Chen  
*Virginia Institute of Marine Science*

Follow this and additional works at: <https://scholarworks.wm.edu/reports>



Part of the [Marine Biology Commons](#)

---

### Recommended Citation

Chen, H. S. (1978) A Storm Surge Model Study: Volume II A Finite Element Storm Surge Analysis and its Application to a Bay-Ocean System. Special Reports in Applied Marine Science and Ocean Engineering (SRAMSOE) No. 189 V2. Virginia Institute of Marine Science, William & Mary. <https://doi.org/10.21220/V5DX72>

This Report is brought to you for free and open access by W&M ScholarWorks. It has been accepted for inclusion in Reports by an authorized administrator of W&M ScholarWorks. For more information, please contact [scholarworks@wm.edu](mailto:scholarworks@wm.edu).

A STORM SURGE MODEL STUDY

Volume II. A FINITE ELEMENT STORM SURGE ANALYSIS  
AND ITS APPLICATION TO A BAY-OCEAN SYSTEM

by

H. S. Chen

A Report to the  
Federal Insurance Administration  
Department of Housing and Urban Development  
under Contract No. H-4508

Special Report No. 189  
in Applied Marine Science and  
Ocean Engineering

Virginia Institute of Marine Science  
Gloucester Point, Virginia 23062

William J. Hargis, Jr.  
Director

September, 1978

## TABLE OF CONTENTS

	Page
List of Figures.....	iii
List of Tables.....	v
Abstract.....	vi
Acknowledgements.....	vii
1. Introduction.....	1
2. Mathematical Formulation of Storm Surge Model.....	8
2.1 Hydrodynamic Model.....	8
2.2 Hurricane Model.....	16
3. Variational Statement and Finite Element Approximation.....	21
3.1 Variational Statement.....	21
3.2 Finite Element Approximation.....	22
3.3 Time Integration.....	32
3.4 Treatment of Boundary Condition.....	34
4. Numerical Results and Discussions.....	37
4.1 Some Computational Aspect.....	37
4.2 Simulation of Tides.....	38
4.3 Storm Surge Calculations.....	54
4.4 Conclusion.....	79
References.....	80
List of Symbols.....	84
Appendix A. Calculated Tides in the Lower James River.....	86
Appendix B. Simulation of Tides in the Chesapeake Bay.....	104
Appendix C. Storm Surge Hindcast in the Chesapeake Bay and its Virginia Atlantic Nearshore Ocean.....	122

## LIST OF FIGURES

Figure		Page
1.1	Map showing Chesapeake Bay.....	2
1.2	Map showing Chesapeake Bay and the Virginia Atlantic nearshore sea.....	5
2.1	Definition sketch of the Cartesian Coordinate System...	9
2.2	Definition sketch of a hurricane.....	19
3.1	Domain and triangular elements.....	26
3.2	Definition sketch of boundary normal.....	35
4.1a	Finite element network of the Lower James River showing nodal positions.....	40
4.1b	Finite element network of the Lower James River showing element positions.....	41
4.1c	Nodal depth of the Lower James River.....	42
4.2a	Time history of water elevation at node.....	45
4.2b	Time history of flow velocity at node.....	46
4.3a	Finite element network of the Chesapeake Bay showing nodal positions.....	48
4.3b	Finite element network of the Chesapeake Bay showing element positions.....	49
4.3c	Nodal depth of the Chesapeake Bay.....	50
4.4a	Time history of water elevation at node.....	52
4.4b	Time history of flow velocity at node.....	53
4.5a	Finite element network of the Chesapeake Bay and its Virginia Atlantic nearshore ocean showing nodal positions.....	55
4.5b	Finite element network of the Chesapeake Bay and its Virginia Atlantic nearshore ocean showing element positions.....	56
4.5c	Nodal depth of the Chesapeake Bay and its Virginia Atlantic nearshore ocean.....	57

List of Figures (Cont'd)

Figure		Page
4.6a	Track of Hurricane Connie 1955.....	60
4.6b	Pressure field of Hurricane Connie 1955.....	61
4.7	The model track of Hurricane Connie 1955.....	63
4.8	Typical pressure and wind field of the simulated hurricane Connie 1955.....	65
4.9	Six tide gauge stations and some element positions.....	66
4.10	Comparison of the calculated surge and the surge deduced from observed tide.....	67
4.11	Three types of hurricane track.....	70
4.12	Maximum surge height in the bay vs. hurricane track.....	73
4.13	Tracks of Hurricanes Connie 1955, Flossy 1956 and Donna 1960.....	75
4.14	Maximum surge height vs. central pressure depression.....	76
4.15	Maximum surge height vs. forward speed.....	77
4.16	Maximum surge height vs. maximum wind radius.....	77
A.1- A.16	Water elevation and circulation of the Lower James River in a tidal cycle.....	88- 103
B.1- B.16	Water elevation and circulation of the Chesapeake Bay in a tidal cycle.....	106- 121
C.1- C.23	Enlarged finite element network for the bay and the results of the storm surge hindcast of model hurricane Connie 1955.....	124- 149

## LIST OF TABLES

Table		Page
4.1a	Some Tide Data of Lower James River.....	43
4.1b	Tidal Input for the Lower James River Hydrodynamic Model..	44
4.2	Tidal Input for the Chesapeake Bay Hydrodynamic Model.....	51
4.3	Calculated Maximum Surge Height vs. Time Step.....	58
4.4	Parameter Values of Calibration Run and Calibrated Coefficients.....	64
4.5a	Maximum Surge Height vs. Various Combinations of Hurricane Parameters for Hurricane HT1.....	71
4.5b	Maximum Surge Height vs. Various Combination of Hurricane HT2 (or HT2').....	72
4.5c	Maximum Surge Height vs. Various Combination of Hurricane Parameters for Hurricane HT3.....	72
4.6	Observed Tide and Deduced Storm Surge.....	74

## ABSTRACT

### A FINITE ELEMENT STORM SURGE ANALYSIS AND ITS APPLICATION TO A BAY-OCEAN SYSTEM

by

H. S. Chen

KEY WORDS: Storm Surge Model, Two Dimensional Hydrodynamic Model, Hurricane Model, Finite Element Approximation, A Bay-Ocean System.

A two dimensional storm surge model has been developed for calculating water elevation and circulation in a bay-ocean system subject to the effect of a hurricane. The model consists of a hydrodynamic model which is based on the continuity and momentum equations for fluid motion, and a hurricane model using semi-empirical formulae based on Wilson (1957) expressing atmospheric pressure and wind fields in terms of hurricane parameters. The hydrodynamic model employs Galerkin's weighted residual finite element numerical scheme.

The storm surge model was first used to simulate tides in the Chesapeake Bay until the tide simulations are satisfactory, then a storm surge hindcast was conducted in the Chesapeake Bay and its Virginia Atlantic nearshore ocean. The response of the surge heights in the Bay to various combination of hurricane parameters were also studied. The result generally agrees with the observed data.

## ACKNOWLEDGEMENTS

This research is part of a larger effort undertaken for the flooding study of the Chesapeake Bay and is supported financially by the Federal Insurance Administration (FIA), Department of Housing and Urban Development (HUD) under contract with the Virginia Institute of Marine Science (VIMS). General contract supervisors were Drs. C. S. Fang and John M. Zeigler.

For his generous supply of his CAFE computer program which has been very helpful in programming in this study, I am greatly indebted to Dr. John D. Wang of University of Miami. Many thanks are due to Dr. John D. Boon, III for supplying the tide data, and to Mr. Robert J. Lukens for the computer graphics and for assistance in some computer access. I also wish to acknowledge the benefits derived from discussions with Drs. John D. Wang, Bryan R. Pearce of MIT, Frank Y. Tsai of HUD and Paul V. Hyer of VIMS.

Special thanks should go to Ms. Shirley Crossley for her patient typing of this report and to many individuals in the Department of Physical Oceanography and Hydraulics of VIMS for their preparation of the figures and tables.



## 1. INTRODUCTION

It is common knowledge that violent storms can cause coastal flooding and damage. The Federal Government has passed a law authorizing a National Flood Insurance Program whereby cities, or towns, or political units of a state can obtain better flood-hazard insurance than they could otherwise get without federal assistance. Basically, this law permits communities to obtain or retain flood protection under the act if the community will assemble certain hydrologic and hydraulic materials relating to probability of flood damage in a required period of time, and adhere to a program of land planning and management. This technically involves establishing flood-flow frequency and flood-elevation frequency, mapping flood boundaries, delineating floodways, and calculating flood hazard factors. For a coastal community, the basic and most important problem is the determination of flood-level frequency. For those who are cognizant of the National Flood Insurance Program there remains the technical problem of assessing realistically flood-level frequency. A few places within the Chesapeake Bay (see figure 1.1) have been settled long enough that reasonably good flood levels are available from tide gages over many years: Norfolk, Kiptopeke, Annapolis, Baltimore and Washington for example. For the most part, however, there are insufficient historical records for accurate flood-level frequency assessment. Each year the problem becomes worse because of rapid population and industry shift to the coastlines. Whole new communities are developed where there are no flood records of any kind. One way to circumvent this problem is to interpolate between the records of nearby tidal gage

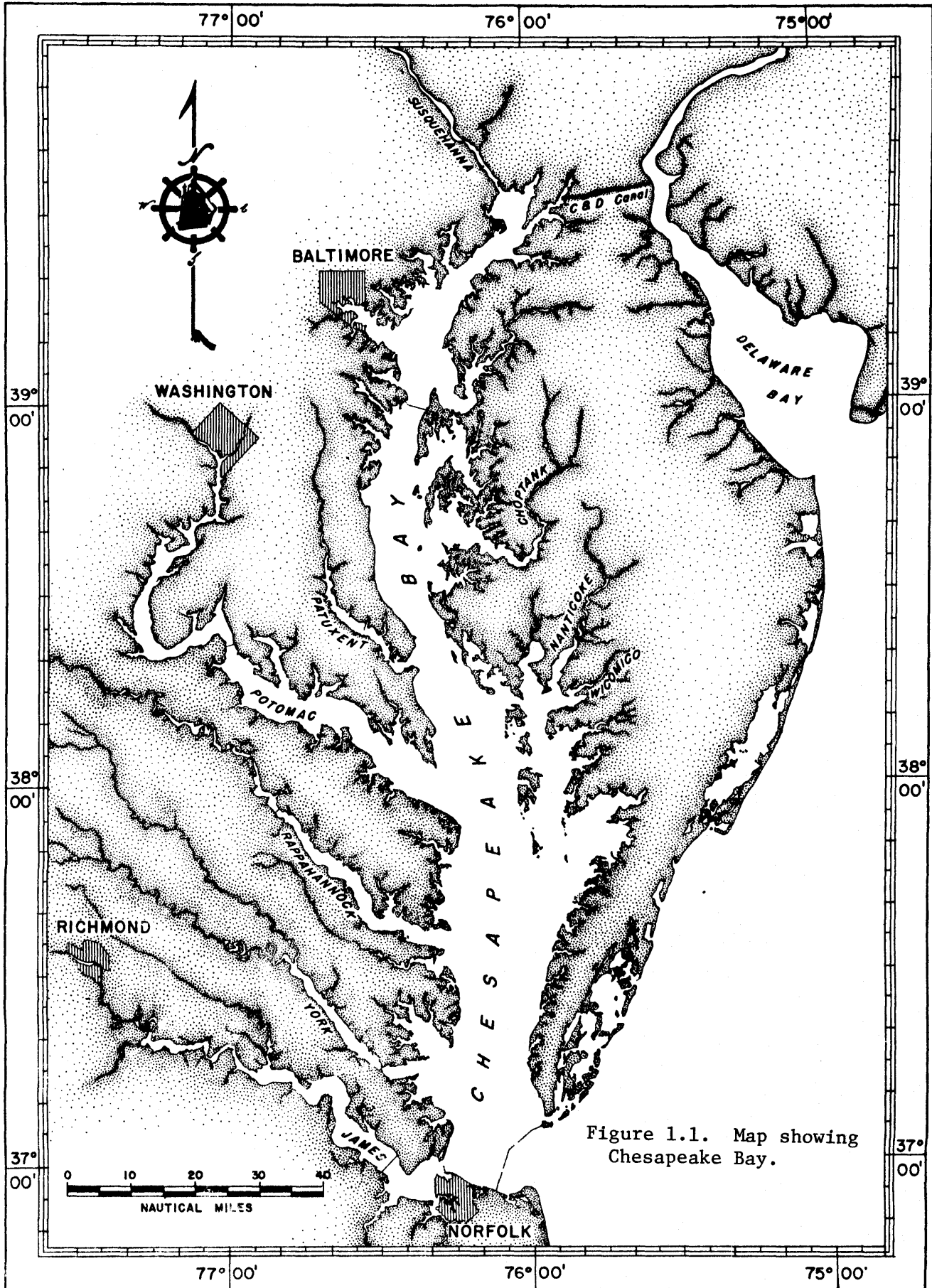


Figure 1.1. Map showing Chesapeake Bay.

stations using engineering judgement. However, when the coastal configuration and topography are complex, this approach becomes inaccurate and impractical, and a more realistic approach should be used. Since flood elevation is the setup of water surface resulting mainly from three basic causes: (1) surge associated with storms (storm surge), (2) astronomical tides, and (3) wave setup superimposed on the raised water level, there is a trend toward using a storm surge model along with prediction techniques of astronomical tides and wave setup to determine the flood-level frequency. A storm surge model should have a sound physical background, and its calculation should not overpredict or underpredict the surge elevations, since these predictions will be used in an effort to establish fair flood insurance rates.

Storm surge is the meteorological (storm) effect on sea level and is usually defined as the observed tide less the astronomical tide. Storm surge in a bay is substantially different from that in an unrestricted water body or on the continental shelf. The spatial variations of the surge in open water are generally of the same order as those of the storm which are on the scale of more than 100 km, while surge level in a bay may vary greatly in a distance of 10 km in order of magnitude. Physical processes also differ in their relative importance. In open water the forced and free inertial-gravitational wave propagations are of primary significance. A bay provides only a restricted area for water mass to bounce around and its shallow water depths also enhance the effects of nonlinearities. Flooding of low terrain can increase the surface area of the bay and converging channels can produce a dramatic local surge height.

The Chesapeake Bay and its Virginia Atlantic nearshore ocean (see figure 1.2) are connected into a interacting bay-ocean system by the water mass exchange through bay entrance. The main factors involved in the generation and modification of storm surge in this bay-ocean system are: (1) Astronomical tide, (2) Inverted barometer effect, (3) Wind fields and wind stress, (4) Coastal configuration, bottom topography and bottom friction, (5) Transport of water by waves and swell, (6) Discharge and surface elevation of rivers.

The storm surge problem has been approached through several hydrodynamic methods by many investigators. All past studies concerned only the nearshore and offshore regions of the ocean or only the bay and did not touch bay-ocean system because previous models have not been compatible with complex coastal configuration and shallow water. Analytic solutions to some simple storm surge problems have been developed by several investigators, such as Lamb (1945), Bretschneider (1966), and Dean and Pearce (1972). Analytic methods are generally impractical in application due to the complexities of actual driving forces, coastal configuration, and topography. A more realistic approach to storm surge problems using numerical techniques was originally proposed by Hansen (1956). Since then many investigators have developed various finite difference numerical schemes for two-dimensional storm surge calculations, such as Platzman (1958), Hansen (1962), Reid and Bodine (1968), Jelesnianski (1965, 1966, 1967, 1970, 1974) and Pearce (1972), just to name a few. Although each makes progress on storm surge calculations, each is limited to some extent in application due either to the treatment of non-linearity, ocean boundary conditions and bottom friction, or to the need

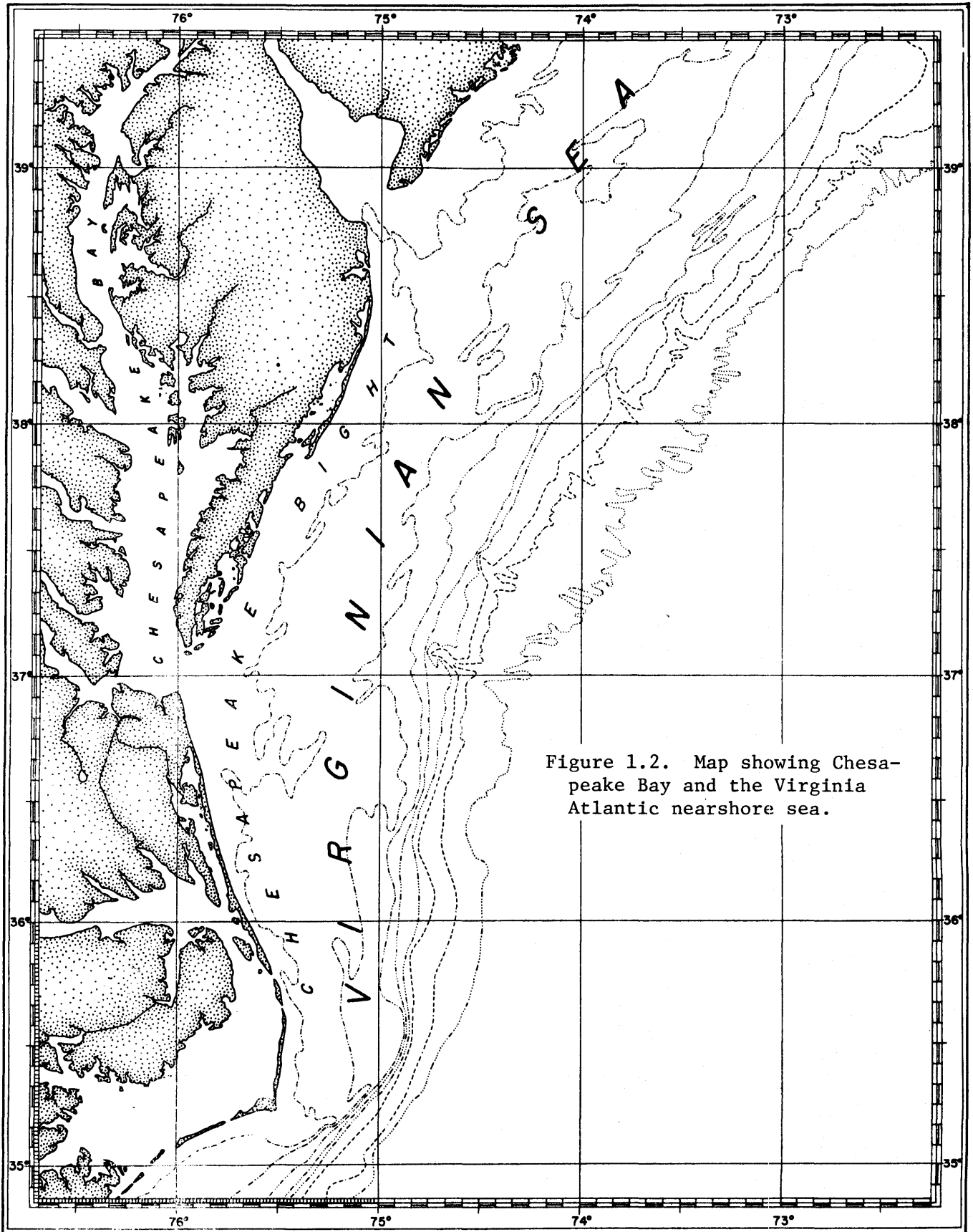


Figure 1.2. Map showing Chesapeake Bay and the Virginia Atlantic nearshore sea.

for calibration through various eddy viscosity and bottom friction coefficients. Recently, a great number of papers and reports have been published on the numerical simulation of storm surge. (Pagenkopf and Pearce 1975, Overland 1975, Damsguard and Dinsmore 1975, Runchal 1975, Yeh and Yeh 1976, etc). Only Overland (1975) dealt with a bay-ocean system by indirectly coupling his bay model with the SPLASH II model (Jelesnianski 1974). This indirect coupling for studying a bay-ocean system may provide a practical tool for engineering purposes, but physically it needs further assessment.

The difficulty of using finite difference schemes in bay-ocean systems is that finite difference schemes generally employ a rectangular uniform grid system and irregular boundaries must be approximated with orthogonal segments. This requires a small grid spacing throughout the entire water domain. Finite element schemes on the contrary, employ more flexible grid networks than finite difference schemes, and have recently and successfully been applied to the hydrodynamic circulation problem by Connor and Wang (1974) and to the offshore storm surge problem by Pagenkopf and Pearce (1975). Indications are that finite element schemes are particularly convenient for problems involving irregular coastal boundaries found in bays, estuaries, or bay-ocean systems.

In this study, a hydrodynamic model which uses meteorological data as input to forecast storm surge response in the Chesapeake Bay and the Virginia Atlantic nearshore is developed. A finite element scheme is used in order to fit the complexities of coastal configuration. Water elevation and water transport, which are related to land flooding,

erosion and circulation respectively in the concerned areas, are quantitatively predicted for a given storm.

Chesapeake Bay, being the largest bay on the Atlantic coast of the United States, has an area of approximately  $62,575 \text{ km}^2$  with an average water depth of 8m. The mean water depth on the inner continental shelf seaward of the bay is about 20m. According to previous studies of storm surge problems, these scales justify the hypothesis that fluid motion is predominantly horizontal and that the vertical accelerations of fluid particles are of small magnitude. Therefore, in Chapter 2, the formulation of the hydrodynamic model is based on two-dimensional depth integrated continuity and momentum equations for fluid motion, along with appropriate initial and boundary conditions. A hurricane model which calculates pressure and wind fields of the storm is also presented and discussed. In Chapter 3, a Galerkin's weighted residual finite element scheme along with the split-time integration scheme is described. The scheme involves variational formulation and finite element approximation. A linear triangular element having three nodes is employed. In Chapter 4, the finite element network is presented. The calibrations and the results of calculations, which include simulations of tides in both the lower James River and the Chesapeake Bay and a storm surge hindcasting in the Chesapeake Bay and its Virginia Atlantic nearshore ocean, are also presented and discussed. In order to test the validity of the system and to study the numerical behavior of the system, a simulation of astronomical tide was conducted in the lower James River. The results of a tidal cycle are shown in Appendix A. The simulation of astronomical tide in the bay proper was also carried out and the results are shown in Appendix B. The calculated results of storm surge hindcast of the model hurricane Connie 1955 are shown in Appendix C.

## 2. MATHEMATICAL FORMULATION OF STORM SURGE MODEL

The storm surge model consists of a hydrodynamic model and a hurricane model. The former describes the water surface fluctuation and circulation, and the latter depicts the pressure and wind fields of a hurricane, which are the driving forces to the hydrodynamic model. In this chapter both models are mathematically formulated.

### 2.1 Hydrodynamic Model

The mathematic hydrodynamic model is based on the principles of conservations of mass and momentum for fluid motion. Since a water domain of shallow depth and great horizontal extent, such as the Chesapeake Bay and its Virginia Atlantic nearshore ocean, is dealt with, the pressure distribution is assumed to be hydrostatic. Therefore, in a Cartesian coordinate system  $(x,y,z)$  as shown in Figure 2.1, the two-dimensional depth integrated hydrodynamic equations with the Boussinesq approximation can be written (Phillips 1966, Connor and Wang, 1974, Nihoul 1975).

$$\frac{\partial H}{\partial t} + \frac{\partial q_x}{\partial x} + \frac{\partial q_y}{\partial y} = Q \quad (2.1)$$

$$\begin{aligned} \frac{\partial q_x}{\partial t} + \frac{\partial H^{-1} q_x^2}{\partial x} + \frac{\partial H^{-1} q_x q_y}{\partial y} - f q_y = -\frac{H}{\rho_o} \frac{\partial}{\partial x} (p^s + \rho g \eta) \\ + \frac{\partial T_{xx}}{\partial x} + \frac{\partial T_{yx}}{\partial y} + \frac{1}{\rho_o} (\tau_x^s - \tau_x^b) \end{aligned} \quad (2.2a)$$

$$\begin{aligned} \frac{\partial q_y}{\partial t} + \frac{\partial H^{-1} q_y q_x}{\partial x} + \frac{\partial H^{-1} q_y^2}{\partial y} + f q_x = -\frac{H}{\rho_o} \frac{\partial}{\partial y} (p^s + \rho g \eta) \\ + \frac{\partial T_{xy}}{\partial x} + \frac{\partial T_{yy}}{\partial y} + \frac{1}{\rho_o} (\tau_y^s - \tau_y^b) \end{aligned} \quad (2.2b)$$



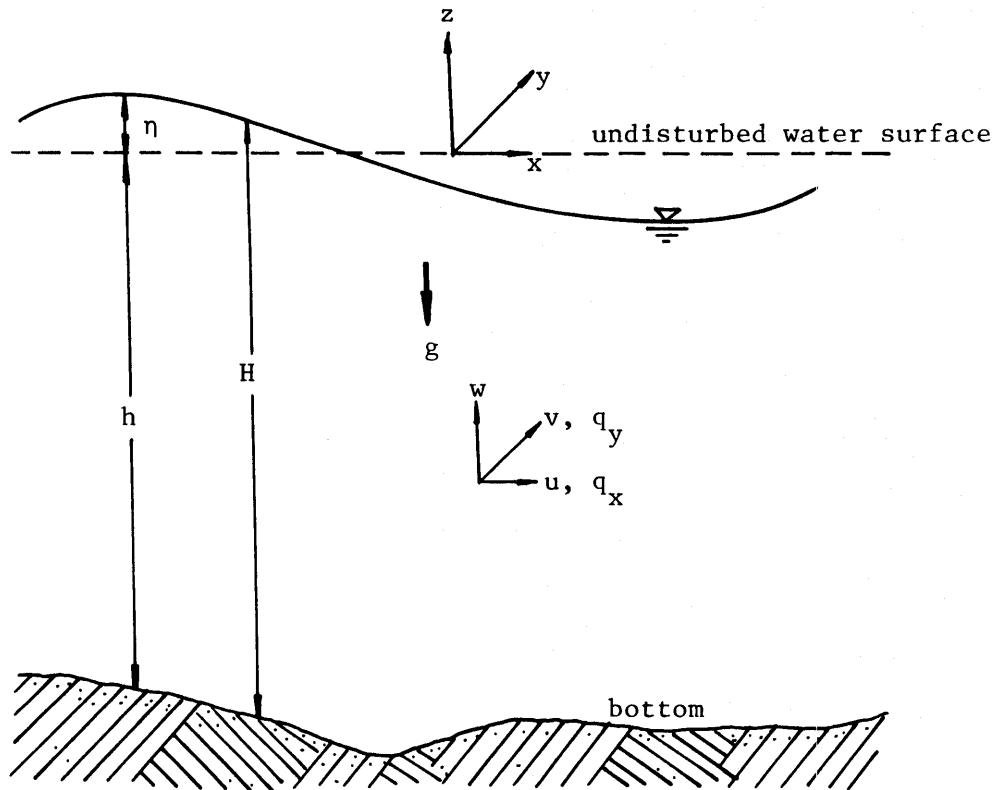


Figure 2.1. Definition sketch of the Cartesian Coordinate System.

where  $H(x,y,t) = h(x,y) + \eta(x,y,t)$  (2.3)

$$q_x(x,y,t) = \int_{-h}^{\eta} u(x,y,z,t) dz, \quad q_y(x,y,t) = \int_{-h}^{\eta} v(x,y,z,t) dz \quad (2.4)$$

$$\rho(x,y,t) = \rho_0 + \Delta\rho(x,y,t) \quad (2.5)$$

The symbols used in equations (2.1) through (2.5) are defined as follows:

$t$  = time variable

$H$  = total water depth

$h$  = undisturbed water depth

$\eta$  = water surface elevation above undisturbed water surface

$\{u,v\}$  = water velocity components in  $x$  and  $y$  directions respectively

$\{q_x, q_y\} = \{q_i\}$  = water transport components in  $x$  and  $y$  directions respectively;  $i = x, y$ .

$Q$  = rate of adding water mass per unit area

$f$  = Coriolis coefficient =  $2\Omega \sin\phi$

$\rho, \rho_0, \Delta\rho$  = water density, constant mean density, density deviation

$p^s$  = atmospheric pressure

$g$  = gravitation acceleration

$$\begin{pmatrix} T_{xx} & T_{xy} \\ T_{yx} & T_{yy} \end{pmatrix} = (T_{ij}) = \text{internal stress tensor; } i, j = x, y$$

$\{\tau_x^s, \tau_y^s\} = \{\tau_i^s\}$  = wind stress components in  $x$  and  $y$  directions respectively;  $i = x, y$

$\{\tau_x^b, \tau_y^b\} = \{\tau_i^b\}$  = bottom friction components in  $x$  and  $y$  directions respectively;  $i = x, y$

Equation (2.1) states that the total rate of change of mass per unit area is equal to the rate of adding mass per unit area, in consequence

of the principle of conservation of mass. While equations (2.2a and b), which follow from the principle of conservation of momentum, include terms reading from left to right representing the inertial term, convective term, Coriolis term, pressure terms, internal stress terms, free surface (wind) stress term and bottom friction term. Water depth is still a function of position.

Among the variables in equations (2.1), (2.2a) and (2.2b),  $p^s$  and  $\tau_i^s$  are the forcing functions from the storm.  $T_{ij}$  and  $\tau_i^b$  are assumed functions of  $H$  and  $q_i$ . Hence, equations (2.1) through (2.2b) constitute a set of three simultaneous partial differential equations for three unknowns;  $H$  (or  $\eta$ ),  $q_x$  and  $q_y$ .

### 2.1.1 Wind Stress

The most sensitive and significant parameter effecting storm surge is the wind shear stress. However, the wind stress on the water surface is too complicated to be accurately estimated due to the complicated nature of the turbulent wind field and the deformable water surface. Nevertheless, it is now widely accepted that the wind stress is related to the wind velocity through the following expression proposed by Van Dorn (1953).

$$\tau_i^s = c_a \rho_a U_{10} U_{10i} \quad ; \quad i = x, y \quad (2.6)$$

where  $c_a$  = wind drag coefficient

$\rho_a$  = air density

$\{U_{10i}\} = \{U_{10x}, U_{10y}\}$  = x and y components of wind velocity at 10-meters above undisturbed water surface

$U_{10} = \sqrt{U_{10x}^2 + U_{10y}^2}$  = wind speed at 10-meters above undisturbed water surface

The wind drag coefficient  $c_a$  is in general a function of wind speed

$$c_a = \begin{cases} c_o & ; U_{10} \leq U_{cr} \\ c_o + c_1 \left(1 - \frac{U_{cr}}{U_{10}}\right) & ; U_{10} \geq U_{cr} \end{cases} \quad (2.7)$$

The values of the coefficients  $c_o$  and  $c_1$  and the critical wind speed  $U_{cr}$  suggested by different investigators are respectively:

	Van Dorn (1953)	Wilson (1960) and Reid and Bodine (1968)
$c_o$	1.2E-3	1.1E-3
$c_1$	2.2E-3	2.5E-3
$U_{cr}$ (m/s)	5.6	7.2

Note that other investigators have used other forms for  $c_a$ , such as Heaps (1969), Wu (1969), Whitaker (1973) and Wang and Connor (1975). All of these expressions of  $c_a$  are consistent with the present state of knowledge, but equation (2.7) works well in this study.  $c_o$  and  $c_1$  are calibrated and obtained by simulating the surge peak of a hurricane in the Bay.

### 2.1.2 Bottom Friction

Bottom friction is another important factor, particularly in shallow water. Although several investigators (Heap 1969; Durance 1974) have attempted to represent the bottom friction by a linear relation to the water transport, it is now commonly accepted that a quadratic relation to the mean water velocity must be used.

$$\tau_i^b = c_f \rho_o H^{-2} \sqrt{q_x^2 + q_y^2} q_i \quad (2.8)$$

where  $c_f$  is the coefficient of bottom friction.  $c_f$  is in general a

function of Reynolds number and bottom roughness, and its order of magnitude may range from 0.001 to 0.1. In this study  $c_f$  is calibrated by the simulation of an astronomical tide in the Bay.

### 2.1.3 Internal Stress

Internal stress originally arises from the eddy and molecular viscosities and the non-uniformity of flow velocity through water depth in the depth integrated approach. Physically it represents the energy dissipation in the fluid and it also serves as a means to control short wave noise generated in numerical processes. In order to obtain a closed formulation, we assume that internal stress is related to mean flow velocity;

$$T_{ij} = \epsilon_{ij} \frac{H}{2} \left( \frac{\partial H^{-1} q_i}{\partial j} + \frac{\partial H^{-1} q_j}{\partial i} \right) \quad i, j = x, y \quad (2.9)$$

where  $\epsilon_{ij}$  may be interpreted as "eddy viscosity" coefficient. Although  $\epsilon_{ij}$  may depend on the mean flow, water depth and flow history, the dependence of  $\epsilon_{ij}$  on the flow conditions is unknown. The value of  $\epsilon_{ij}$  is therefore mainly determined from experience and by trial. An estimate of  $\epsilon_{ij}$  is suggested by Wang and Connor (1975) by comparing the internal stress term with the pressure term

$$\epsilon \sim a g \frac{\eta^*}{U^*} \Delta s^*$$

where  $a$  is constant and ranges from 0.1 ~ 0.01.  $\eta^*$  is the typical free surface displacement,  $U^*$  the typical mean flow velocity and  $\Delta s^*$  the typical spatial grid size.

### 2.1.4 Initial and Boundary Conditions

In order to complete the mathematic formulation of the storm

surge problem, the initial and boundary conditions should be properly prescribed.

The initial conditions specify free surface elevation and water transport in the entire water domain at the initial time

$$\begin{aligned} \eta(x,y,t) &= \eta_0(x,y) & \text{or } H(x,y,0) &= H_0(x,y) \\ q_i(x,y,t) &= q_{i0}(x,y); \quad i = x,y & & \text{for all } (x,y) \\ & & & \text{at } t=0 \end{aligned} \quad (2.10)$$

The boundary condition encountered in the storm surge problem normally are of three types. They are: the land boundaries at the water-land interface, the seaward open boundary at the artificial termination of the computational grid system which is usually chosen to be beyond the continental shelf, and the lateral open boundaries at the connecting lines of the end points of the land boundary and the seaward open boundary, more or less perpendicular to the shoreline. For an enclosed water body, such as a lake, only the land boundary need to be considered. For an open coastal area, such as the Chesapeake Bay and its Virginia Atlantic near-shore sea, all three types of boundaries must be considered.

Before specifying the boundary conditions, we define at the boundaries the normal and tangential water transports

$$\begin{aligned} q_n &= \alpha_{nx}q_x + \alpha_{ny}q_y \\ q_s &= -\alpha_{ny}q_x + \alpha_{nx}q_y \end{aligned} \quad (2.11)$$

where  $n$  is the unit normal vector outward from the water domain,  $s$  the unit tangential vector along the boundary, and the direction cosines

$$\begin{aligned} \alpha_{nx} &= \cos(n,x) \\ \alpha_{ny} &= \cos(n,y) \end{aligned} \quad (2.12)$$

consequently

$$\begin{aligned} q_x &= \alpha_{nx} q_n - \alpha_{ny} q_s \\ q_y &= \alpha_{nx} q_s + \alpha_{ny} q_y \end{aligned} \quad (2.13)$$

Define the x and y components of force measures due to internal stress

$$\begin{aligned} T_x &= \alpha_{nx} T_{xx} + \alpha_{ny} T_{yx} \\ T_y &= \alpha_{nx} T_{xy} + \alpha_{ny} T_{yy} \end{aligned} \quad (2.14)$$

At the land boundary a fixed vertical solid wall is assumed, and the normal water transport is specified to be zero.

$$q_n = q_n^* = 0 \quad (2.15)$$

where the superscript \* denotes (and hereafter except when noted) a prescribed value.

At the seaward open boundary, which is usually beyond the continental shelf, the magnitude of the wind setup is insignificant due to the great water depth and the decreased hindrance of the land boundary. The barometric and astronomical tides still exist at the seaward open boundary, therefore the water surface elevation is

$$\eta = \eta_a^* + \eta_b \quad (2.16)$$

in which  $\eta_a^*$  is the astronomical tide. The barometric tide  $\eta_b$  is calculated from the atmospheric pressure depression  $\Delta p$ , which in turn is obtained from the hurricane model.

$$\eta_b = \frac{\Delta p}{\rho g} \quad (2.17)$$

The lateral open boundary condition from a physical point of view is the most difficult and also the most controversial to specify.

However, they are necessary for a complete mathematic formulation. Since no real physical limitation exists, the conditions must be chosen that least disturb the model and therefore allow a realistic solution to be obtained. Although several different specifications for the lateral open boundaries have been proposed such as radiative boundary condition (Reid and Bodine 1968), zero onshore transport (Pearce 1972), zero gradient of surge elevation and/or zero gradient of total water depth across the lateral boundaries (Yeh and Yeh 1976), all computational experience indicates that any of the three forementioned conditions would yield practically the same surge, if the lateral open boundaries are located far away (in the sense of wave propagation) from the domain of interest. Indications are that any reasonable boundary conditions at the far-away lateral boundaries have only a second order effect. In the present study, the lateral boundaries are chosen to be a great distance from the Bay entrance and equation (2.16) is again adopted for simplicity as the lateral boundary condition.

The boundary conditions which specify the x and y component of force measures are written

$$\begin{aligned} T_x &= T_x^* \\ T_y &= T_y^* \end{aligned} \tag{2.18}$$

In this study  $T_x^*$  and  $T_y^*$  are assumed to be of second order significance and are imposed to be zero in the calculation.

## 2.2 Hurricane Model

"Hurricane" is the West Indian name for the intense tropical cyclones which originate over the oceans within 5 to 15 degrees of



latitude from the equator. In this work all tropical cyclones will be called hurricanes. The most prominent characteristic of the hurricane is a large scale (some 1000 km order of magnitude) doughnut-shaped ring of strong winds often exceeding 50 m/s surrounding an area of very low pressure at the center, some 50 mb below that of the periphery. A hurricane also contains tremendous volumes of warm, moist air and torrential rainfall may be anticipated as it passes.

The analytical representations of the (atmospheric) pressure and wind fields of a hurricane are of great interest and are obtained semi-empirically on the basis of previous works (Holmboe 1945, Myers 1954, Wilson 1957, Pagenkopf and Pearce 1975). An idealized hurricane could be characterized by the central pressure depression (or anomaly)  $\Delta p$ , the distance from the hurricane center to the point of maximum winds, which is called the radius of maximum winds  $R_m$ , and the forward velocity of the hurricane  $V_f$ . These three parameters are also reported by the National Weather Service when characterizing a hurricane, thereby providing valuable information for the study of hurricane surges.

The central pressure anomaly is defined

$$\Delta p = p_\infty - p_c \quad (2.19)$$

where  $p_\infty$  is the atmospheric pressure at the outer periphery of the hurricane, and  $p_c$  the pressure at the center of the hurricane. According to the Hydrometeorological Section of the Weather Bureau, through studies of the various hurricanes (Myers 1954), the rate of change of pressure with a distance  $r$  from the hurricane center is given in the form

$$\frac{dp}{dr} = \Delta p \frac{R_m}{r^2} e^{-\frac{R_m}{r}} \quad (2.20)$$

This equation can be deduced explicitly to (Wilson 1957)

$$p = p_c + \Delta p e^{-\frac{R_m}{r}} \quad (2.21)$$

Equations (2.20) and (2.21) give adequate pictures of the pressure field, and equation (2.21) shows that the isobars are circular with the lowest pressure at the center.

Surface wind velocities of an idealized hurricane are obtained by the forces balance on a control volume of air mass, which according to Holmboe (1945) and Wilson (1957) is

$$\frac{U^2}{r} + \left( f + \frac{V_f \sin \theta}{r} \right) U - \frac{1}{\rho_a} \frac{\partial p}{\partial r} = 0 \quad (2.22)$$

in which  $f$  is the Coriolis coefficient,  $r$  is the distance from the hurricane center, and  $\theta$  is the counter clockwise angle between the point and the line of forward direction, and  $\rho_a$  the air density (see figure 2.2). The terms in equation (2.22) from the left to the right are respectively the centrifugal acceleration, the Coriolis acceleration, the turning acceleration of the wind vector and the pressure gradient. Invoking equation (2.20),  $U$  is obtained from equation (2.22).

$$U = \frac{1}{2} \left\{ - (fr + V_f \sin \theta) + \left[ (fr + V_f \sin \theta)^2 + 4 \frac{\Delta p}{\rho_a} \frac{R_m}{r} e^{-\frac{R_m}{r}} \right]^{1/2} \right\} \quad (2.23)$$

In order to reduce the gradient wind  $U$  to the 10-meter elevation a reduction factor  $c_r$  is needed. This factor depends on latitude, divergence of wind direction from the isobars, condition of the earth surface

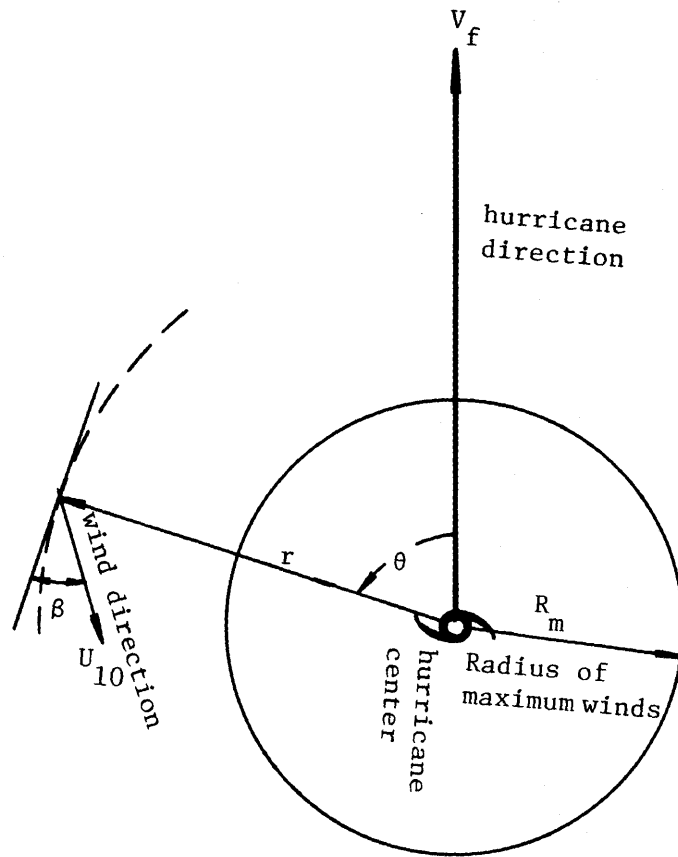


Figure 2.2. Definition sketch of a hurricane.

and other factors. Reduction factors for various North American coastal regions have been reported by Gram and Nun (1959). In addition, a deflection angle  $\beta$ , being defined as the angle between true wind direction and a tangent to a circle with center at the hurricane center, must also be considered to correct the gradient wind computation. The values of  $\beta$  in the following table are adapted from the standard project hurricane (Graham and Nun 1959).

$\beta$	Location
$20^\circ$	center to $R_m$
$20^\circ-25^\circ$	$R_m$ to $1.2 R_m$
$25^\circ$	beyond $1.2 R_m$

Therefore equation (2.23) is thus modified to be

$$U_{10} = \frac{1}{2} \left\{ - \left[ c_r f r + V_f \sin(\theta + \beta) \right] \left[ \left( c_r f r + V_f \sin(\theta + \beta) \right)^2 + c_r^2 \frac{4\Delta p}{\rho_a} \frac{R_m}{r} e^{-\frac{R_m}{r}} \right]^{1/2} \right\} \quad (2.24)$$

where  $U_{10}$  is the 10-meter surface wind. A definition sketch is shown in figure 2.2. Equation (2.24) has the same expression used by Pagenkopf and Pearce (1975).

For a given hurricane, equations (2.21) and (2.24) provide the pressure and wind fields of the hurricane to the hydrodynamic model for calculation of the storm surge.

### 3. VARIATIONAL STATEMENT AND FINITE ELEMENT APPROXIMATION

The system of governing equations (2.1) and (2.2a and b) with proper initial and boundary conditions is too complicated to be solved by analytical means. However, it permits a great number of different numerical approximations. The literature on the theoretical and numerical behavior of finite difference techniques for solving equations of hyperbolic and parabolic types is quite extensive, but so far only a few computational models that could serve as general guides have been developed. In the study of storm surge of a complicated bay-ocean system, a finite element scheme is used in order to have a grid system that fits the physical coastal boundaries well.

#### 3.1 Variational Statement

The Galerkin's weighted residual finite element numerical technique is employed in this work. In most cases, Galerkin's process (Finlayson 1972) is a simple and more direct formulation than the functional construction (which sometimes may not exist) and the subsequent extremization. When the equation is self-adjoint, the variational process is identical to that of the Galerkin's weighted residual method. (Oden and Oliveira 1973) The Galerkin's formulation is a weak form (Strang and Fix 1973) and the variational statements for equations (2.1) and (2.2a and b) with equation (2.18) can be obtained by invoking Stokes' theorem as follows:

$$\iint_A \left( \frac{\partial H}{\partial t} + \frac{\partial q_x}{\partial x} + \frac{\partial q_y}{\partial y} - Q \right) \delta H \, dA = 0 \quad (3.1)$$

$$\iint_A \left\{ \left( \frac{\partial q_x}{\partial t} + \frac{\partial H^{-1} q_x^2}{\partial x} + \frac{\partial H^{-1} q_y q_x}{\partial y} - f_{q_y} + \frac{H}{\rho_o} \frac{\partial}{\partial x} (p^s + \rho g \eta) \right. \right. \\ \left. \left. - \frac{\tau_x^s - \tau_x^b}{\rho_o} \right) \delta q_x + T_{xx} \frac{\partial \delta q_x}{\partial x} + T_{yx} \frac{\partial \delta q_x}{\partial y} \right\} dA - \int_{\partial A} T_x^* \delta q_x dL = 0 \quad (3.2a)$$

$$\iint_A \left\{ \left( \frac{\partial q_y}{\partial t} + \frac{\partial H^{-1} q_x q_y}{\partial x} + \frac{\partial H^{-1} q_y^2}{\partial t} + f_{q_x} + \frac{H}{\rho_o} \frac{\partial}{\partial y} (p^s + \rho g \eta) \right. \right. \\ \left. \left. - \frac{\tau_y^s - \tau_y^b}{\rho_o} \right) \delta q_y + T_{xy} \frac{\partial \delta q_y}{\partial x} + T_{yy} \frac{\partial \delta q_y}{\partial y} \right\} dA - \int_{\partial A} T_y^* \delta q_y dL = 0 \quad (3.2b)$$

where A is the water domain of interest,  $\partial A$  is the boundary curve of the domain A.  $dA$  and  $dL$  are associated with area and line integrals.  $\delta H$ ,  $\delta q_x$  and  $\delta q_y$  are the weighting functions. Note that the second order derivative contained in the internal stress terms in equations (2.2a and b) has been reduced to a first order derivative in equations (3.2a and b). In this situation, a linear interpolation function is also an admissible function and can be used for approximation. However, a linear interpolation function chosen to describe a large domain A will lose accuracy in general. Therefore, the entire domain A will be divided into finite elements, and an approximate solution within each element will be sought by using a simple linear interpolation function with unknown nodal variables  $H$ ,  $q_x$ ,  $q_y$ .

### 3.2 Finite Element Approximation

The finite element method is a technique of numerical approximation. In this method a domain is divided by lines or surfaces into a finite number of nonoverlapping subdomains which are called the elements.

The procedure is first to approximate the solution within each element by admissible interpolation functions in terms of a finite number of unknown parameters. An assembling procedure is then employed to combine the relations for individual elements into a system of equations for all the unknown parameters. In this way the original problem, having infinite degrees of freedom, is transformed into a problem with a finite number of degrees of freedom. As the element size becomes smaller and smaller, it is hoped that the discretization error of the field variables vanishes and the exact solution can be obtained. The unknown parameters are usually the values of field variables (nodal variables) at a finite number of points, which are called nodes. The establishment of the system of equations for unknown parameters is usually based on the extremization of a variational statement. With the exception of very elementary problems, practical application of the finite element method entails a considerable amount of computation and the use of a high speed electronic computer. The reader can find a very full exposition of the finite element method in recent books by Zenkiewicz (1971), Martin and Cary (1973), Norrie and deVries (1973), Oden and Oliverira (1973), Strang and Fix (1973), and Brebbia and Connor (1974), for example.

### 3.2.1 Linear Triangular Element

In this study the entire water domain of interest is divided into small triangular elements, each with three nodes. Within each element, the field variables  $H$ ,  $q_x$  and  $q_y$  are approximated by a linear interpolation (shape) function  $N_i^e$  ( $i=1,2,3$  corresponding to three nodes)

with unknowns being the nodal variables  $H_i^e$ ,  $q_{xi}^e$  and  $q_{yi}^e$  at the element nodal point, i.e., in the "e" element

$$H^e = N_1^e H_1^e + N_2^e H_2^e + N_3^e H_3^e = \{N^e\}^T \{H^e\} = \{H^e\}^T \{N^e\} \quad (3.3)$$

$$q_x^e = N_1^e q_{x1}^e + N_2^e q_{x2}^e + N_3^e q_{x3}^e = \{N^e\}^T \{q_x^e\} = \{q_x^e\}^T \{N^e\} \quad (3.4a)$$

$$q_y^e = N_1^e q_{y1}^e + N_2^e q_{y2}^e + N_3^e q_{y3}^e = \{N^e\}^T \{q_y^e\} = \{q_y^e\}^T \{N^e\} \quad (3.4b)$$

In the preceding, the transposes of arrays  $\{H^e\}$ ,  $\{q_x^e\}$  and  $\{q_y^e\}$  are respectively

$$\{H^e\}^T = \{H_1^e, H_2^e, H_3^e\} \quad (3.5)$$

$$\{q_x^e\}^T = \{q_{x1}^e, q_{x2}^e, q_{x3}^e\} \quad (3.6a)$$

$$\{q_y^e\}^T = \{q_{y1}^e, q_{y2}^e, q_{y3}^e\} \quad (3.6b)$$

With the numerical subscripts referring to the nodes,  $\{N^e\}^T$  is the row vector

$$\{N^e\}^T = \{N_1^e, N_2^e, N_3^e\} \quad (3.7)$$

with

$$N_i^e = (a_i + b_i x + c_i y) / 2\Delta^e \quad ; \quad i = 1, 2, 3 \quad (3.8a)$$

$$a_1 = x_2^e y_3^e - x_3^e y_2^e \quad (3.8b)$$

$$b_1 = y_2^e - y_3^e \quad (3.8c)$$

$$c_1 = x_3^e - x_2^e \quad (3.8d)$$

(equations for  $a_2, a_3, b_2, b_3, c_2, c_3$  are cyclic permutations on 1, 2, 3)



$$\text{and } \Delta^e = \text{the area of the element } e = \frac{1}{2} \begin{vmatrix} 1 & x_1^e & y_1^e \\ 1 & x_2^e & y_2^e \\ 1 & x_3^e & y_3^e \end{vmatrix} \quad (3.8e)$$

where  $(x_i^e, y_i^e)$  are the coordinates of the element nodal point  $i$  as shown in figure 3.1. The interpolation functions  $N_i^e$  are linear functions of the coordinate. It is obvious that each interpolation function  $N_i^e$  is a pyramid, being unity at one node and going linearly to zero at surrounding nodes. These linear interpolation functions are employed to approximate the solution for each three nodal triangular elements in the domain  $A$ .

### 3.2.2 Evaluation of the Variational Statements

The interpolation functions given by equations (3.3) through (3.7) are used to evaluate the integral equations (3.1) and (3.2a and b). In the following calculation of the integrals, we shall omit, for brevity, the symbols  $dA$  in all area integrals and  $dL$  in all line integral, and also omit, when not ambiguous, the superscript  $e$ .

The calculation of each integral of equation (3.1) is sequently obtained to be

$$\begin{aligned} \iint_A \frac{\partial H}{\partial t} \delta H &= \sum_{e \in A} \iint_e \frac{\partial H}{\partial t} \delta H = \sum_{e \in A} \{\delta H\}^T \iint_e \{N\} \{N\}^T \frac{\partial \{H\}}{\partial t} \\ &= \sum_{e \in A} \{\delta H\}^T (M_h) \frac{\partial \{H\}}{\partial t} \end{aligned} \quad (3.9a)$$

$$\begin{aligned} \iint_A \frac{\partial q_x}{\partial x} \delta H &= \sum_{e \in A} \iint_e \frac{\partial q_x}{\partial x} \delta H = \sum_{e \in A} \{\delta H\}^T \iint_e \{N\} \frac{\partial \{N\}^T}{\partial x} \{q_x\} \\ &= \sum_{e \in A} \{\delta H\}^T (G_x) \{q_x\} \end{aligned} \quad (3.9b)$$

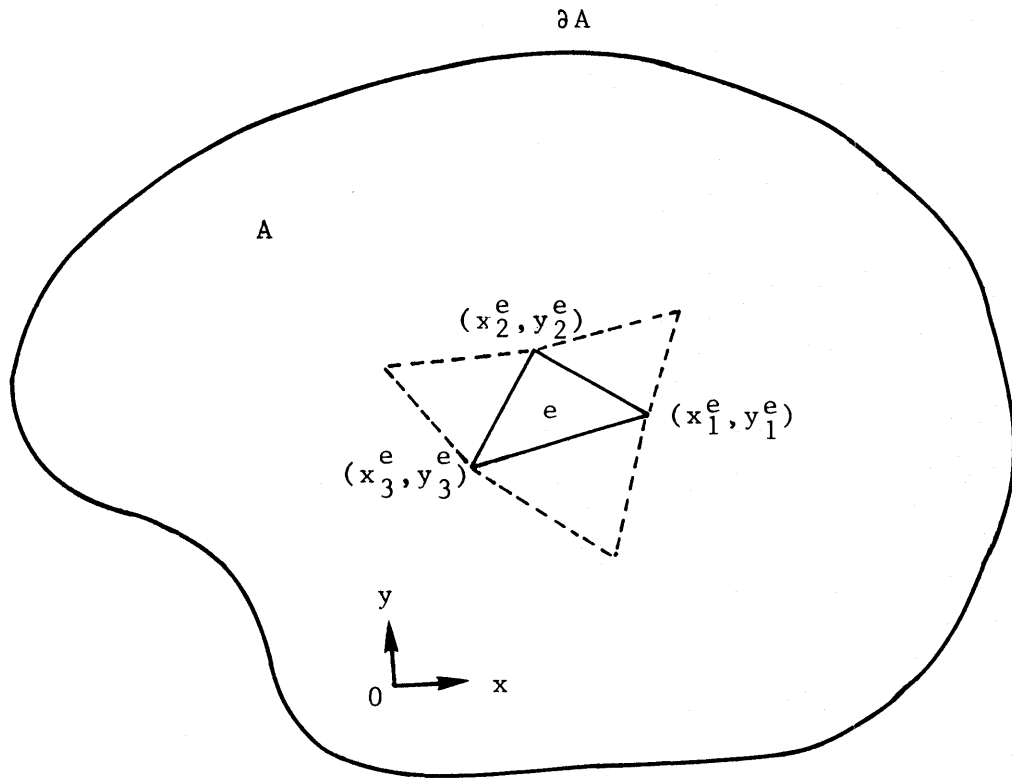


Figure 3.1. Domain and triangular elements

$$\begin{aligned} \iint_A \frac{\partial q_y}{\partial y} \delta H &= \sum_{e \in A} \iint_e \frac{\partial q_y}{\partial y} \delta H = \sum_{e \in A} \{\delta H\}^T \iint_e \{N\} \frac{\partial \{N\}}{\partial y} \{q_y\} \\ &= \sum_{e \in A} \{\delta H\}^T (G_y) \{q_y\} \end{aligned} \quad (3.9c)$$

$$\begin{aligned} \iint_A Q \delta H &= \sum_{e \in A} \iint_e Q \delta H = \sum_{e \in A} \{\delta H\}^T \iint_e \{N\} \{N\}^T \{Q\} \\ &= \sum_{e \in A} \{\delta H\}^T (M_h) \{Q\} \end{aligned} \quad (3.9d)$$

where the matrices

$$(M_h^e) = \iint_e \{N\} \{N\}^T = \frac{\Delta}{12} \begin{pmatrix} 2 & 1 & 1 \\ 1 & 2 & 1 \\ 1 & 1 & 2 \end{pmatrix} \quad (3.10a)$$

$$(G_x^e) = \iint_e \{N\} \frac{\partial \{N\}^T}{\partial x} = \frac{1}{6} \begin{pmatrix} b_1 & b_2 & b_3 \\ b_1 & b_2 & b_3 \\ b_1 & b_2 & b_3 \end{pmatrix} \quad (3.10b)$$

$$(G_y^e) = \iint_e \{N\} \frac{\partial \{N\}^T}{\partial y} = \frac{1}{6} \begin{pmatrix} c_1 & c_2 & c_3 \\ c_1 & c_2 & c_3 \\ c_1 & c_2 & c_3 \end{pmatrix} \quad (3.10c)$$

Equation (3.1) is then reduced to

$$\sum_{e \in A} \{\delta H\}^T \left\{ (M_h) \frac{\partial \{H\}}{\partial t} + (G_x) \{q_x\} + (G_y) \{q_y\} - (M_h) \{Q\} \right\} = 0 \quad (3.11)$$

Next we define the global vector arrays as follows

$$\{\delta H\} = \text{union of all } \{\delta H^e\} \quad (3.12a)$$

$$\{H\} = \text{union of all } \{H^e\} \quad (3.12b)$$

$$\{\delta q\} = \text{union of all } \{\delta q_x^e\} \text{ and } \{\delta q_y^e\} \quad (3.12c)$$

$$\{q\} = \text{union of all } \{q_x^e\} \text{ and } \{q_y^e\} \quad ; \quad e \in A \quad (3.12d)$$

Then equation (3.18) can be assembled into a simple equation in matrix form

$$\{\delta H\}^T \left\{ (M_h) \frac{\partial \{H\}}{\partial t} + (G_h) \{q\} + \{R_h\} \right\} = 0 \quad (3.13)$$

where the global matrices  $(M_h)$ ,  $(G_h)$  and  $\{R_h\}$  are known from the assemblage of the element matrices  $(M_h^e)$ ,  $(G_x^e)$  and  $\{G_y^e\}$ , and  $(M_h^e)(Q^e)$  respectively. Since the element of  $\{\delta H\}$  determines the test function, which is an arbitrary function, the terms within the brackets must vanish; i.e.

$$(M_h) \frac{\partial \{H\}}{\partial t} + (G_h) \{q\} + \{R_h\} = 0 \quad (3.14)$$

Note that  $(M_h)$  is symmetric. Equation (3.14) represents a set of first order differential equations in time.

The calculation of each integral of equations (3.2a and b) in element  $e$  is given as follows:

For equation (3.2a)

$$\iint_e \frac{\partial q_x}{\partial t} \delta q_x = \{\delta q_x\}^T (M_h) \frac{\partial \{q_x\}}{\partial t}$$

$$\text{Defining } c_{ij} = H^{-1} q_i q_j ; \quad i, j = x, y$$

$$\iint_e \frac{\partial H^{-1} q_x^2}{\partial x} \delta q_x \cong \{\delta q_x\}^T (G_x) \{c_{xx}\}$$

$$\iint_e \frac{\partial H^{-1} q_y q_x}{\partial y} \delta q_y = \{\delta q_x\}^T (G_y) \{c_{yx}\}$$

$$\iint_e f q_y \delta q_x = \{\delta q_x\}^T f(M_h) \{q_y\}$$

$$\iint_e \frac{H}{\rho_o} \frac{\partial p^s}{\partial x} \delta q_x = \{\delta q_x\} (M_h) \{H\} \frac{(b_1 p_1 + b_2 p_2 + b_3 p_3)}{2\rho_o \Delta}$$

$$\iint_e gH \frac{\partial \eta}{\partial x} \delta q_x = \{\delta q_x\}^T (M_h) \{H\} \frac{g(b_1 \eta_1 + b_2 \eta_2 + b_3 \eta_3)}{2\Delta}$$

Defining  $(M_{3\gamma}) = \iint_e \{N\} \{N\}^T \{H\} \{N\}^T \{\gamma\}$

$$= \frac{\Delta}{60} \begin{pmatrix} 2\bar{\gamma} + 4\gamma_1 & 2\bar{\gamma} - \gamma_3 & 2\bar{\gamma} - \gamma_2 \\ 2\bar{\gamma} - \gamma_3 & 2\bar{\gamma} + 4\gamma_2 & 2\bar{\gamma} - \gamma_1 \\ 2\bar{\gamma} - \gamma_2 & 2\bar{\gamma} - \gamma_1 & 2\bar{\gamma} + 4\gamma_3 \end{pmatrix}$$

$$\text{and } \bar{\gamma} = \gamma_1 + \gamma_2 + \gamma_3$$

(3.15\*)

$$\iint_e \frac{gH\Delta\rho}{\rho_o} \frac{\partial \eta}{\partial x} \delta q_x \cong \{\delta q_x\}^T \frac{g(b_1 \eta_1 + b_2 \eta_2 + b_3 \eta_3)}{2\rho_o \Delta} (M_{3\Delta\rho}) \{H\}$$

$$\iint_e \frac{gH\eta}{\rho_o} \frac{\partial \Delta\rho}{\partial x} \delta q_x \cong \{\delta q_x\}^T \frac{g(b_1 \Delta\rho_1 + b_2 \Delta\rho_2 + b_3 \Delta\rho_3)}{2\rho_o \Delta} (M_{3\eta}) \{H\}$$

$$\iint_e \frac{\tau_x^s}{\rho_o} \delta q_x = \{\delta q_x\}^T \frac{1}{\rho_o} (M_h) \{\tau_x^s\}$$

$$\iint_e \frac{\tau_x^b}{\rho_o} \delta q_x \cong \{\delta q_x\}^T \frac{1}{\rho_o} (M_h) \{\tau_x^b\}$$

Defining  $\bar{H} = (H_1 + H_2 + H_3)$  as in equation (3.15\*) and flow velocities  $(u, v) = H^{-1}(q_x, q_y)$

$$\iint_e T_{xx} \frac{\partial \delta q_x}{\partial x} \cong \{\delta q_x\}^T \frac{\epsilon_{xx} \bar{H}}{12\Delta} (M_{bb}) \{u\} \quad ;$$

$$\text{where } (M_{bb}) = \begin{pmatrix} b_1^2 & b_1 b_2 & b_1 b_3 \\ b_2 b_1 & b_2^2 & b_2 b_3 \\ b_3 b_1 & b_3 b_2 & b_3^2 \end{pmatrix}$$

$$\iint_e T_{yx} \frac{\partial \delta q_x}{\partial y} \cong \{\delta q_x\}^T \frac{\epsilon_{yx} \bar{H}}{24\Delta} \left\{ (M_{cb}) \{v\} + (M_{cc}) \{u\} \right\} \quad ;$$

$$\text{where } (M_{cb}) = \begin{pmatrix} c_1 b_1 & c_1 b_2 & c_1 b_3 \\ c_2 b_1 & c_2 b_2 & c_2 b_3 \\ c_3 b_1 & c_3 b_2 & c_3 b_3 \end{pmatrix}$$

$$\text{and } (M_{cc}) = \begin{pmatrix} c_1^2 & c_1 c_2 & c_1 c_3 \\ c_2 c_1 & c_2^2 & c_2 c_3 \\ c_3 c_1 & c_3 c_2 & c_3^2 \end{pmatrix}$$

$$\int_{\partial e} T_x^* \delta q_x = \{\delta q_x\}^T \int_{\partial e} \{N\} \{N\}^T \{T_x^*\} = \{\delta q_x\}^T \frac{L^e}{6} \begin{pmatrix} 2 & 1 \\ 1 & 2 \end{pmatrix} \{T_x^*\}$$

For equation (3.2b)

$$\iint_e \frac{\partial q_y}{\partial t} \delta q_y = \{\delta q_y\}^T (M_h) \frac{\partial \{q_y\}}{\partial t}$$

$$\iint_e \frac{\partial H^{-1} q_x q_y}{\partial x} \delta q_y \cong \{\delta q_y\}^T (G_x) \{c_{xy}\}$$

$$\iint_e \frac{\partial H^{-1} q_y^2}{\partial y} \delta q_y \cong \{\delta q_y\}^T (G_y) \{c_{yy}\}$$

$$\iint_e f q_x \delta q_y = \{\delta q_y\}^T f (M_h) \{q_x\}$$

$$\iint_e \frac{H}{\rho_o} \frac{\partial p^s}{\partial y} \delta q_y = \{\delta q_y\}^T (M_h) \{H\} \frac{(c_1 p_1 + c_2 p_2 + c_3 p_3)}{2\rho_o \Delta}$$

$$\iint_e g H \frac{\partial \eta}{\partial y} \delta q_y = \{\delta q_y\}^T (M_h) \{H\} \frac{g(c_1 \eta_1 + c_2 \eta_2 + c_3 \eta_3)}{2\Delta}$$

$$\iint_e \frac{g H \Delta \rho}{\rho_o} \frac{\partial \eta}{\partial y} \delta q_y \cong \{\delta q_y\}^T \frac{g(c_1 \eta_1 + c_2 \eta_2 + c_3 \eta_3)}{2\rho_o \Delta} (M_{3\Delta\rho}) \{H\}$$

$$\iint_e \frac{g H \eta}{\rho_o} \frac{\partial \Delta \rho}{\partial y} \delta q_y \cong \{\delta q_y\}^T \frac{g(c_1 \Delta \rho_1 + c_2 \Delta \rho_2 + c_3 \Delta \rho_3)}{2\rho_o \Delta} (M_{3\eta}) \{H\}$$

$$\iint_e \frac{\tau_y^s}{\rho_o} \delta q_y = \{\delta q_y\}^T \frac{1}{\rho_o} (M_h) \{\tau_y^s\}$$

$$\iint_e \frac{\tau_y^b}{\rho_o} \delta q_y \cong \{\delta q_y\}^T \frac{1}{\rho_o} (M_h) \{\tau_y^b\}$$

$$\iint_e T_{xy} \frac{\partial \delta q_y}{\partial x} \cong \{\delta q_y\}^T \frac{\epsilon_{xy} \bar{H}}{24\Delta} \left\{ (M_{cb})^T \{u\} + (M_{bb}) \{v\} \right\}$$

$$\iint_e T_{yy} \frac{\partial \delta q_y}{\partial y} \cong \{\delta q_y\}^T \frac{\epsilon_{yy} \bar{H}}{12\Delta} (M_{cc}) \{v\}$$

$$\int_{\partial e} T_y^* \delta q_y = \{\delta q_y\}^T \frac{L^e}{6} \begin{pmatrix} 2 & 1 \\ 1 & 2 \end{pmatrix} \{T_y^*\}$$

Now all the integrals are substituted into equations (3.2a and b) and assemblage is performed, the resultant equation can be represented by the matrix form

$$\left(M_m\right) \frac{\partial\{q\}}{\partial t} + \left(G_m\right)\{q\} + \left(K_m\right)\{\eta\} + \{R_m\} = 0 \quad (3.15)$$

where the matrices  $\left(M_m\right)$ ,  $\left(G_m\right)$ ,  $\left(K_m\right)$  and  $\{R_m\}$  are obtained through the assemblage of all the element in domain A. Note that the variables in the higher order integration terms, such as convection and bottom friction, have been lumped into a simple form for approximation as self-explained in the preceding integrals.

### 3.3 Time Integration

After using the finite element integration in spatial coordinates, the original continuous system of equations (3.1) and (3.2a and b) reduce to a system of first order ordinary differential equation in time, equations (3.14) and (3.15). To complete the model, an effective technique must be used to advance the solution in time from a given initial condition. The choice of the scheme depends on the required features of accuracy, stability and efficiency. The literature on these features is very extensive. (Richtmyer and Morton 1967, Roache 1972). In this study the split-time method (Wang and Connor 1975) is employed in order to achieve a faster and more efficient computational procedure to deal with a large complicated bay-ocean system. The scheme is actually inspired by the time split explicit (TSE) scheme in the finite difference method. The computational procedure is expressed as follows.

Equations (3.14) and (3.15) can be reformed into



$$(M_h) \frac{\partial \{H\}}{\partial t} = \{P_h\} \quad (3.16a)$$

$$(M_m) \frac{\partial \{q\}}{\partial t} = \{P_m\} \quad (3.16b)$$

where the elements of  $\{P_h\}$  and  $\{P_m\}$  are in general functions of  $H$ ,  $q$ ,  $t$ . If the trapezoidal rule in time is used and  $H$  and  $q$  are staggered in time such that  $H$  is evaluated at times  $t_{n-\frac{1}{2}}$  and  $q$  at  $t_n$  ( $n=1,2,3,\dots$ ), equations (3.16a and b) reduce to

$$(M_h) \left\{ \{H\}_{n+\frac{1}{2}} - \{H\}_{n-\frac{1}{2}} \right\} = \Delta t \{P_h(\{H\}_{n-\frac{1}{2}}, \{q\}_n, t_n)\} \quad (3.17a)$$

$$(M_m) \left\{ \{q\}_{n+1} - \{q\}_n \right\} = \Delta t \{P_m(\{H\}_{n+\frac{1}{2}}, \{q\}_n, t_{n+\frac{1}{2}})\} \quad (3.17b)$$

or

$$\{H\}_{n+\frac{1}{2}} = \{H\}_{n-\frac{1}{2}} + \Delta t (M_h)^{-1} \{P_h(\{H\}_{n-\frac{1}{2}}, \{q\}_n, t_n)\} \quad (3.18a)$$

$$\{q\}_{n+1} = \{q\}_n + \Delta t (M_m)^{-1} \{P_m(\{H\}_{n+\frac{1}{2}}, \{q\}_n, t_{n+\frac{1}{2}})\} \quad (3.18b)$$

by assuming given initial conditions  $\{H\}_{n-\frac{1}{2}}$  and  $\{q\}_n$ . The solution is obtained by first solving equation (3.18a) and then equation (3.18b) and then sequentially repeating the process. The stability condition of this scheme for the present problem is difficult to obtain analytically since so many physical terms are considered. Nevertheless, according to the present study and the study by Wang and Connor(1975), the critical time step for onset of instability is about  $1.5 \Delta t_{cr}$ .

$$1.5 \Delta t_{cr} = \frac{1.5 \Delta s^*}{\sqrt{2gh}} > \Delta t \quad (3.19)$$

where  $\Delta s^*$  is typical grid size. Equation (3.19) without the factor 1.5 is the well known Courant condition.

### 3.4 Treatment of Boundary Condition

Since the grid system of a physical problem is somewhat arbitrary, the definition of the normal at the boundary needs to be reasonably resolved for a better imposition of normal and tangential water transport  $q_n$  and  $q_s$ . The concept of "flow leaked in equals to flow leaked out across the boundaries" developed by Wang and Connor (1975) is adapted in this study. Define the angle  $\theta_n$  of the normal at point  $P_2$  as shown in figure 3.2.

$$\cot \theta_n = \frac{L_2 \sin \theta_o}{L_1 - L_2 \cos \theta_o} \quad \frac{\pi}{2} < \theta_o < 2\pi \quad (3.20)$$

where  $P_1$ ,  $P_2$  and  $P_3$  are three immediate adjoining points,  $L_1$  and  $L_2$  are two lengths of element boundaries, and  $\theta_o$  is the angle between  $L_1$  and  $L_2$ . Experience shows that the condition of zero velocity is appropriate for an acute angle,  $\theta_o \leq \frac{\pi}{2}$ .

Boundary conditions are specified in terms of  $q_n$  and  $q_s$ , instead of  $q_x$  and  $q_y$ . The transformation of field variables (water transport) from the global (x,y) coordinate system to the local (n,s) coordinate system is performed according to the geometric relation

$$\begin{pmatrix} n \\ s \end{pmatrix} = (T) \begin{pmatrix} x \\ y \end{pmatrix}, \quad \begin{pmatrix} x \\ y \end{pmatrix} = (T)^T \begin{pmatrix} n \\ s \end{pmatrix} \quad (3.21a)$$

$$\begin{pmatrix} q_n \\ q_s \end{pmatrix} = (T) \begin{pmatrix} q_x \\ q_y \end{pmatrix}, \quad \begin{pmatrix} q_x \\ q_y \end{pmatrix} = (T)^T \begin{pmatrix} q_n \\ q_s \end{pmatrix} \quad (3.21b)$$

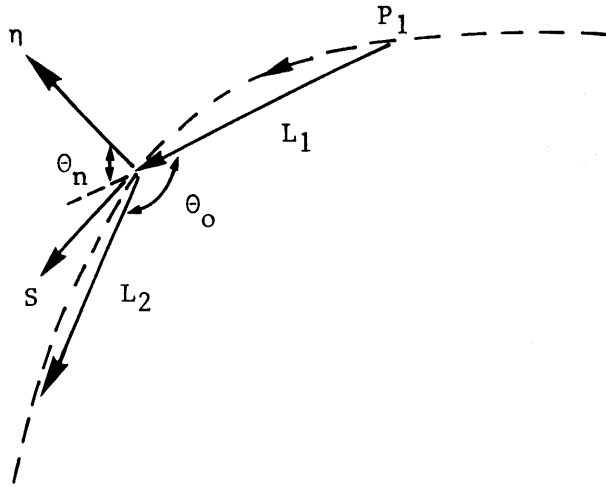


Figure 3.2. Definition sketch of boundary normal

where  $(T) = \begin{pmatrix} \cos\theta & \sin\theta \\ -\sin\theta & \cos\theta \end{pmatrix}$  (3.21c)

Note that  $(T)$  is an orthonormal matrix such that  $(T)^{-1} = (T)^T$ .

The boundary condition (2.15) and (2.16) are specified by using a standard row-column elimination technique on the coefficient matrices of respective equations (3.18a and b).

#### 4. NUMERICAL RESULTS AND DISCUSSIONS

In this chapter computational aspects of the hydrodynamic model and finite element layout are described in general terms. Numerical results are presented for three cases: tide simulation of the lower James River, tide simulation of the Chesapeake Bay, and storm surge hindcasting of the Chesapeake Bay. The purpose of simulating tide in the lower James River is to provide an economical way to test the validity of the hydrodynamic model and to study the numerical behavior of the model. The tide simulation in the bay was done mainly to calibrate the bottom friction coefficient. A storm surge hindcast in the bay using observations from hurricane Connie 1955 was conducted to determine the wind field and wind stress.

##### 4.1 Some Computational Aspects

The computational procedures and program for the storm surge calculation have been developed according to Chapters 2 and 3. Since the approach for solving the hydrodynamic model described in Chapter 3 is somewhat similar to the works by Connor and Wang (1975), the associated computer program CAFE (Circulation Analysis by Finite Element) has been used with modifications in this study.

The layout of the finite element system depends on variations of water elevation, coastal configuration and water depth. The maximum element size is chosen, according to Chen and Mei (1974)

$$\frac{\ell^e}{\lambda} \leq 0.1 \quad (4.1)$$

i.e. the element size  $\ell^e$  is chosen to be smallest in estuary (less than

5 km), somewhat larger in the bay (less than 10 km), and to increase gradually with distance of the grid point from the bay entrance. A Numonics Digitizer which reads to the accuracy of one hundredth of a centimeter, has been used to measure the coordinates of nodal points. The critical time step for instability was found by computational trials to be  $1.5 \Delta t_{cr}$  (see equation 3.19 and section 3.3), which is more relaxed than the Courant condition.

Computational experience also reached the same conclusions as found by Wang and Connor (1975); that the increase of the bottom friction coefficient  $c_f$  tends to increase the phase lag in the direction of water wave propagation. The water elevation was fairly insensitive to the change of  $c_f$ , but noticeable changes in the flow currents were calculated. Eddy viscosity ( $\epsilon_{xx}$ ,  $\epsilon_{xy}$  and  $\epsilon_{yy}$ ) have little effect on phase and range of water elevation, but affect flow currents.

## 4.2 Simulation of Tides

The physical unknown coefficients included in the storm surge model are bottom friction coefficient  $c_f$ , eddy viscosity coefficients  $\epsilon_{ij}$ , wind drag coefficients  $c_o$  and  $c_1$ , and wind reduction factor  $c_r$ . Values of these coefficients have to be determined before the model is used for prediction. Although these values are within some typical ranges, they generally vary for each different geographic area. In this study  $c_f$  and  $\epsilon_{ij}$  were calibrated by the tide simulations and  $c_o$ ,  $c_1$  and  $c_r$  by a storm surge hindcast.

### 4.2.1 Tide Simulation of the Lower James River

The location of the James River is shown in Figure 1.1. Three U.S.C&G maps (1974), numbered 562, 529 and 530, were used to provide

the information on coastal configuration and topography for the geometric input to the system. The finite element network of the lower James River, from Sandy Point and Sloop Point to the river mouth (Old Point Comfort and Willoughby Beach), is shown in Figure 4.1a and b. The figures illustrate the nodal and element positions. The typical length of an element is 1.2 to 4 km, depending on the desired accuracy. Figure 4.1c is the locally averaged mean water depth, being the mean low water depth corrected by mean tidal height and NGVD (1929) (National Geodetic Vertical Datum 1929).

The tidal information is obtained from U. S. Tide Tables (1976) and is adjusted by NGVD (1929) data. The inputs of free surface super-elevation (mean sea level minus NGVD (1929)), tidal height and phase lag at fifteen locations are listed in Tables 4.1a and b. It is believed that the free surface super-elevation is partly contributed by freshwater discharge from upstream and from tributaries.

Tidal heights and tidal currents from the U. S. Tide Tables and the U. S. Tidal Current Tables (1976), and the intensive survey field current data from VIMS (Virginia Institute of Marine Science) were used to calibrate the bottom friction coefficient  $c_f$  and eddy viscosity coefficients  $\epsilon_{ij}$ . The results show a good fit for  $c_f = 0.0064$ ,  $\epsilon_{xx} = \epsilon_{xy} = \epsilon_{yy} = 100 \text{ m}^2/\text{s}$ . The time step is 2 minutes. The water elevation and flow current reached periodic equilibrium state in only about 2 hours after starting from initial conditions. Examples of transient response are illustrated in Figures 4.2a and b. This fast convergence is due to the even distribution of the tidal force imposed over the water domain. The calculated results of water elevation and

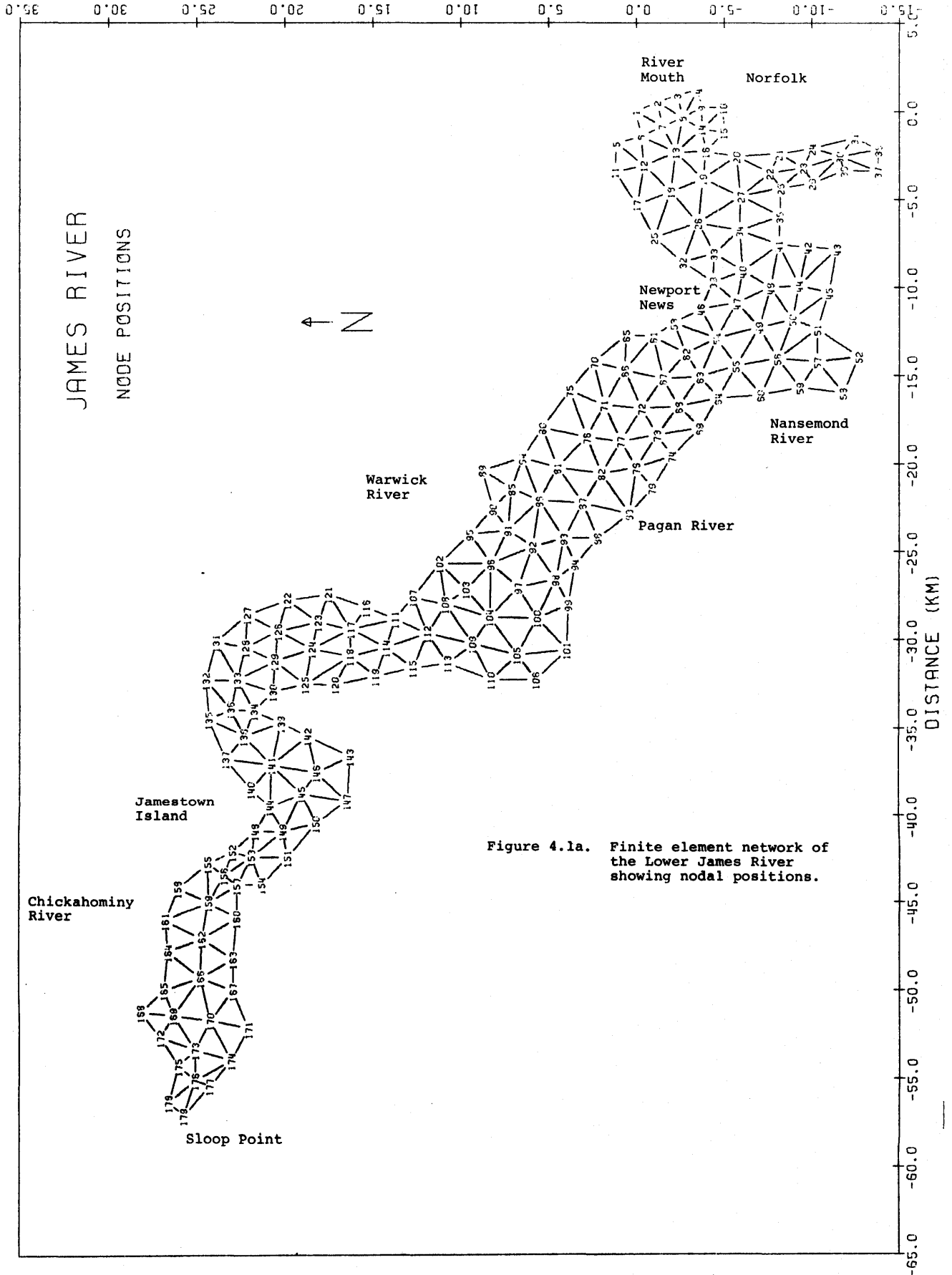


Figure 4.1a. Finite element network of the Lower James River showing nodal positions.





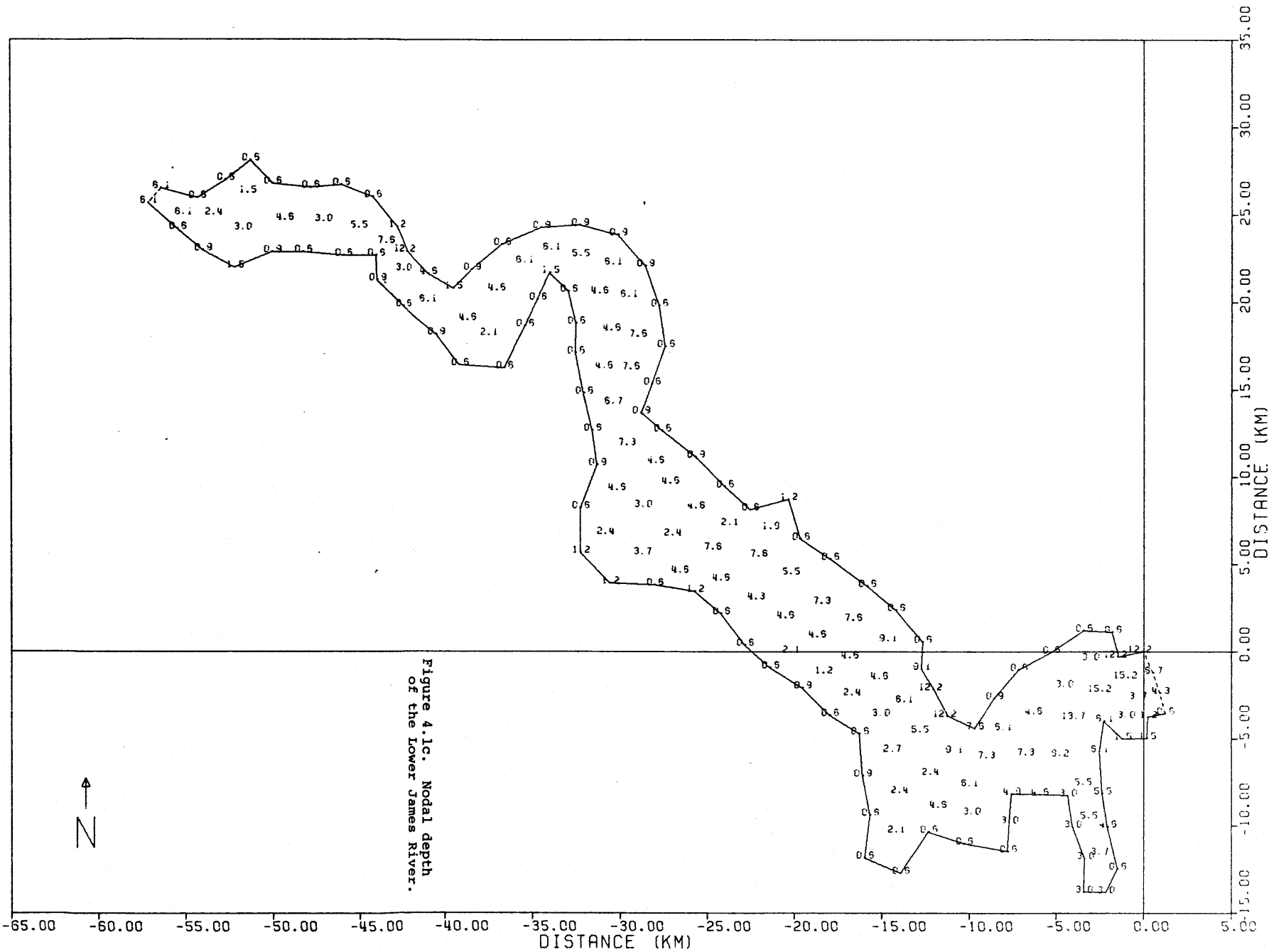


Figure 4.1c. Nodal depth of the Lower James River.

Table 4.1a. Some Tide Data of Lower James River.

Location	NGVD (1929)- MLW (m)	Mean Tidal Height (m)	Phase Lag		
			High Water	Low Water (hr:min)	Average
Old Point Comfort	0.396	0.366	-00:11	-00:35	-00:23
Sewells Point	0.390	0.366	00:00	00:00	00:00
Norfolk Harbor	0.466	0.396	00:13	00:19	00:16
Newport News	0.399	0.396	00:20	00:18	00:19
Chuckatuck Creek Entrance	0.463	0.427	00:41	00:47	00:44
Menchville	0.421	0.396	00:54	01:09	01:02
Burwell Bay	0.357	0.366	01:14	01:42	01:28
Ferry Point Chickahominy R.	0.247	0.274	03:54	04:26	04:10
Claremont Wharf	0.238	0.274	04:02	04:38	04:20

Table 4.1b. Tidal Input for the Lower James River Hydrodynamic Model.

Nodal Point	Free Surface Superelevation (is Referenced to NGVD (1929)) (m)	Tidal Height (m)	Phase Lag (is Referenced to Sewells Point) (sec)
1	-0.015	0.38	-1380
2	-0.015	0.38	-1380
3	-0.015	0.38	-1380
4	-0.015	0.38	-1380
20	-0.009	0.38	0
37	-0.041	0.42	945
38	-0.041	0.42	945
46	-0.003	0.40	1140
59	-0.036	0.43	2640
60	-0.036	0.43	2640
89	-0.025	0.40	3696
106	0.009	0.36	5280
168	0.043	0.29	15000
178	0.052	0.29	15600
179	0.052	0.29	15600

(see Figure 4.1a for nodal point)

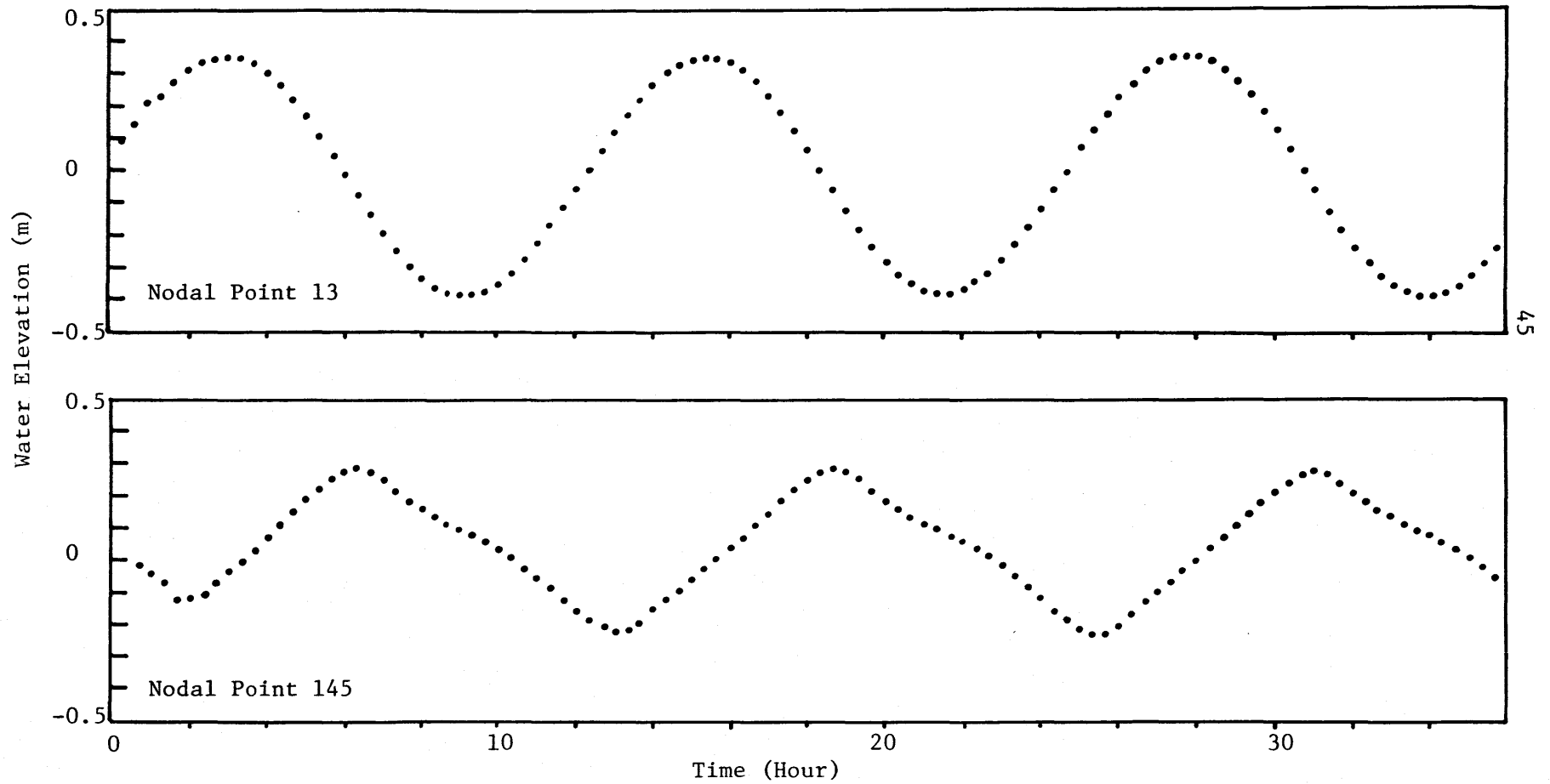


Figure 4.2a. Time history of water elevation at Node. (See Figure 4.1a for nodal position).

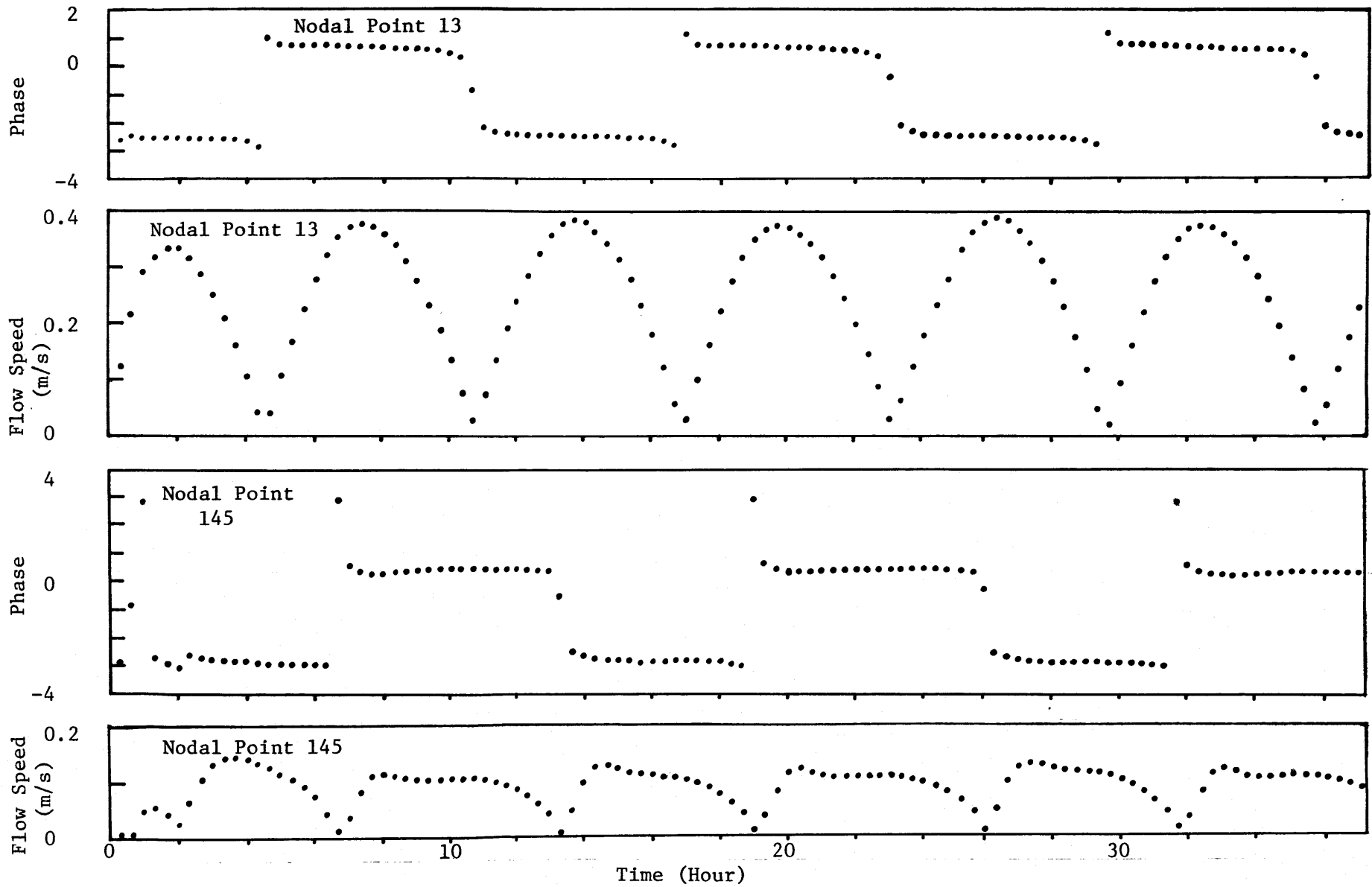


Figure 4.2b. Time history of flow velocity at node. (See Figure 4.1a for nodal position).

flow circulation within a tidal cycle are illustrated in Appendix A.

#### 4.2.2 Tidal Simulation of the Chesapeake Bay

"The Bathymetry of the Chesapeake Bay" published by VIMS was used to produce the geometric information of the coastal configuration and topography. The finite element network of the bay proper is shown in Figures 4.3a and b. The typical length of an element ranges from 5 km to 10 km, depending on the coastal configuration and water depth. Figure 4.3c shows the locally averaged mean water depth, which is adjusted to refer to NGVD (1929).

Since tidal current information at the Bay entrance and at each river mouth was lacking, the free surface super-elevation, tidal height and phase lag was again used to represent the only driving forces at the boundary. Some of these inputs was obtained from U. S. Tide Tables and adjusted by NGVD (1929), while others were interpolated from the results of Hicks (1964). These input data are listed in Table 4.2.

The calibration was conducted by comparing the calculated results with the results by Hicks (1964) and the information from the U. S. Tide Tables and U. S. Tidal Current Tables (1976), although this comparison is technically difficult due to the scarcity of the existing data. The calibrated result shows that  $C_f = 0.0064$  and  $\epsilon_{xx} = \epsilon_{xy} = \epsilon_{yy} = 300 \text{ m}^2/\text{s}$ . The time step was 4 minutes. The water elevation and flow velocity reach periodic equilibrium state about 6 hours after starting from initial conditions. Two typical nodal points are shown in Figure 4.4a and b. The results of water elevation and flow circulation within a tidal cycle are illustrated in Appendix B.

NODE POSITIONS

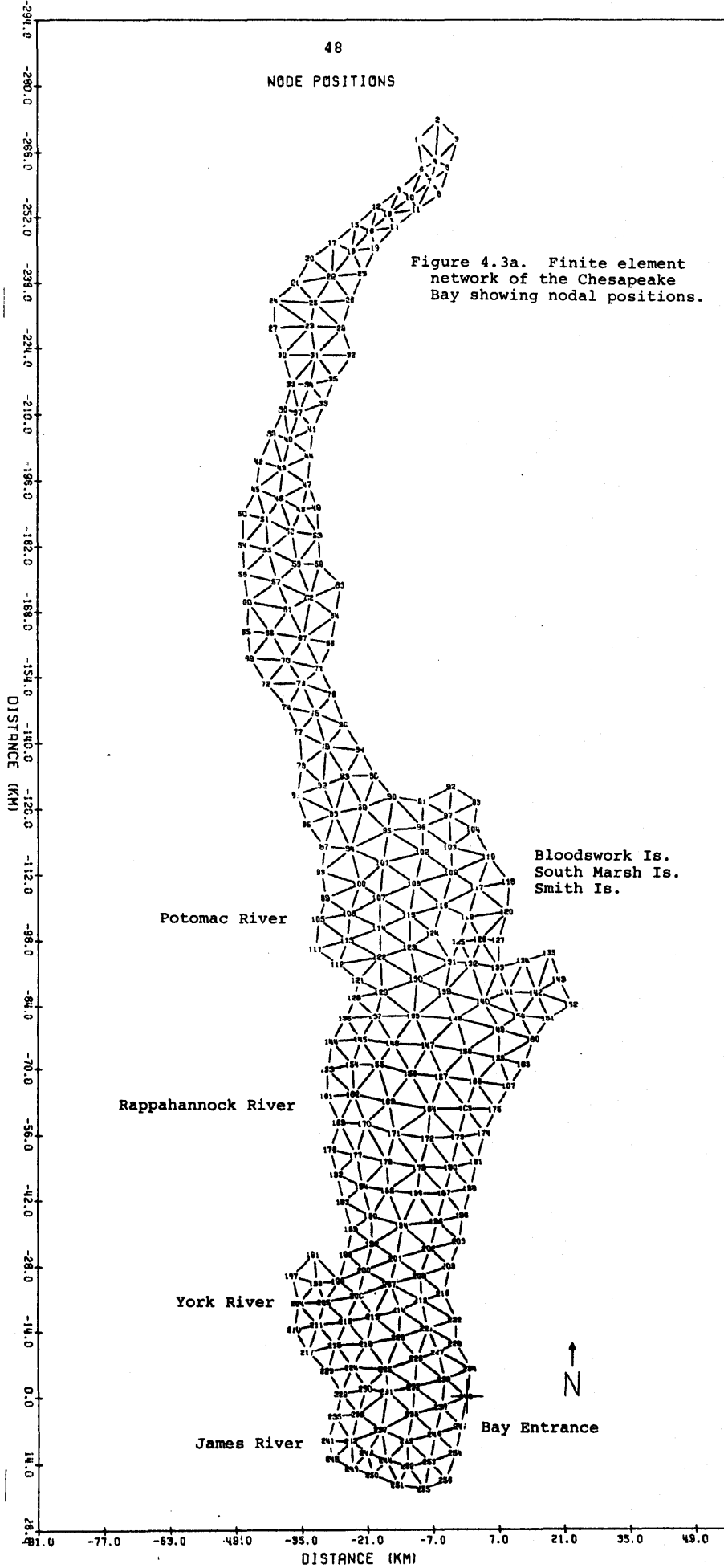


Figure 4.3a. Finite element network of the Chesapeake Bay showing nodal positions.

Potomac River

Rappahannock River

York River

James River

Bloodwork Is.  
South Marsh Is.  
Smith Is.



Bay Entrance

DISTANCE (KM)

DISTANCE (KM)



FINITE ELEMENTS

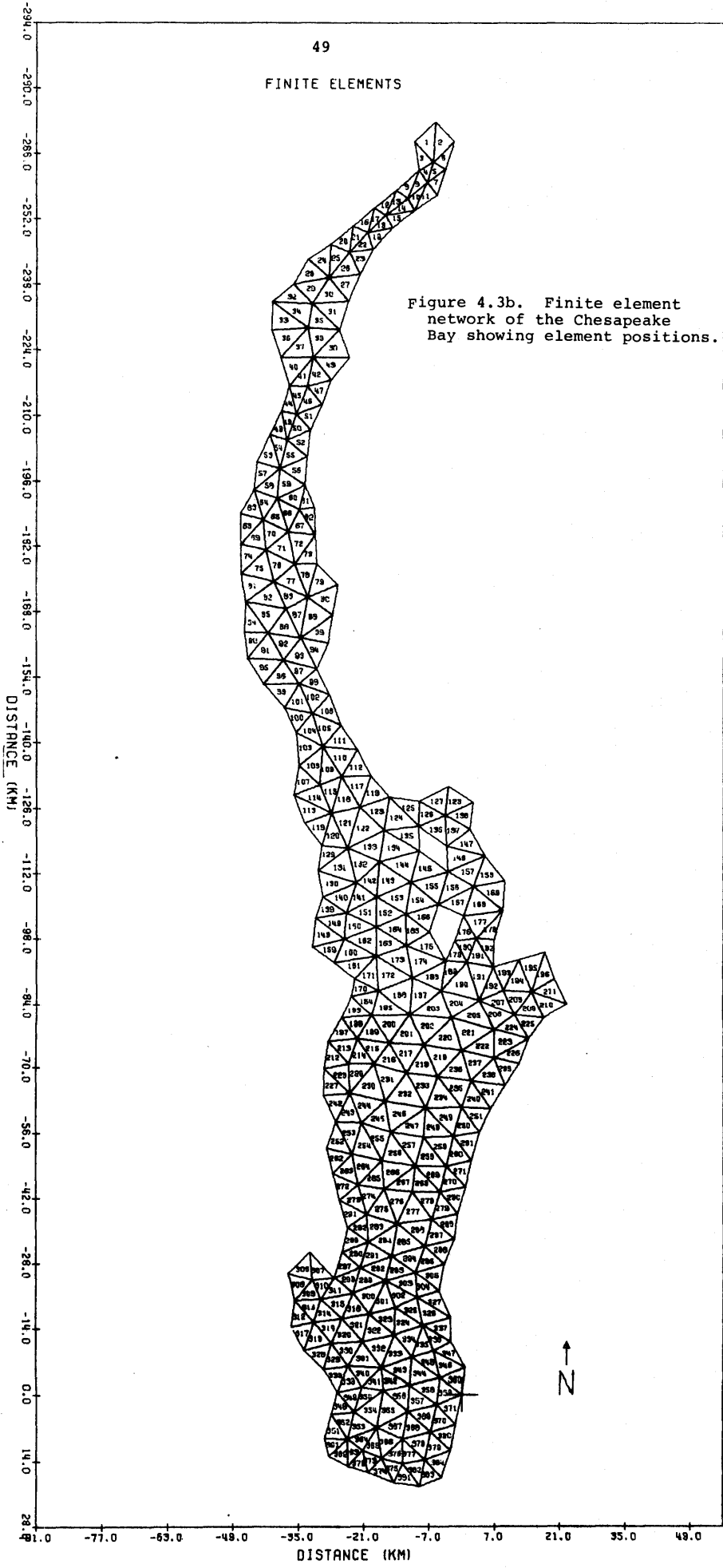


Figure 4.3b. Finite element network of the Chesapeake Bay showing element positions.

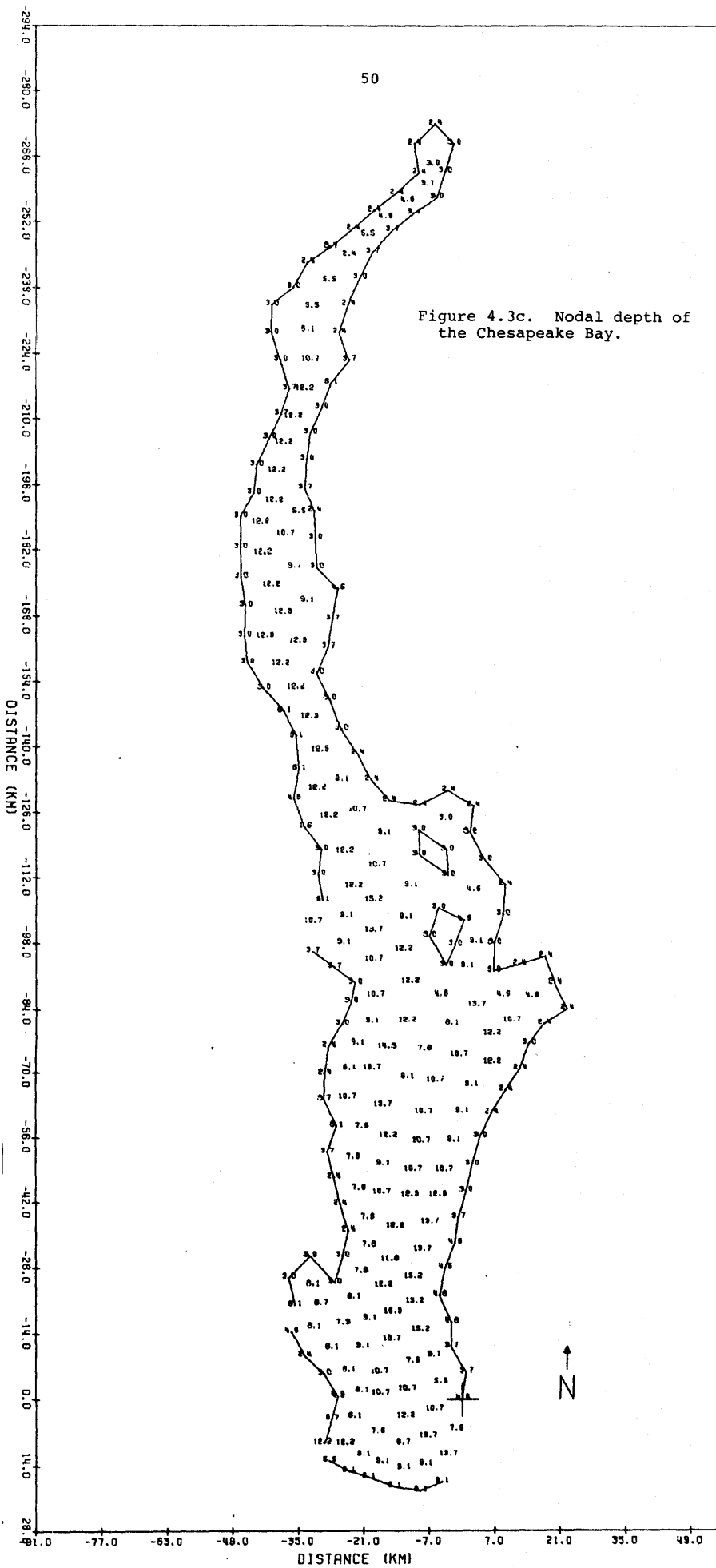


Figure 4.3c. Nodal depth of the Chesapeake Bay.

Table 4.2. Tidal Input for the Chesapeake Bay Hydrodynamic Model

Nodal Point	Free Surface Superelevation (is Referenced to NGVD (1929)) (m)	Tidal Height (m)	Phase Lag (is Referenced to Sewells Point) (sec)
1	0.2286	0.26	49380
2	0.2286	0.26	49380
36	0.1250	0.14	31230
37	0.1250	0.14	30030
77	0.1190	0.18	18870
99	0.5490	0.18	16260
105	0.5490	0.20	14460
111	0.5490	0.18	12660
168	0.0396	0.27	10800
169	0.0030	0.18	6750
176	0.0030	0.18	5850
181	0.0	0.26	5850
204	-0.0121	0.35	-300
210	-0.0121	0.33	-300
216	-0.0061	0.36	-660
222	-0.0061	0.37	-600
234	-0.0213	0.43	-2280
240	-0.0305	0.46	-3210
241	-0.0152	0.38	-1380
247	-0.0335	0.46	-3340
248	-0.0152	0.38	-1020
251	-0.0488	0.40	-3120
254	-0.0366	0.44	-3470
256	-0.0396	0.43	-3600

(see Figure 4.3a for nodal point)

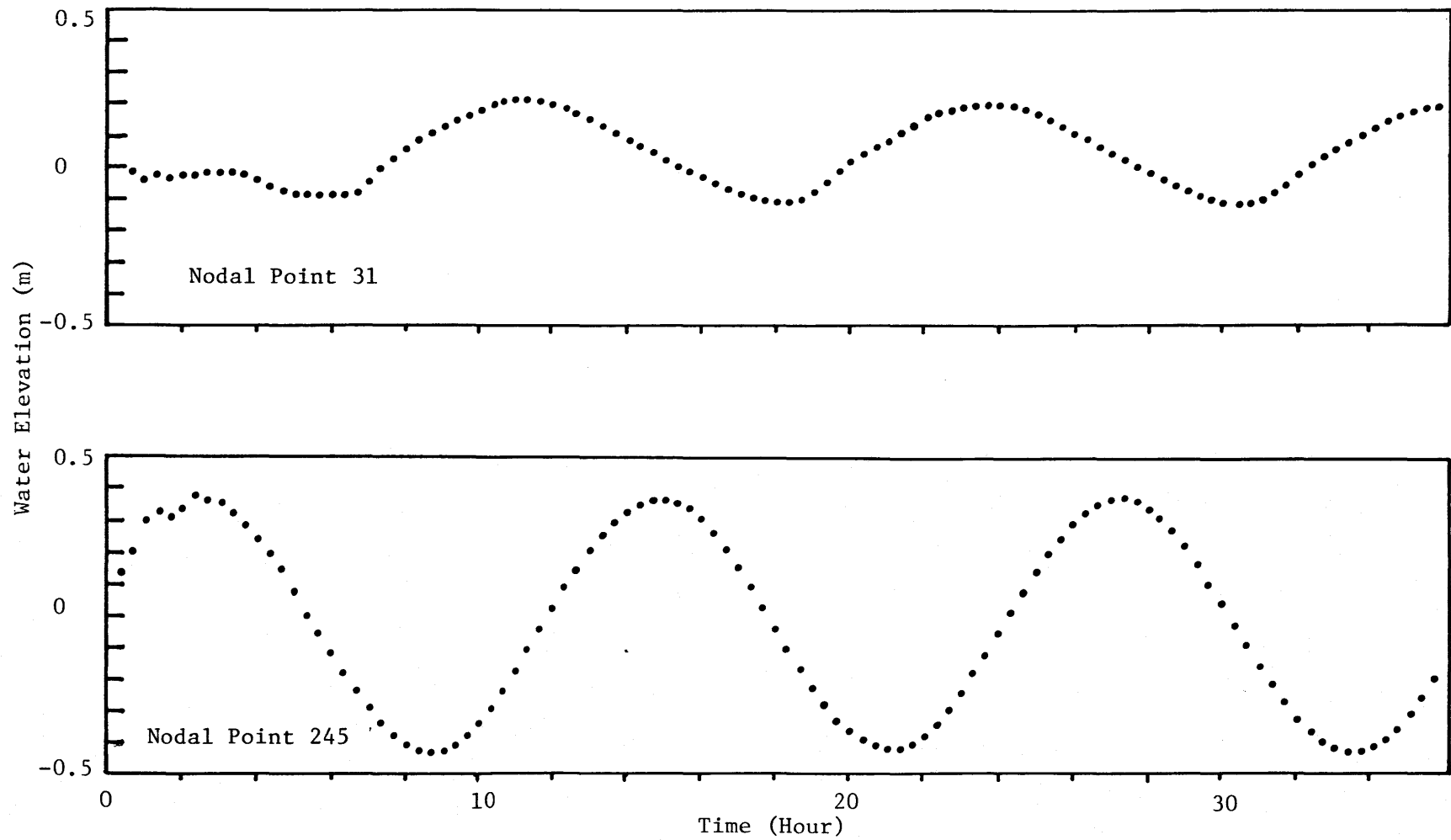


Figure 4.4a. Time history of water elevation at node. (See Figure 4.3a for nodal position).

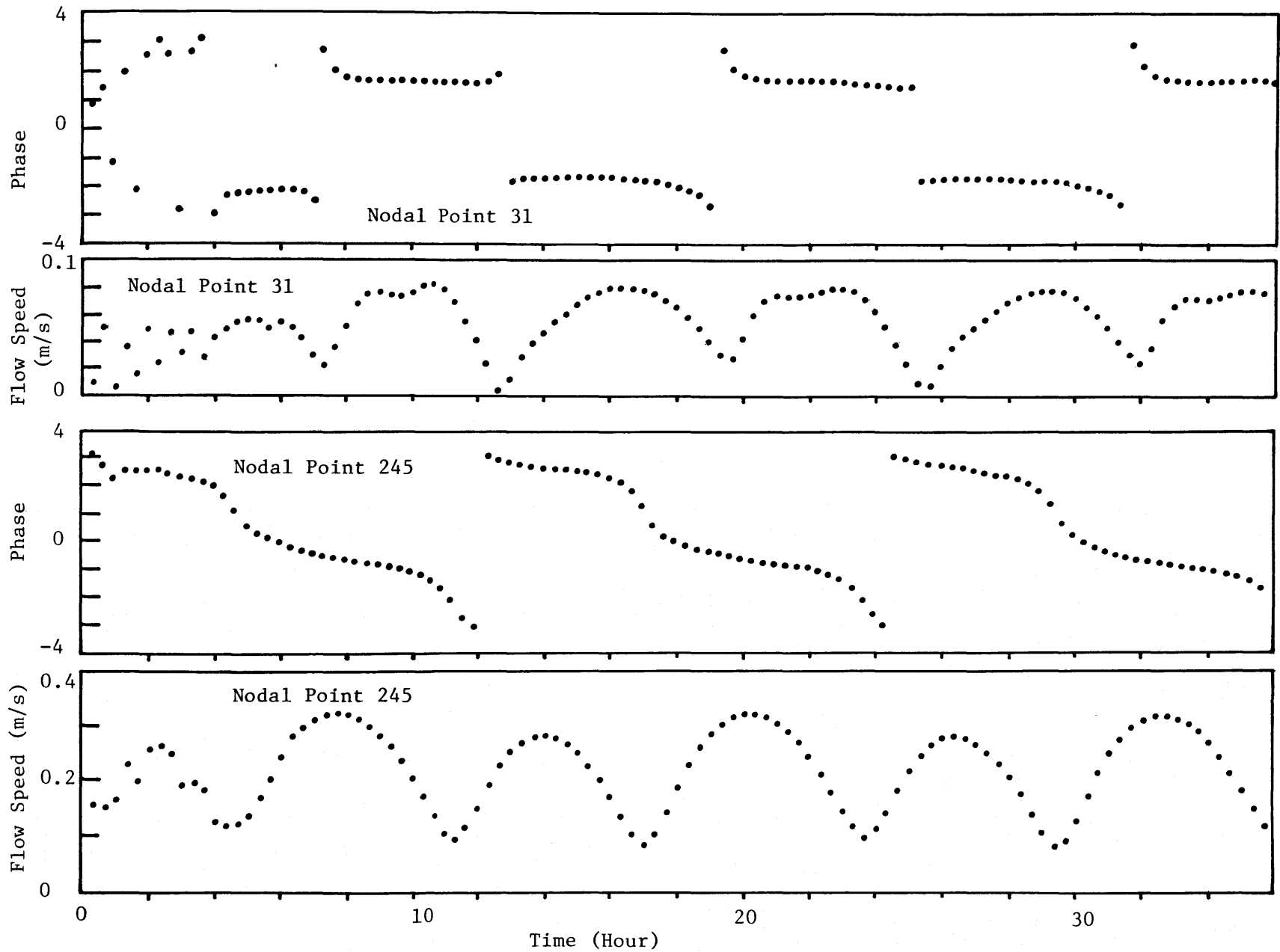


Figure 4.4b. Time history of flow velocity at node. (See Figure 4.3a for nodal position).

### 4.3 Storm Surge Calculations

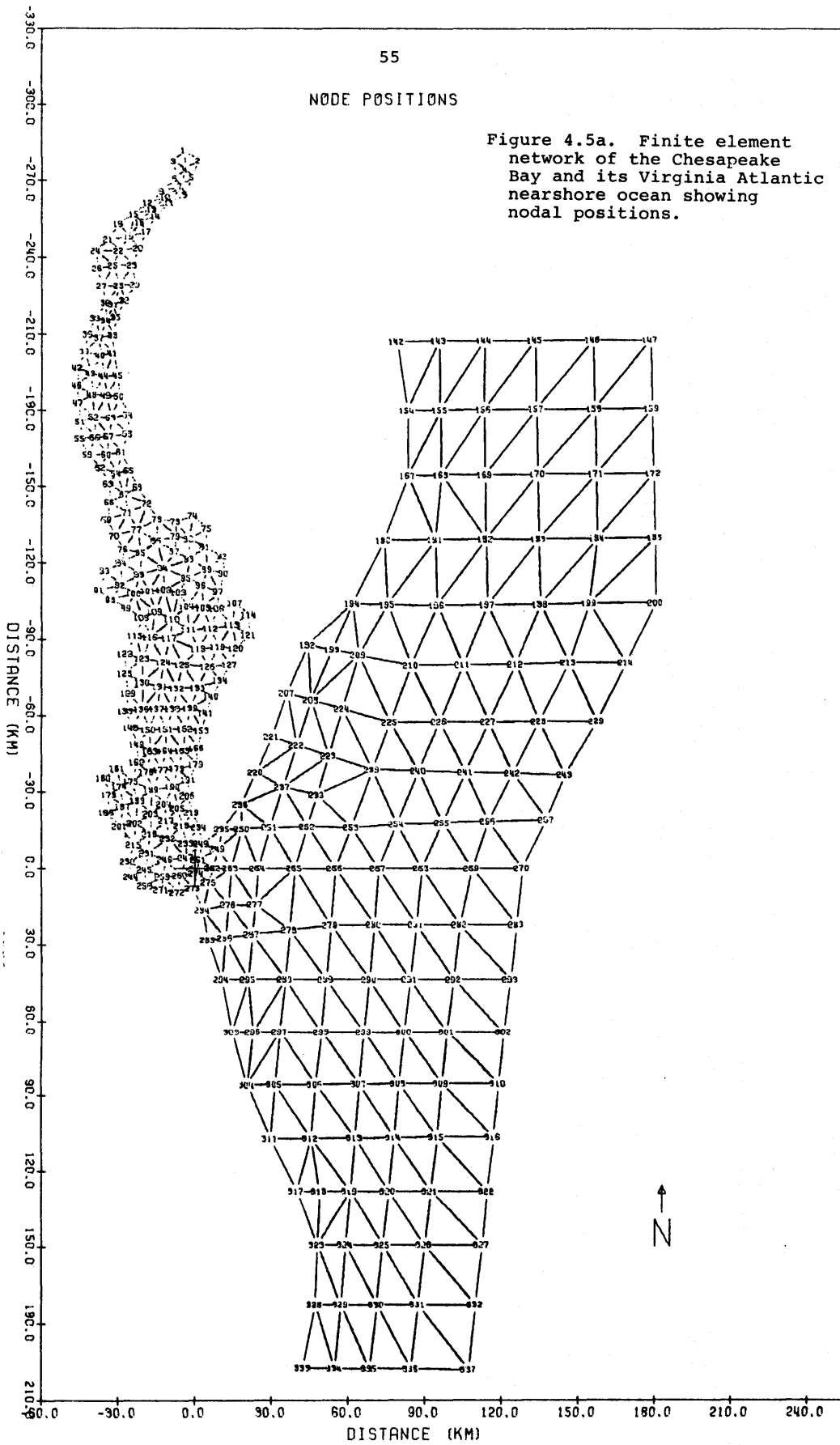
#### 4.3.1 Finite Element Network and Time Step

"The Bathymetry of the Chesapeake Bay" and "The Bathymetry of the Virginia Sea" both by VIMS were used to generate the geometric information of coastal configuration and topography. The finite element network of the Chesapeake Bay and its Virginia Atlantic near-shore ocean is shown in Figures 4.5a and b. Enlarged figures of the bay are also shown in Appendix C for clarity. The network includes the entire bay and extends offshore eastward beyond the edge of the continental shelf, as far north as Cape May, New Jersey, and as far south as Cape Hatteras, North Carolina. Note that the grid dimension increases gradually from inside the bay and bay entrance to the continental shelf and nearshore ocean away from bay mouth. The grid size in the bay and near the bay entrance, being the areas of concern, ranges from 5 to 10 km, depending on required accuracy, while that in the areas of less concern was made larger in order to reduce computational effort by having fewer nodal points and a higher overall time step. Depth variation is shown in Figure 4.5c. The water depth is locally averaged mean water depth, being the mean low water depth adjusted by tidal height and NGVD (1929).

Computational time step is limited by  $1.5 \Delta t_{cr}$  as described in Section 3.3. In the present grid system,  $\Delta t \leq 1.5 \Delta t_{cr} = 430$  seconds, which is equivalent to an element having 15 m water depth and 5 km element size. The calculated maximum surge heights by using  $\Delta t = 4$  min and 6 min indicate little difference as shown in Table 4.3. Time step  $\Delta t = 6$  min is used for all storm surge calculation.

NODE POSITIONS

Figure 4.5a. Finite element network of the Chesapeake Bay and its Virginia Atlantic nearshore ocean showing nodal positions.



56  
FINITE ELEMENTS

Figure 4.5b. Finite element network of the Chesapeake Bay and its Virginia Atlantic nearshore ocean showing element positions.

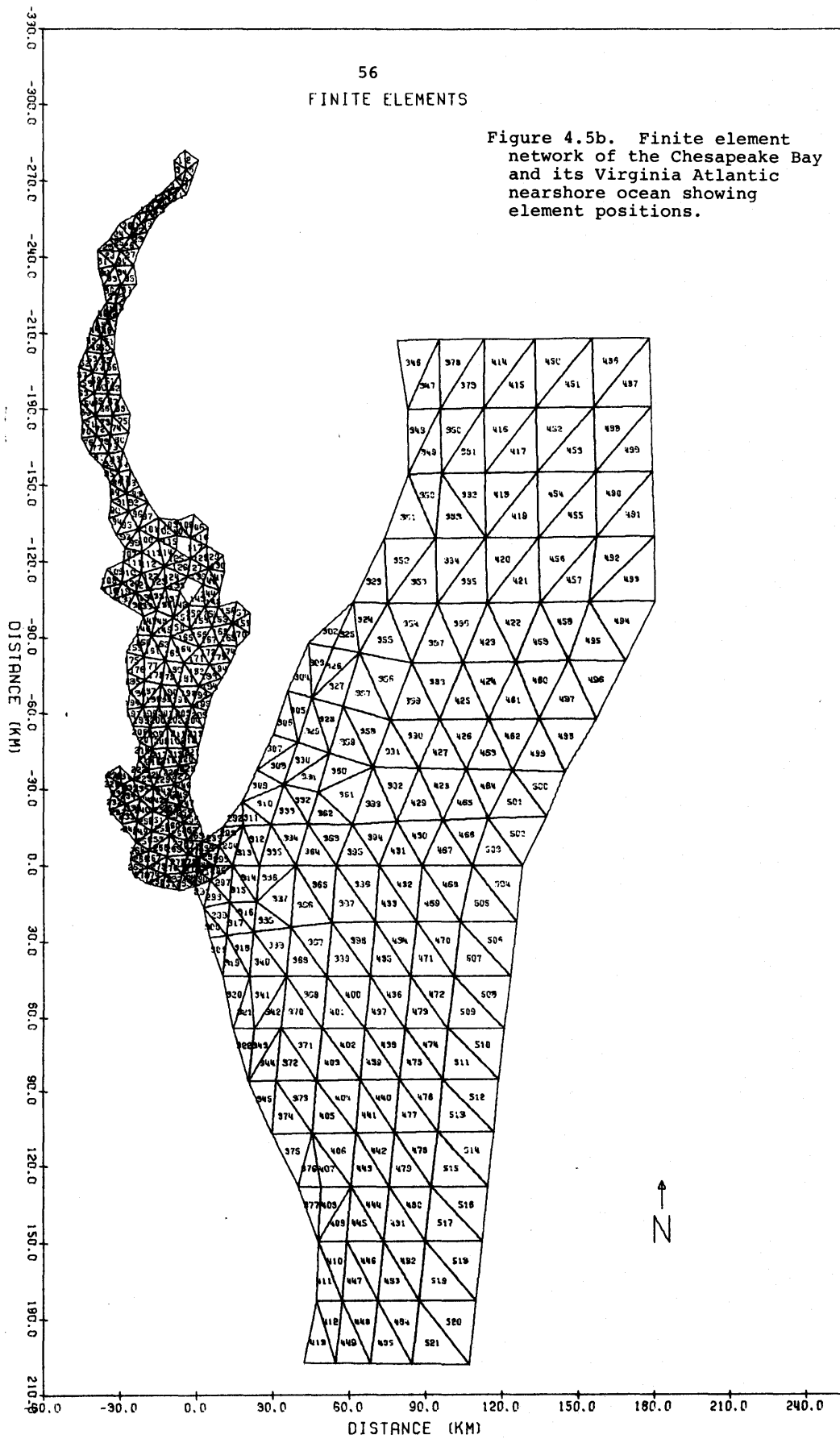




Figure 4.5c. Nodal depth of the Chesapeake Bay and its Virginia Atlantic nearshore ocean.

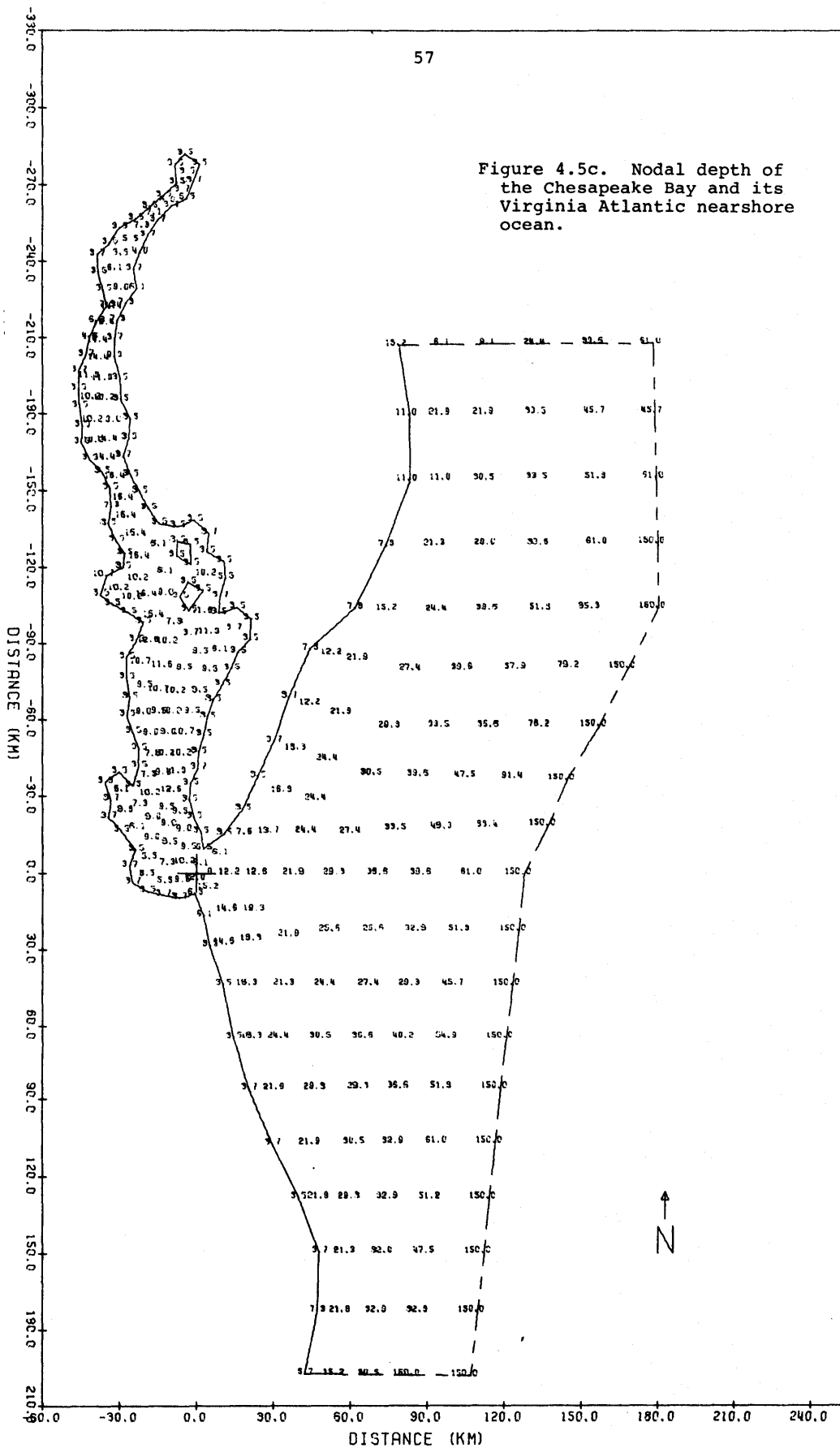


Table 4.3. Calculated Maximum Surge Height vs. Time Step

Time Step \ Localities		1	40	62	232	262	265
		4 (min)	Height (m)	3.102	1.461	1.249	1.377
Phase Lag (min)	2000		1748	1684	972	980	936
6 (min)	Height (m)	3.098	1.460	1.224	1.376	1.136	1.492
	Phase Lag (min)	2010	1752	1692	978	990	942

Note that Localities refer to the element number in figure 4.9, Phase Lags refer to the starting time of the hurricane in model calculation

#### 4.3.2 Storm Surge Hindcasting of Hurricane Connie 1955

A storm surge is driven primarily by the pressure anomaly and wind drag of the hurricane. The pressure and wind fields were calculated from equations (2.21) and (2.24), and the wind drag from equation (2.6). Therefore, the storm surge calculation requires not only the information of hurricane parameters but also the correct wind stress coefficients and wind reduction factor. These coefficients and factors are determined by a storm surge hindcasting of hurricane Connie 1955.

Hurricane Connie 1955 was chosen for calibration. According to Chapman and Sloan (1955), Connie was first detected at 0630 GMT August 4 about 1920 km east of San Juan, P. R.. It crossed the North Carolina coast near Cherry Point at 1500 GMT August 12. On crossing the coastline, Connie weakened, but remained an intensive storm as it continued generally northward to near the latitude of Washington, D. C.. It then turned northwestward. It also released as much as 12.7 to 15.2 cm of rainfall along the eastern coast of U. S. (Namias and Dunn 1955). Figure 4.6a shows the track of hurricane Connie 1955, and Figure 4.6b shows a typical atmospheric pressure field of the hurricane near the Chesapeake Bay.

Precise simulation of an actual hurricane is very crucial to storm surge calculation in a large bay, where many tide gauge stations are involved simultaneously in calibration. Particularly, the determination of the hurricane track is of great significance, since the right hand side of the hurricane generates stronger wind, therefore higher surge, than that at the left hand side. However, since field data is scarce, the construction of a hurricane on a spatial scale of 5 km and

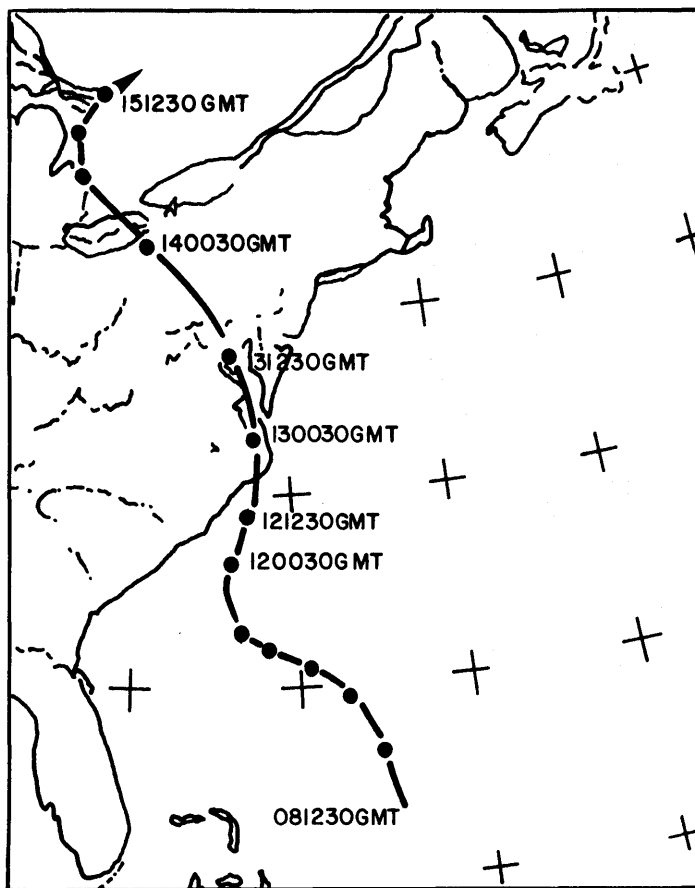


Figure 4.6a. Track of Hurricane Connie 1955.  
(recorded from Chapman and Sloan 1955)

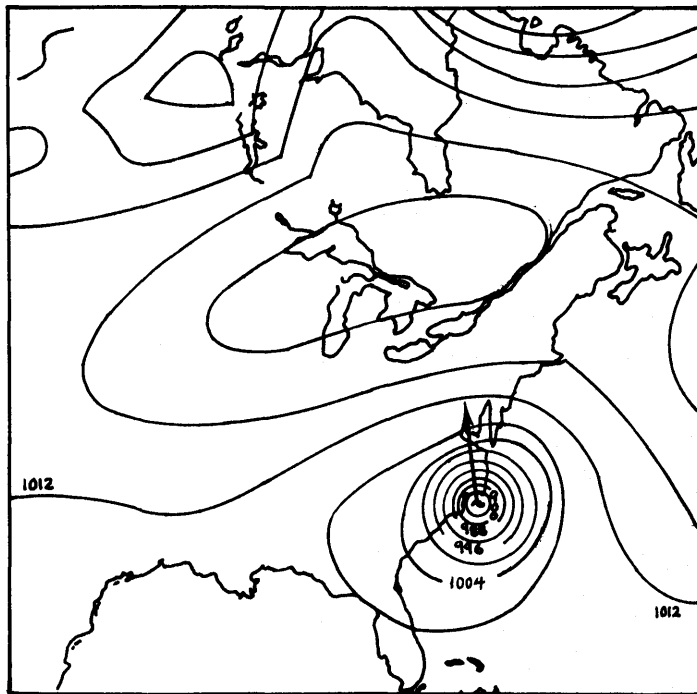


Figure 4.6b. Pressure field of Hurricane Connie 1955. (recorded from Chapman and Sloan 1955)

time scale less than one hour is very difficult. Parameters and the model set-up for hurricane Connie 1955 were estimated as shown in Figure 4.7 and Table 4.4. Note that a two-straight-line track was selected to approximate the actual track. The forward speeds are the averaged speeds estimated from Figure 4.6a. The values of central pressure depression and maximum wind radius as shown in Table 4.4 were obtained from the report by Ho, Richard and Goodyear (1975).

In the model computation, the hurricane center advances a distance calculated from hurricane forward speed along the chosen track at each new time increment. The forcing functions of pressure depression and wind drag are calculated at each nodal point at each time step by equations (2.21), (2.24) and (2.6). Then the response of the water body to these forcings is calculated at each nodal point at each time step. Typical pressure and wind field calculated from the hurricane model are illustrated in Figure 4.8.

#### 4.3.3 Storm Surge Calibrated Results and Discussion

The storm surge results due to the simulated hurricane Connie 1955 were calculated. Surge data obtained for six tide gauge stations: Baltimore, Annapolis, Solomons Island, Gloucester Point, Kiptopeke Beach, and Hampton Roads, as shown in Figure 4.9 were used for calibration. These six stations are those having the longest period of tide record in the Chesapeake Bay. The field surge data, being calculated from the observed tides minus the predicted astronomical tide, was supplied by Dr. Boon of VIMS (personal communication). The comparison of the calculated results and the deduced field data is shown in Figure 4.10. The maximum surge heights and the general pattern of surge variations generally

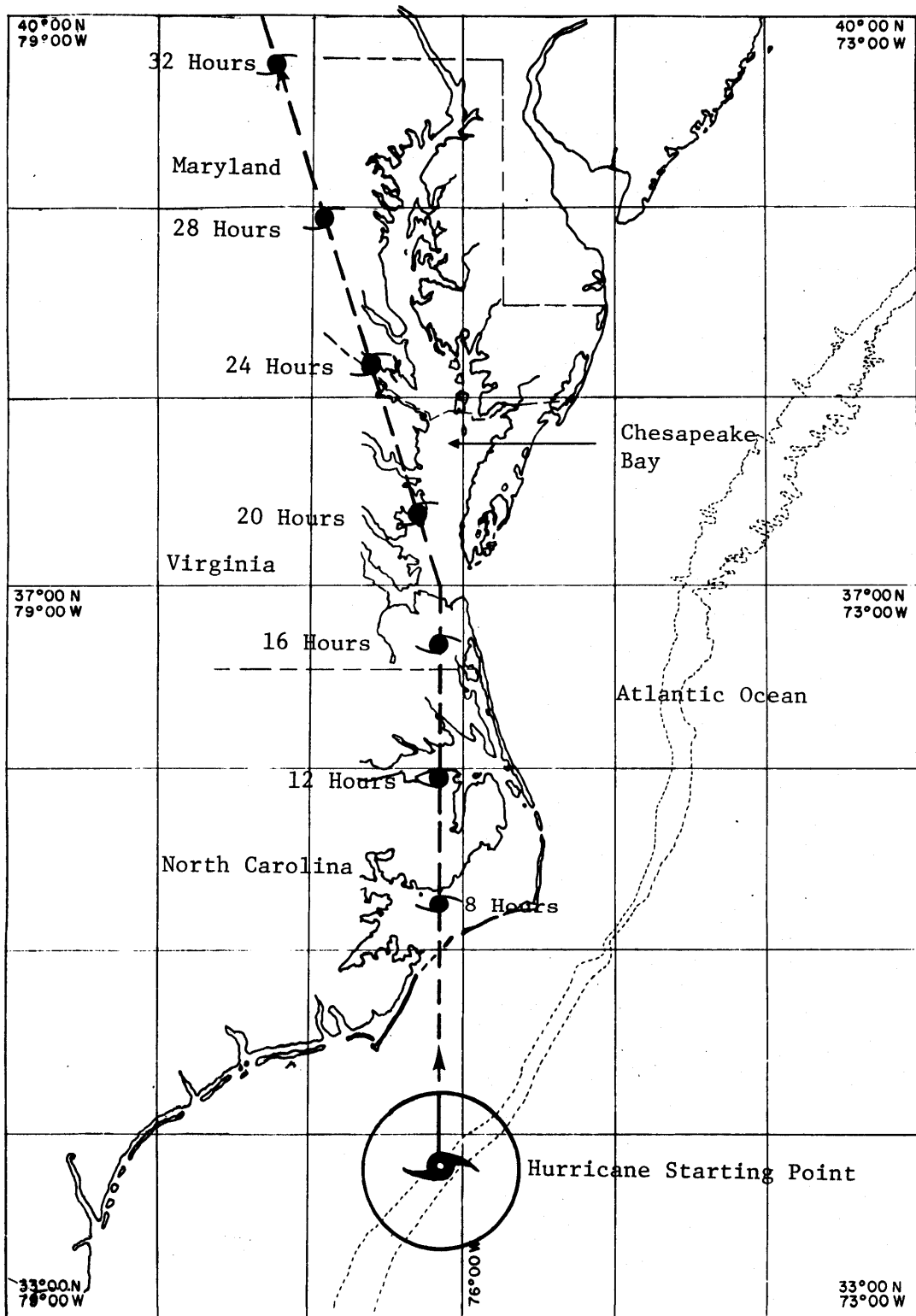


Figure 4.7. The model track of Hurricane Connie, 1955

Table 4.4. Parameter Values of Calibration Run and Calibrated Coefficients

Hurricane Starting Point: (referred to original point at  $73^{\circ}\text{E}$ ,  $37^{\circ}\text{N}$ , see figure 4.7).

$$(x_o, y_o) = (-12000, -352296) \text{ m}$$

Hurricane Forward Velocity:  $V_f = 5.4 \text{ m/s}$  When hurricane center is below  $37^{\circ}\text{N}$ , direction  $V_{\text{ang}} = 0^{\circ}$  (referred to North)

$V_f = 6.4 \text{ m/s}$  When hurricane center is above  $37^{\circ}\text{N}$ , direction  $V_{\text{ang}} = 17^{\circ}$  (referred to North)

Hurricane Central Pressure Depression:  $\Delta p = 5190 \text{ kg/m/s}^2$   
( $1\text{mb} = 100 \text{ kg/m/s}^2$ )

Hurricane Maximum Winds Radius:  $R_m = 83300 \text{ m}$

Bottom Friction Coefficient:  $C_f = 0.0048$  in bay and near bay entrance varying to 0.0 near continental shelf

"Eddy Viscosity" Coefficients:  $\epsilon_{xx}, \epsilon_{xy}, \epsilon_{yy} = 1500 \text{ (m}^2/\text{s)}$  in bay and near bay entrance varying to 4000 near continental shelf

Wind Stress Coefficients:  $C_o = 0.0011, C_1 = 0.0022$

Wind Reduction Factor:  $C_r = 0.7$

Time Step:  $\Delta t = 6 \text{ minutes}$



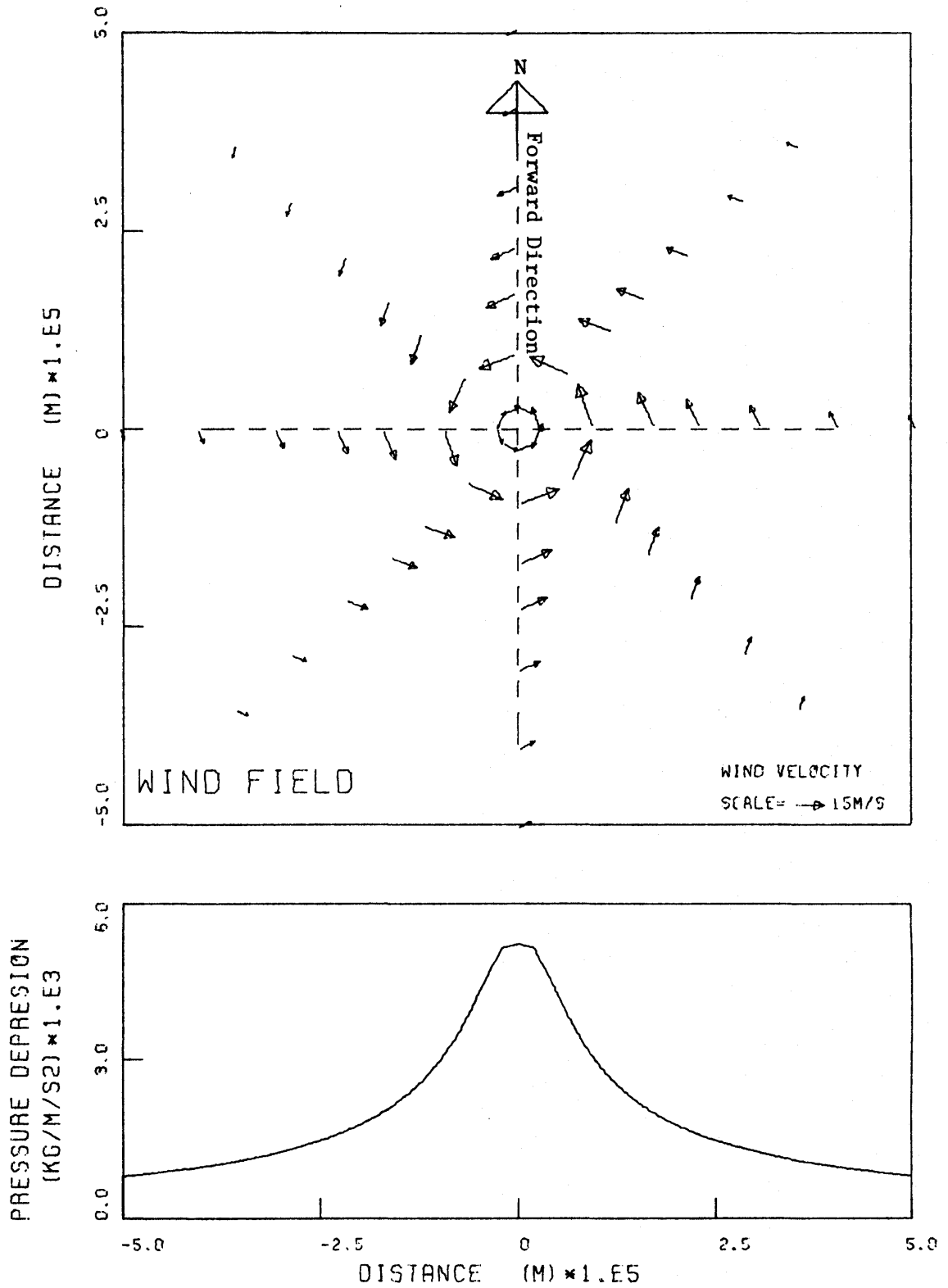


Figure 4.8. Typical pressure and wind field of the simulated hurricane Connie 1955.

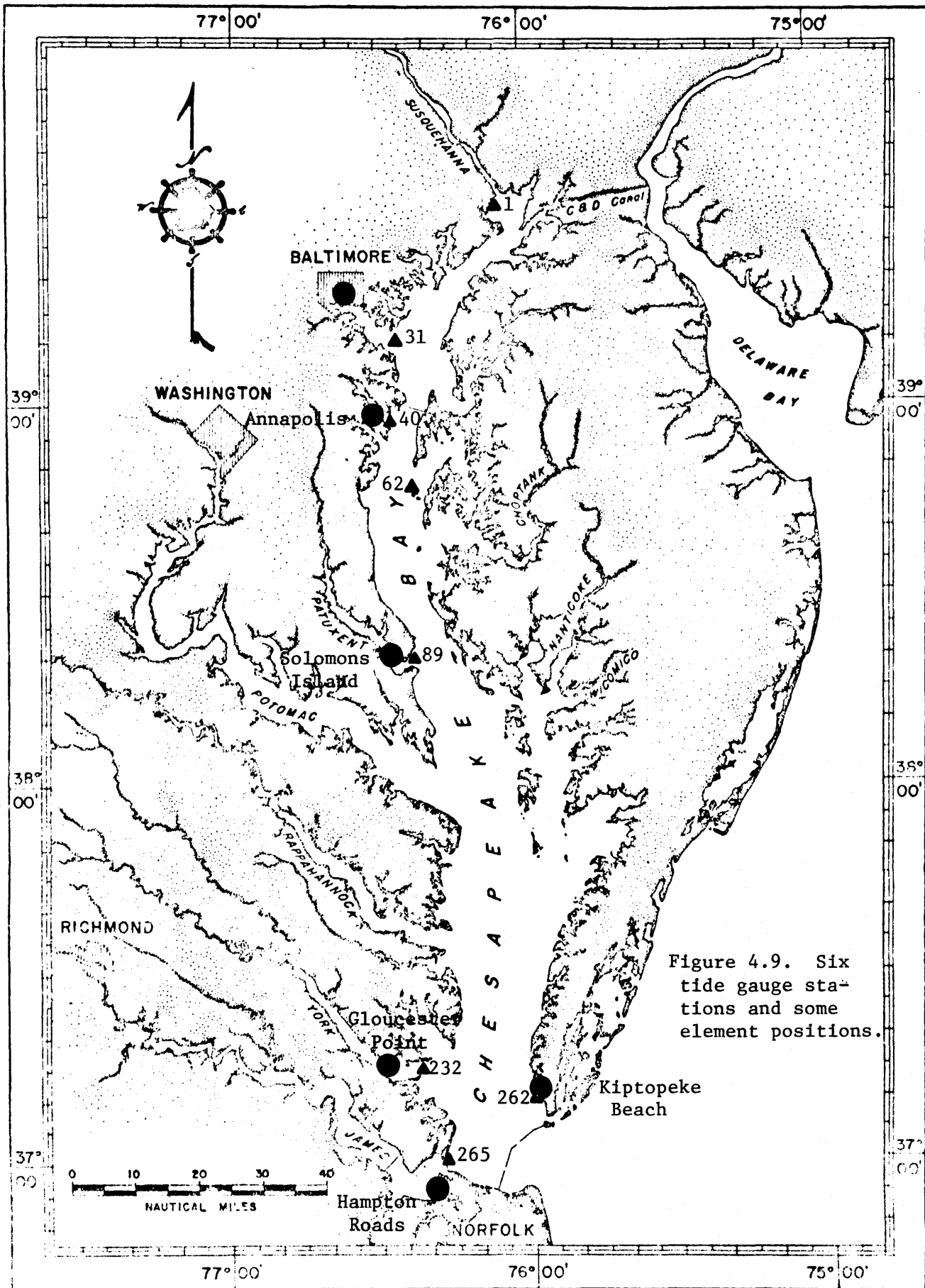


Figure 4.9. Six tide gauge stations and some element positions.

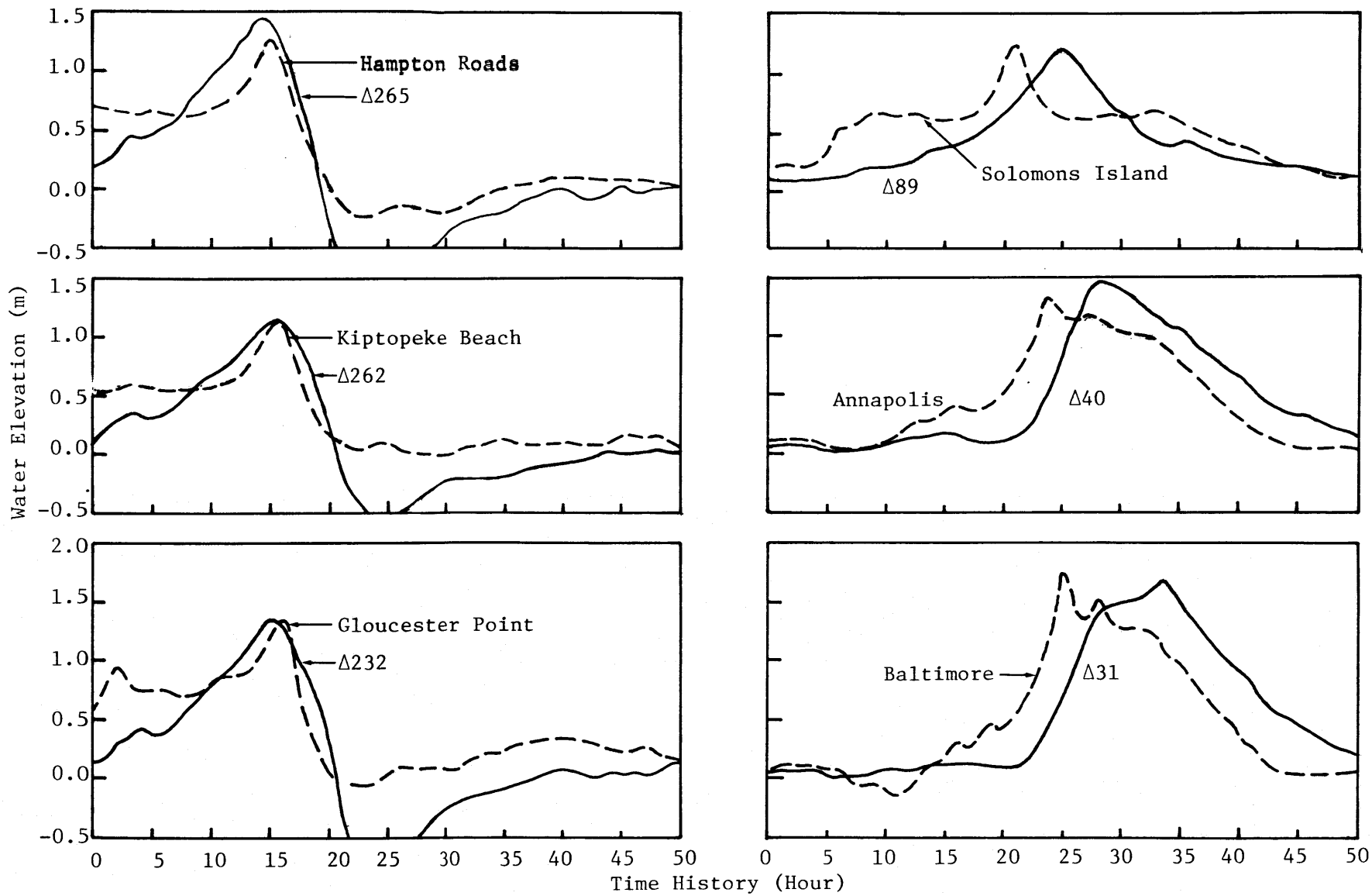


Figure 4.10. Comparison of the calculated surge and the surge deduced from observed tide. (See Figure 4.9 for the position of station and element).

agree very well. Several slight disagreements of the lowest surge heights and phase lags are due partly to the absolute error in comparison of two distinctive locations\*, and partly to the approximation made in formulating the model hurricane. In addition, rainfall and short waves may also contribute to this disagreement. Note that error may also be inherited from the method of calculating the observed surges, i.e. subtracting out the predicted astronomical tides from the observed total tides. Examples of the calibrated water elevation and flow circulation are shown in Appendix C. Note that calculated results show strong current occurring at the bay entrance, see flow circulation figures in Appendix C. The calibration for the time being is generally satisfactory. The calibrated coefficients are shown in Table 4.4.

#### 4.3.4 The Response of Maximum Surge Height and Hurricane Parameters

Analysis of the sensitivity of the maximum surge height to systematic variations in hurricane parameters should be able to indicate the general response of the Chesapeake Bay. Several calculated results are typically illustrated in Table 4.5a, b and c.

#### Hurricane Track

The hurricane wind field is counterclockwise and is strongest in the rear right hand quarter of the hurricane. Obviously the response of maximum surge height at a station in the bay depends very much on the hurricane track. Three types of tracks are of great interest in the Chesapeake Bay. They are the track passing to the left of the bay center, the track passing to the right of the bay center, and the track passing to the south of the bay from east to west. They are denoted as

---

\* Particularly, some field data reported by Corps of Engineers (1968) indicate that the maximum surge difference between Old Point Comfort ( $\Delta 265$ ) and Sewells Point (Hampton Roads) may range from 0 m to 0.34 m, depending on the characteristics of hurricane.

HT1, HT2 (or HT2'), and HT3 respectively are shown in Figure 4.11. Tables 4.5a, b and c and Figure 4.12 indicate that for the HT1 type, the area of maximum winds of the hurricane passes directly over the entire bay and the surge is very significant in the entire bay. For the HT2 type, the surge in the lower bay is generally greater than that in the upper bay, and this surge difference is very significant when hurricane passes the bay center with a distance of maximum wind radius from the hurricane center. The observed field surges also support this behavior as indicated in Table 4.6, which shows the results of Connie 1955, Flossy 1956 and Donna 1960. Their tracks are shown in Figure 4.13. Such surge response to the HT2 type hurricane is because the surge, built up in the lower bay before the hurricane center arrives in the bay area, encounters the opposite winds as it propagates to the upper bay. Finally, for the HT3 type the surge in the lower bay is much greater than that in the upper bay. In addition, the surge in the western shore of the bay is generally greater than that in the eastern shore due to the effect of east wind generated by the hurricane.

#### Central Pressure Depression

The response of maximum surge height in the bay to increasing hurricane intensity is nearly linear with central pressure depression as shown for typical points in Figure 4.14 (see also Table 4.5a, b and c). This nearly linear relation was also found by Overland (1975) in studying storm surge in Apalachicola Bay, Florida by using a different model.

#### Forward Speed

The response of maximum surge height in the Bay to hurricane forward speed  $V_f$  proportionally increases up to 30 m/sec (Pagenkopf and Pearce 1975) which is shown in Figure 4.15 (see also Table

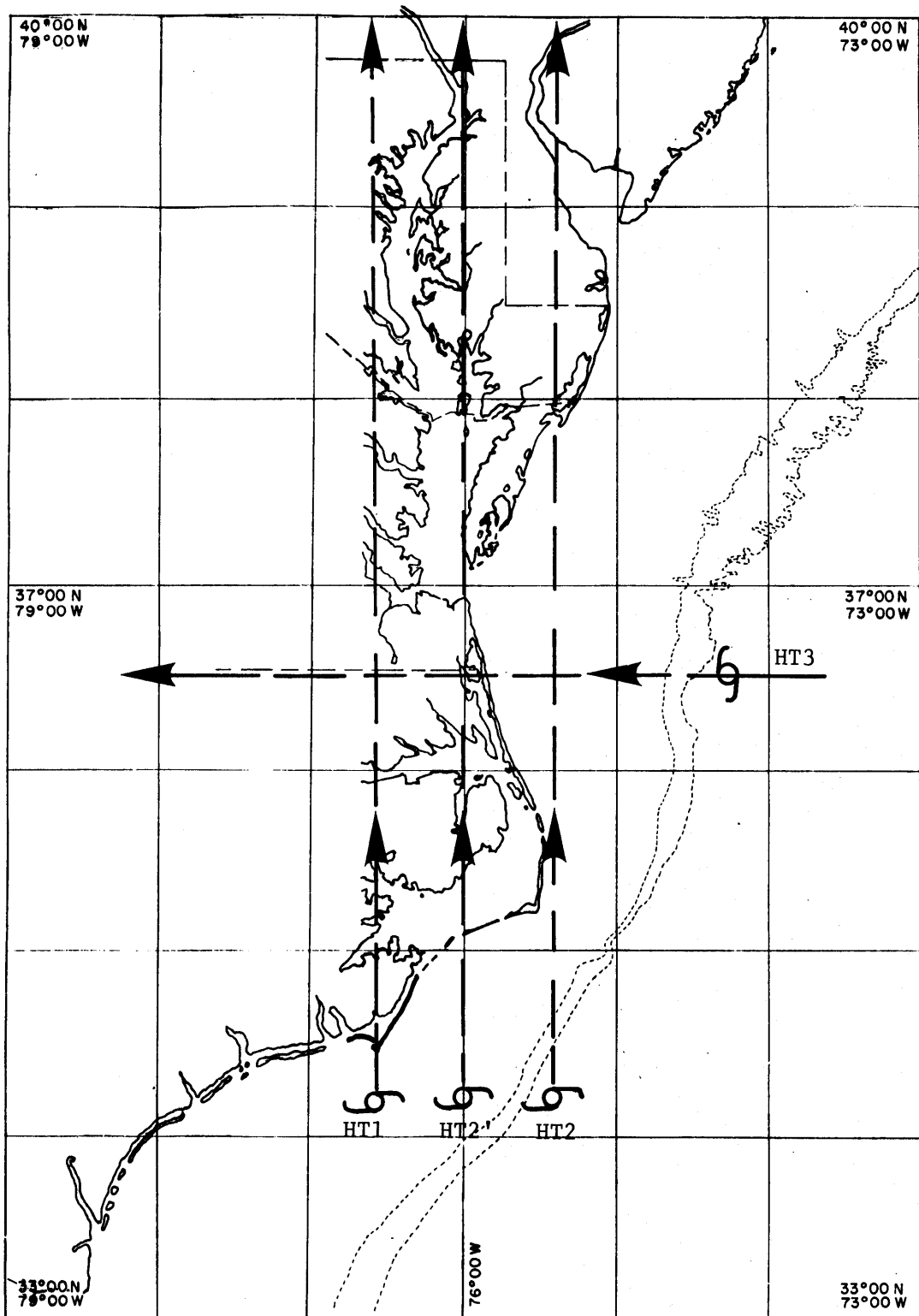


Figure 4.11. Three types of hurricane track.

Table 4.5a. Maximum Surge Height vs. Various Combinations of Hurricane Parameters for Hurricane HT1

Hurricane Starting Point		Central Pressure Depression	Maximum Winds Radius	Forward Speed	Station							
$x_o$ (km)	$y_o$ (km)	$\Delta p$ (mb)	$R_m$ (km)	$V_f$ (m/s)	1	31	40	62	89	232	262	265
-51.85	-443.79	53.60	75.00	30.	1.50	0.90	0.75	0.79	0.98	1.31	1.71	1.91
-51.85	-443.79	53.60	75.00	22.	1.63	0.97	0.84	0.91	1.03	1.44	1.63	1.31
-51.85	-443.79	53.60	75.00	16.	1.99	1.05	1.00	1.09	1.14	1.49	1.41	1.39
-51.85	-443.79	53.60	75.00	10.	2.84	1.24	1.43	1.40	1.43	1.52	1.17	1.42
-51.85	-332.84	53.60	75.00	5.	3.58	1.87	1.85	1.76	1.70	0.83	1.20	1.08
-51.85	-332.84	38.30	75.00	5.	2.63	1.37	1.34	1.27	1.23	0.60	0.82	0.74
-51.85	-332.84	23.60	75.00	5.	1.64	0.86	0.83	0.79	0.76	0.58	0.40	0.51
-51.85	-332.84	8.30	75.00	5.	0.51	0.31	0.29	0.27	0.26	0.16	0.12	0.13
-51.85	-332.84	53.60	47.50	5.	3.73	2.13	2.03	1.88	1.89	1.43	0.87	1.21
-51.85	-332.84	38.60	47.50	5.	2.81	1.61	1.51	1.39	1.40	1.00	0.10	0.82
-51.85	-332.84	23.60	47.50	5.	1.79	1.04	0.96	0.87	0.88	0.57	0.35	0.45
-51.85	-332.84	8.30	47.50	5.	0.61	0.38	0.34	0.31	0.31	0.17	0.10	0.12
-51.85	-332.84	53.60	20.00	5.	3.05	2.06	1.87	1.51	1.57	1.06	0.48	0.72
-51.85	-332.84	38.60	20.00	5.	2.31	1.56	1.40	1.12	1.16	0.74	0.33	0.49
-51.85	-332.84	23.60	20.00	5.	1.50	1.01	0.89	0.71	0.73	0.43	0.19	0.27
-51.85	-332.84	8.60	20.00	5.	0.56	0.39	0.34	0.27	0.26	0.13	0.06	0.08

(see Figure 4.9 for station position and Figure 4.11 for hurricane type)

Table 4.5b. Maximum Surge Height vs. Various Combination of Hurricane Parameters for Hurricane HT2 (or HT2').

Hurricane Starting Point		Central Pressure Depression	Maximum Winds Radius	Forward Speed	Station							
$x_o$ (km)	$y_o$ (km)	$\Delta p$ (mb)	$R_m$ (km)	$V_f$ (m/s)	1	31	40	62	89	232	262	265
0	-443.79	53.60	75.00	30.	0.57	0.28	0.24	0.14	0.49	0.50	1.46	0.73
0	-443.79	53.60	75.00	22.	0.48	0.27	0.19	0.14	0.56	0.76	1.18	1.40
0	-443.79	53.60	75.00	16.	0.56	0.22	0.13	0.22	0.59	1.01	1.01	1.20
0	-443.79	53.60	75.00	10.	0.96	0.23	0.14	0.27	0.38	1.23	1.28	1.42
0	-443.79	53.60	20.00	30.	0.30	0.15	0.14	0.08	0.30	0.45	1.01	0.65
0	-443.79	53.60	20.00	22.	0.26	0.16	0.11	0.09	0.35	0.56	1.31	0.66
0	-443.79	53.60	20.00	16.	0.20	0.06	0.03	0.13	0.41	0.61	1.45	0.71
0	-443.79	53.60	20.00	10.	0.25	0.02	0.03	0.14	0.36	0.60	1.30	0.95

Table 4.5c. Maximum Surge Height vs. Various Combination of Hurricane Parameters for Hurricane HT3.

(Headings for this table are the same as for the above table)

444.00	-50.00	53.60	75.00	30.	0.77	0.64	0.62	0.58	0.79	2.43	2.29	2.47
444.00	-50.00	53.60	75.00	16.	0.60	0.51	0.49	0.46	0.62	2.59	2.13	2.54
444.00	-50.00	53.60	75.00	5.	0.17	0.42	0.55	0.55	0.74	1.67	1.32	1.87
444.00	-50.00	23.60	75.00	30.	0.49	0.37	0.36	0.31	0.38	1.58	1.45	1.59
444.00	-50.00	23.60	75.00	16.	0.39	0.26	0.26	0.25	0.34	1.43	1.11	1.40
444.00	-50.00	23.60	75.00	5.	0.37	0.38	0.39	0.36	0.37	0.70	0.57	0.79
444.00	-50.00	53.60	20.00	30.	0.45	0.33	0.32	0.28	0.35	1.53	1.70	1.87
444.00	-50.00	53.60	20.00	16.	0.37	0.23	0.24	0.22	0.33	1.63	1.41	1.89
444.00	-50.00	53.60	20.00	5.	0.43	0.39	0.38	0.34	0.37	0.96	0.81	1.25
444.00	-50.00	23.60	20.00	30.	0.32	0.19	0.19	0.18	0.25	0.93	0.76	1.06
444.00	-50.00	23.60	20.00	5.	0.28	0.23	0.21	0.19	0.20	0.39	0.33	0.50

(See Figure 4.9 for station position and Figure 4.11 for hurricane type)



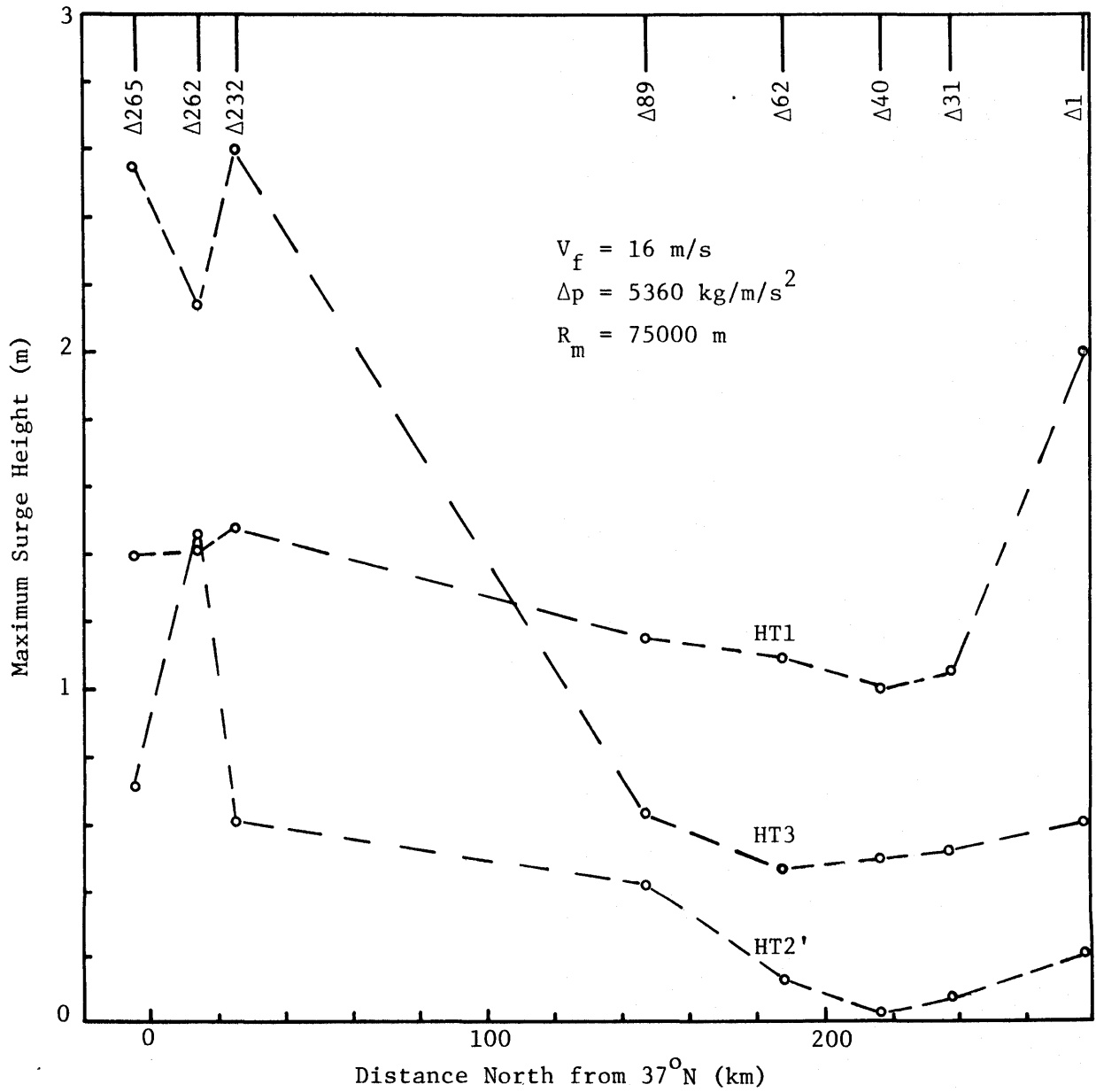


Figure 4.12. Maximum surge height in the bay vs. hurricane track.  
 (see Figure 4.9 for element position)

Table 4.6. Observed Tide and Deduced Storm Surge (in meters)

Hurricane	Name of Tide	Tidal Stations					
		Baltimore	Annapolis	Solomon Island	Gloucester Point	Kiptopeke Beach	Hampton Roads
Connie 1955	Observed Tide	1.82	1.31	1.21	1.04	0.83	1.02
	Predicted Astronomical Tide	0.06	0.04	-0.02	-0.31	-0.26	-0.23
	Deduced Surge	1.76	1.27	1.23	1.35	1.09	1.25
Flossy 1956	Observed Tide	0.54	0.42	0.63	1.37	0.80	1.39
	Predicted Astronomical Tide	0.11	-0.05	-0.12	0.22	-0.14	0.12
	Deduced Surge	0.43	0.47	0.75	1.15	0.94	1.27
Donna 1960	Observed Tide	0.42	0.30	0.45	1.28	1.17	1.48
	Predicted Astronomical Tide	0.17	0.08	0.10	-0.09	-0.20	-0.05
	Deduced Surge	0.25	0.22	0.35	1.37	1.37	1.53

Note that Deduced Surge = Observed Tide - Predicted Astronomical Tide

See Figure 4.9 for station location

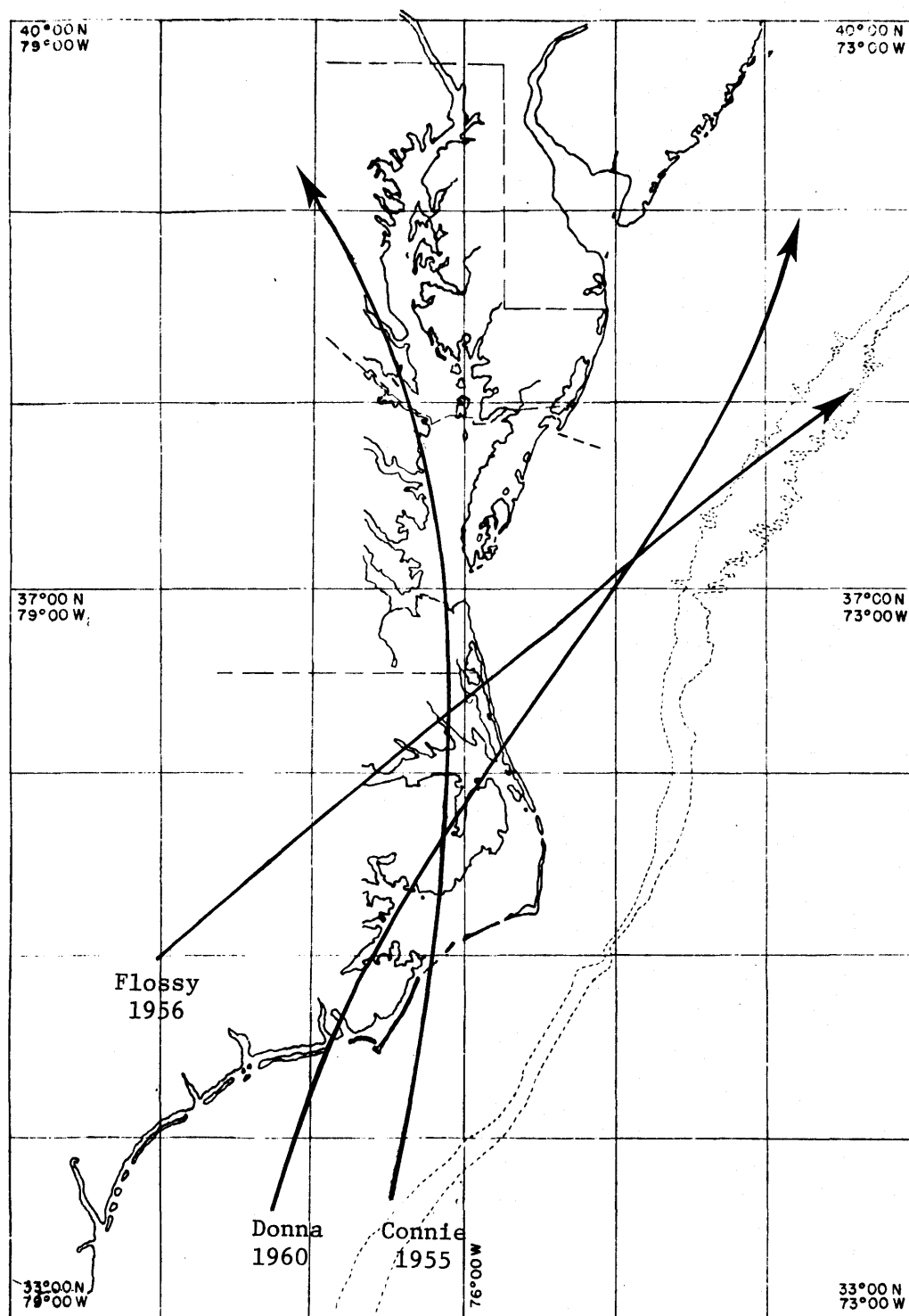


Figure 4.13. Tracks of Hurricanes Connie 1955, Flossy 1956 and Donna 1960. (Chapman and Sloan 1955, Dunn, Davis and Moor 1956, and Dunn 1961).

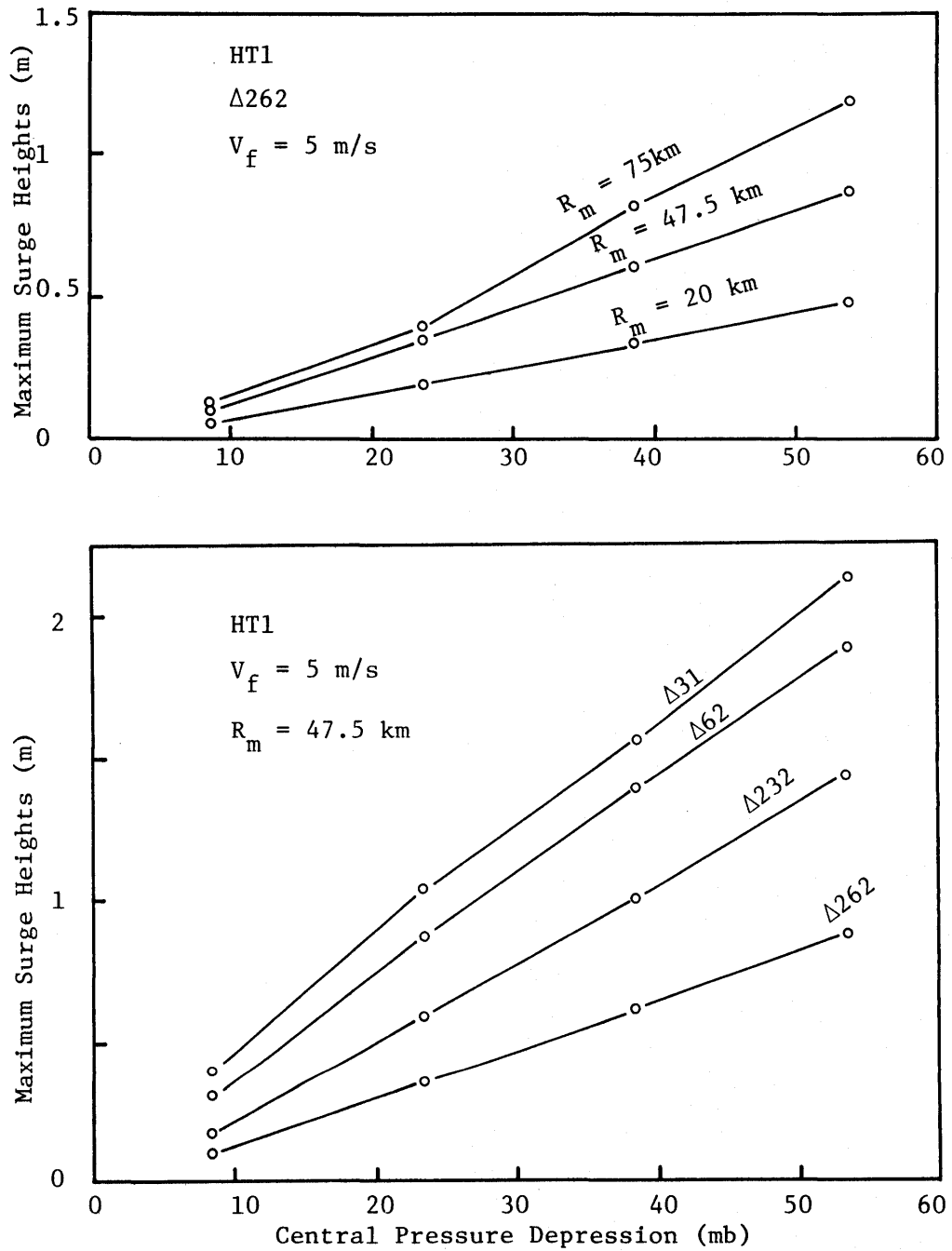


Figure 4.14. Maximum surge height vs. central pressure depression. (See Figure 4.9 for element position).

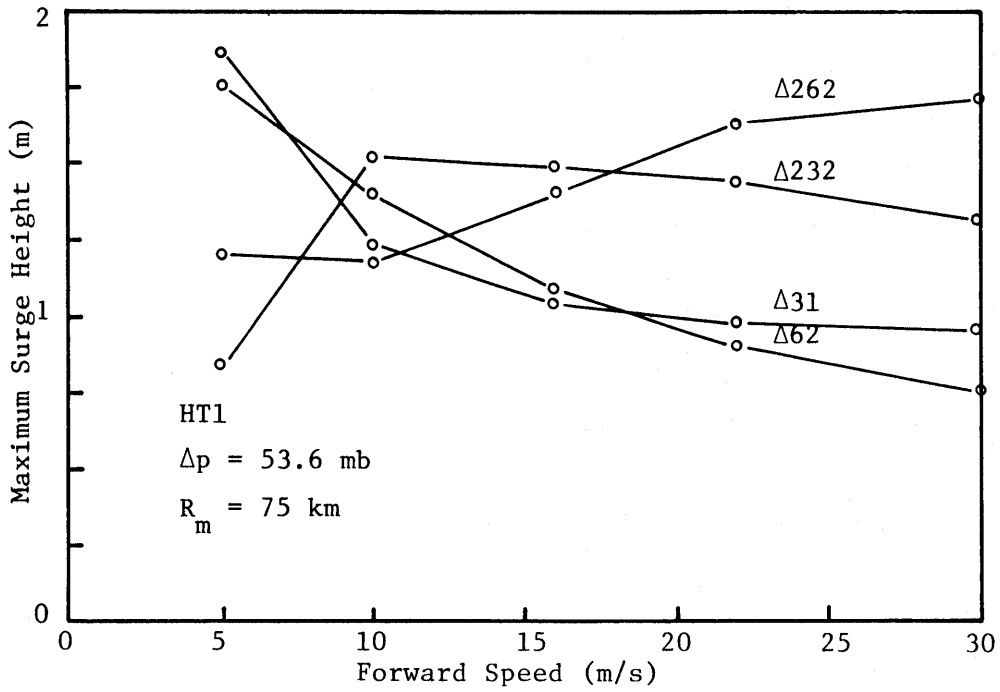


Figure 4.15. Maximum surge height vs. forward speed.  
(See Figure 4.9 for element position)

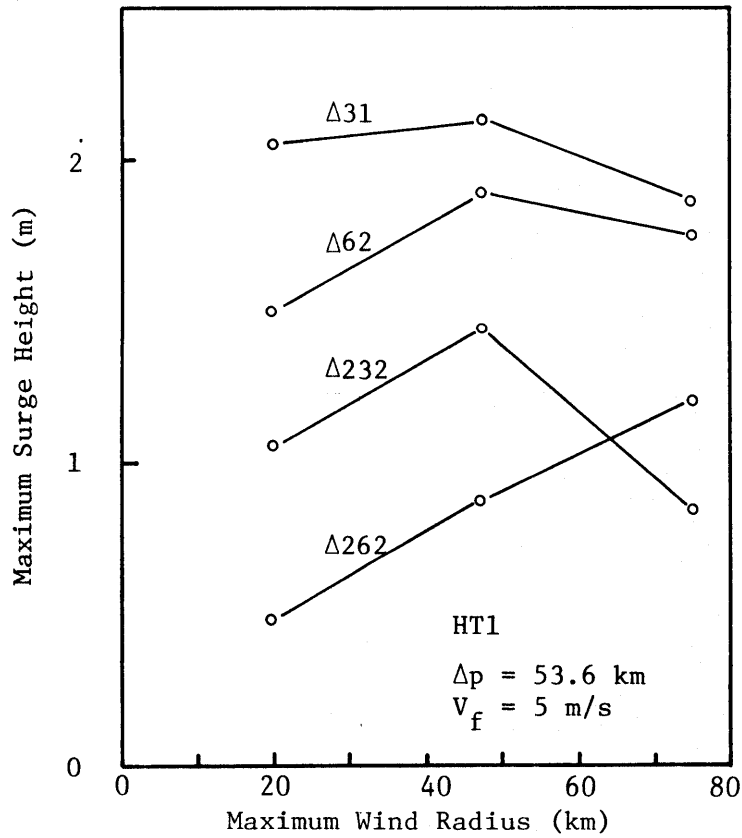


Figure 4.16. Maximum surge height vs. maximum wind radius. (See Figure 4.9 for element position).

4.5a, b and c). This is unlike the open coast surge which increases as the forward speed,  $V_f$ , increases. The surge in the bay is effected by two opposing influences, i.e. surge excited at the bay entrance and wind duration limited by bay area. As the hurricane forward speed increases, the open coast surge near the bay entrance increases. On the contrary, with faster forward speed, the wind duration for filling the basin of the bay is shorter. The net effect is that the higher open coast surge exciting the bay interior through the bay entrance competes with the lower surge set-up by the shorter wind duration in the bay, producing high surge near the bay entrance and low surge in the upper bay. The situation is reversed for slow forward speed.

#### Maximum Wind Radius

The response of the maximum surge height to the maximum wind radius is typically shown in Figure 4.16. (see also Table 4,5a, b and c). Note that the maximum of the maximum surge height curve at a station occurs when the hurricane passes the station with a distance from hurricane center approximately equal to the maximum wind radius. For example the model hurricane passes stations 31, 62 and 232 (see Figure 4.9 for station position) with an approximate distance of 50 km and passes station 262 with an approximate distance of 80 km. This coincidence suggests that the maximum surge height depends on the hurricane track rather than the maximum wind radius. This is probably due to the fact that the wind fetch is limited by the area of the bay and the typical size of a hurricane generally covers the entire bay so that a higher surge at a station is generated only when maximum wind area of the hurricane passes directly over the station.

#### 4.4 Conclusion

A two dimensional depth integrated finite element storm surge model has been developed. The model, being capable of reproducing the major feature of the storm surge in the Chesapeake Bay, can be considered at present one of the best two-dimensional formulations of the bay-ocean system. Possible studies for further improvement are specification of the hurricane parameters which describe the transition over land and bay, a more sophisticated treatment of water-land boundaries, and consideration of the interaction with the astronomical tides.

Since the primary objective in this study is to develop a more rational storm surge model for the study of flood levels and flood frequencies in the Chesapeake Bay, the model is then employed to calculate the storm surge height subject to various combination of hurricane parameters. The calculated results are separately reported.

## REFERENCES

- Brebbia, C. A. and J. J. Connor. 1974. "Fundamentals of Finite Element Techniques", A Halster Press Book, John Wiley & Sons.
- Bretschneider, C. L. 1966. "Engineering Aspects of Hurricane Surge", in Estuary and Coastline Hydrodynamics, ed. by A. T. Ippen, McGraw-Hill, Inc.
- Chapman, William T., Jr. and T. Sloan Young. 1955. "The Paths of Hurricanes Connie and Diane", Monthly Weather Review, August.
- Chen, H. S. and C. C. Mei. 1974. "Oscillations and Wave Forces in a Man-Made Harbor in the Open Sea", Proceeding of 10th Naval Hydrodynamics Symposium, June.
- Connor, J. and J. Wang. 1974. "Finite Element Modelling of Hydrodynamic Circulation", in Numerical Methods in Fluid Dynamics, ed. by Brebbia and Connor, Pentech Press.
- Corps of Engineers. 1968. "Flood Plain Information, Coastal Flooding, Hampton, Virginia", U.S. Army Norfolk, Virginia District, October.
- Damsguard, A. and A. F. Dinsmore. 1975. "Numerical Simulation of Storm Surges in Bays", Modeling 75, Symposium of Modeling Techniques, WW, ASCE, September.
- Dean, R. G. and B. R. Pearce. 1972. "Storm Tide Response on Idealized Continental Shelves: Effects of Steady Wind Fields of Limited Lateral Extent", Dept. of Coastal and Oceanographic Engineering, Univ. of Florida Technical Report No. 9, January.
- Dunn, Gordon E. 1961. "The Hurricane Season of 1960", Monthly Weather Review, March.
- Dunn, Gordon E, Walter R. Davis, and Paul L. Moore. 1956. "Hurricane Season of 1956", Monthly Weather Review, December.
- Durance, A. 1974. "A Mathematical Model of the Residual Circulation of the Southern North Sea", Sixth Liège Colloquium on Ocean Hydrodynamics, Mém. Soc. Roy. Sc de Liège.
- Finlayson, B. A. 1972. "The Method of Weighted Residuals and Variational Principles", Academic Press.
- Francis, P. H., Richard W. Schwerdt and Hugo V. Goodyear. 1975. "Some Climatological Characteristics of Hurricanes and Tropical Storms, Gulf and East Coasts of the United States", NOAA Technical Report NWS 15, May.
- Graham, Howard E. and Dwight E. Bun. 1959. "Meteorological Considerations Pertinent to Standard Project Hurricane, Atlantic and Gulf Coasts of the United States", National Hurricane Research Project, Report No. 33, November.



- Hansen, W. 1956. "Theorie zur Errechnung des Wasserstandes und der Stromungen in Randmeeren Nebst Anwendungen", Tellus, No. 3.
- Hansen, W. 1962. "Hydrodynamical Methods Applied to Oceanographic Problems", Proceedings of the Symposium, Mathematical-Hydrodynamical Methods of Physical Oceanography, Institute Fur Meereskunde Der Universitat Hamburg.
- Heaps, N. S. 1969. "A Two-Dimensional Numerical Sea Model", Royal Society of London, Philosophical Transactions, Ser. A, Vol. 265, No. 1160, October.
- Hicks, Steacy, D. 1964. "Tidal Wave Characteristics of Chesapeake Bay", Chesapeake Science, Vol. 5, No. 3, pp. 103-113, Fall.
- Holmboe, Jorgen. 1945. "Dynamic Meteorology", John Wiley & Sons, Inc., New York.
- Jelesnianski, C. P. 1965. "A Numerical Computation of Storm Tides Induced by a Tropical Storm Impinging on a Continental Shelf", Monthly Weather Review, Vol. 93, No. 6.
- Jelesnianski, C. P. 1966. "Numerical Computations of Storm Surges Without Bottom Stress", Monthly Weather Review, Vol. 94, No. 6.
- Jelesnianski, C. P. 1967. "Numerical Computations of Storm Surges With Bottom Stress", Monthly Weather Review, Vol. 95, No. 11.
- Jelesnianski, C. P. 1970. "Bottom Stress Time-History in Linearized Equations of Motion of Storm Surge", Monthly Weather Review, Vol. 98, No. 6.
- Jelesnianski, C. P. 1974. "SPLASH - Special Program to List Amplitude of Surge from Hurricane, Part II - General Track and Variant Storm Conditions, NWS, NOAA, Technical Memorandum, NWS TOL-52.
- Lamb, Sir Horace. 1945. "Hydrodynamics", Dover Publications, 6th edition.
- Martin, H. C. and G. F. Carey. 1973. "Introduction to Finite Element Analysis", McGraw-Hill, Inc.
- Myers, V. A. 1954. "Characteristics of United States Hurricanes Pertinent to Levee Design for Lake Okeechobee, Florida", Hydrometeorological Report No. 32, Weather Bureau, U. S. Dept. of Commerce, Washington, D. C., March.
- Namias, Jerome and Carlos R. Dunn. 1955. "The Weather and Circulation of August 1955", Monthly Weather Review, August.

- Nihoul, J. C. J. 1975. "Modelling of Marine Systems", Elsevier Publ. Co., Amsterdam.
- Norrie, D. H. and G. deVries. 1973. "The Finite Element Method", Academic Press.
- Oden, J. T. and E. R. A. Oliveira. 1973. "Lectures on Finite Element Methods in Continuum Mechanics", The University of Alabama Press.
- Overland, James E. 1975. "Estimation of Hurricane Storm Surge in Apalachicola Bay, Florida", NOAA Technical Report NWS 17, June.
- Pagenkopf, James R. and Bryan R. Pearce. 1975. "Evaluation of Techniques for Numerical Calculation of Storm Surges", MIT Ralph M. Parsons Lab. Report No. 199, February.
- Pearce, B. R. 1972. "Numerical Calculation of the Response of Coastal Waters to Storm Systems", Technical Report No. 12, Coastal and Oceanographic Engineering Lab. Univ. of Florida.
- Phillips, O. M. 1966. "The Dynamics of the Upper Ocean", Cambridge University Press.
- Platzman, G. W. 1958. "A Numerical Computation of the Surge of 26 June 1954 on Lake Michigan", Geophysica, Vol. 6.
- Reid, Robert O. and Bernie R. Bodine. 1968. "Numerical Model for Storm Surge in Galveston Bay", WWI, ASCE, February.
- Richtmyer, Robert D. and K. W. Morton. 1967. "Difference Method for Initial-Value Problems", Interscience Publishers, 2nd edition.
- Roache, Patrick J. 1972. "Computational Fluid Dynamics", Hermosa Publishers.
- Runchal, Akshai Kumar. 1975. "Numerical Model for Storm Surge and Tidal Run-up Studies", Modeling 75, Symposium on Modeling Techniques, WW, ASCE, September.
- Strang, Gilbert and George J. Fix. 1973. "An Analysis of the Finite Element Method", Prentice-Hall, Inc.
- U. S. Dept. of Commerce, National Ocean Survey, NOAA. 1975. "Tide Tables 1976, High and Low Water Predictions, East Coast of North and South America including Greenland".
- U. S. Dept. of Commerce, National Ocean Survey, NOAA. 1975. "Tidal Current Tables 1976, Atlantic Coast of North America".

- Van Dorn, William G. 1953. "Wind Stress on an Artificial Pond",  
Journal of Marine Research, Vol. 12, No. 3.
- Wang, John D. and Jerome J. Connor. 1975. "Mathematical Modeling  
of Near Coastal Circulation", MIT, Ralph M. Parsons Laboratory,  
Report No. 200, April.
- Whitaker, R. E., et al. 1973. "Drag Coefficients at Hurricane Wind  
Speeds as Deduced from the Numerical Simulation of Dynamical  
Water Level Changed in Lake Okeechobee", Ref. 73-13-5,  
Texas A&M, August.
- Wilson, Basil W. 1957. "Hurricane Wave Statistics for the Gulf of  
Mexico", Dept. of the Army Technical Memorandum No. 98,  
June.
- Wilson, B. W. 1960. "Note on Surface Wind Stress Over Water at  
Low and High Wind Speeds", Journal of Geophysical Research,  
Vol. 65, No. 10.
- Wu, J. 1969. "Wind Stress and Surface Roughness at Air-Sea Interface",  
Journal of Geophysical Research, Vol. 74, No. 2, January.
- Yeh, Gour-Tsyh and Fei-Fan Yeh. 1976. "Generalized Model for Storm  
Surges", Proceeding, Fifteen International Conference on  
Coastal Engineering, Vol. I, Chapter 54, July.

## List of Symbols

$c_o, c_1, c_a$	wind drag coefficients
$c_f$	bottom friction coefficient
$c_r$	wind reduction factor
$f$	Coriolis coefficient
$g$	gravitational acceleration
$h$	undisturbed water depth
$H$	total water depth
$L_1, L_2$	lengths shown in Figure 3.2
$N_i, N_1, N_2, N_3$	interpolation functions of triangular element
$p, p^s$	atmospheric pressure
$p_c$	atmospheric pressure at hurricane center
$p_\infty$	atmospheric pressure at the outer periphery of the hurricane
$P_1, P_2, P_3$	points shown in Figure 3.2
$q, q_i, q_x, q_y$	water transport and its components
$q_n, q_s$	normal and tangential components of water transport
$Q$	rate of adding water mass per unit area
$r$	distance from hurricane center
$R_m$	maximum wind radius
$t$	time variables
$T_{ij}, T_{xx}, T_{xy}, T_{yx}, T_{yy}$	internal stresses
$(u, v, w)$	components of water velocity in x-, y- and z-direction respectively
$U$	wind speed
$U_{cr}$	critical wind speed
$U_{10}, U_{10x}, U_{10y}$	wind speed at 10-meters above undisturbed water surface and its components.

$V_f$	hurricane forward speed
$x, y$	horizontal coordinates
$z$	vertical coordinate
$\alpha_{nx}, \alpha_{ny}$	cosines directions
$\beta$	wind deflection angle
$\delta$	referring to weighting function
$\Delta$	area of a triangular element
$\Delta p$	hurricane central pressure depression
$\Delta t$	time step
$\Delta t_{cr}$	critical time step
$\varepsilon_{ij}, \varepsilon_{xx}, \varepsilon_{xy}, \varepsilon_{yx}, \varepsilon_{yy}$	eddy viscosity coefficients
$\eta$	water elevation above undisturbed water surface
$\eta_a$	water elevation of astronomical tide
$\eta_b$	water elevation of barometric tide
$\theta$	angle shown in Figure
$\theta_o, \theta_n$	angles shown in Figure 3.2
$\lambda$	water wave length
$\rho, \rho_o, \Delta\rho$	water density, constant mean density, density deviation
$\rho_a$	air density
$\tau_i^b, \tau_x^b, \tau_y^b$	bottom friction components
$\tau_i^s, \tau_x^s, \tau_y^s$	wind stress components
$\phi$	latitude degree
{ }	column vector
{ } <sup>T</sup>	transport of column vector, row vector
( )	matrix
superscript *	referring to a prescribed value
superscript e	referring to element e

## APPENDIX A

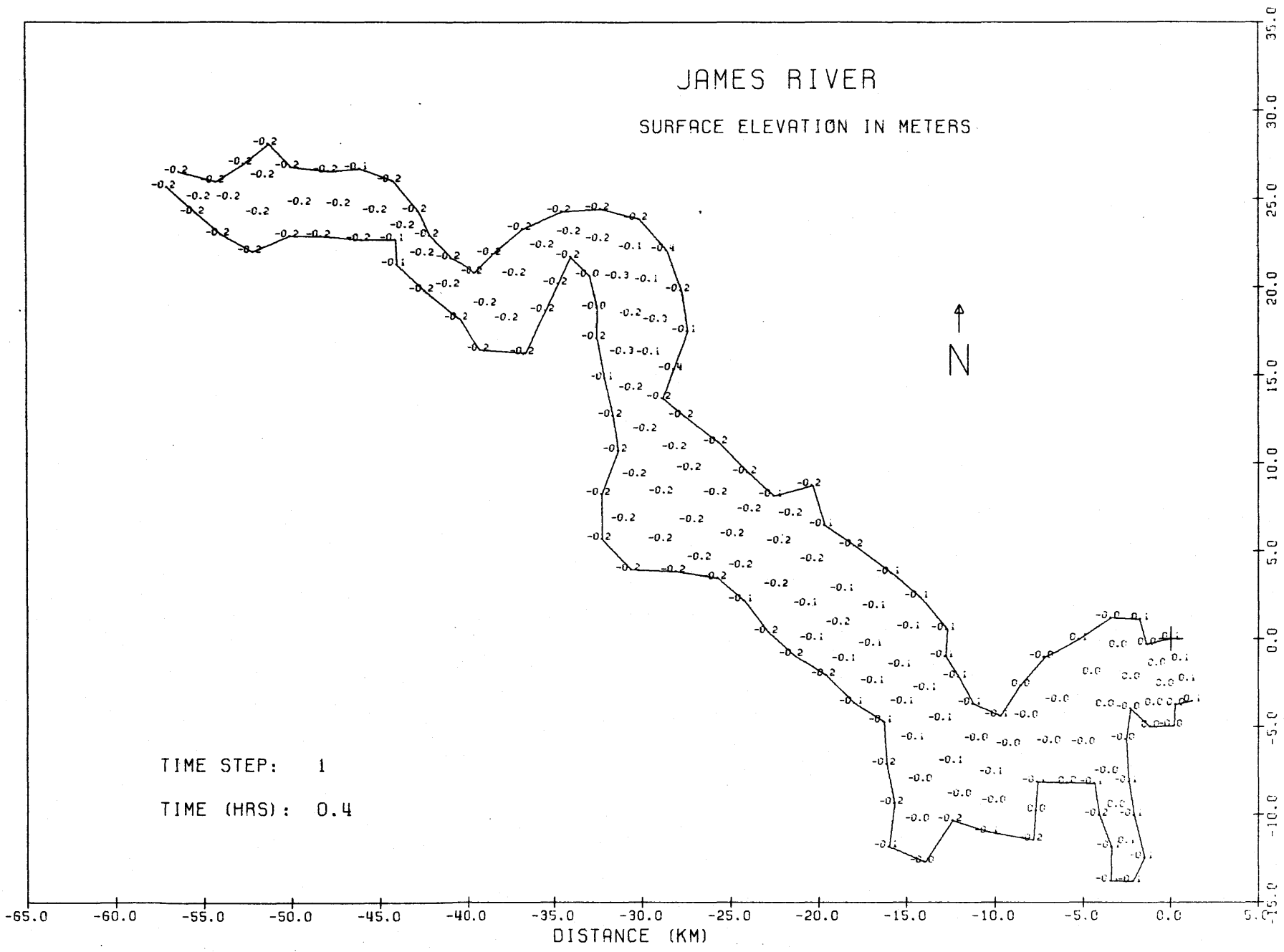
## CALCULATED TIDES IN THE LOWER JAMES RIVER

This appendix shows a sequence of the calculated results of the water elevation and flow circulation within a tidal cycle in the lower James River. The water elevation is referred to the NGVD (1929). The time step shown in the figures is not actual computational time step, it only indicates the sequence of the figures.

Figures A.1 - A.16. Water elevation and circulation of the Lower James River in a tidal cycle.

# JAMES RIVER

SURFACE ELEVATION IN METERS



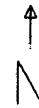
TIME STEP: 1  
TIME (HRS): 0.4

DISTANCE (KM)  
SCALE (METERS/INCH) : 5000  
88

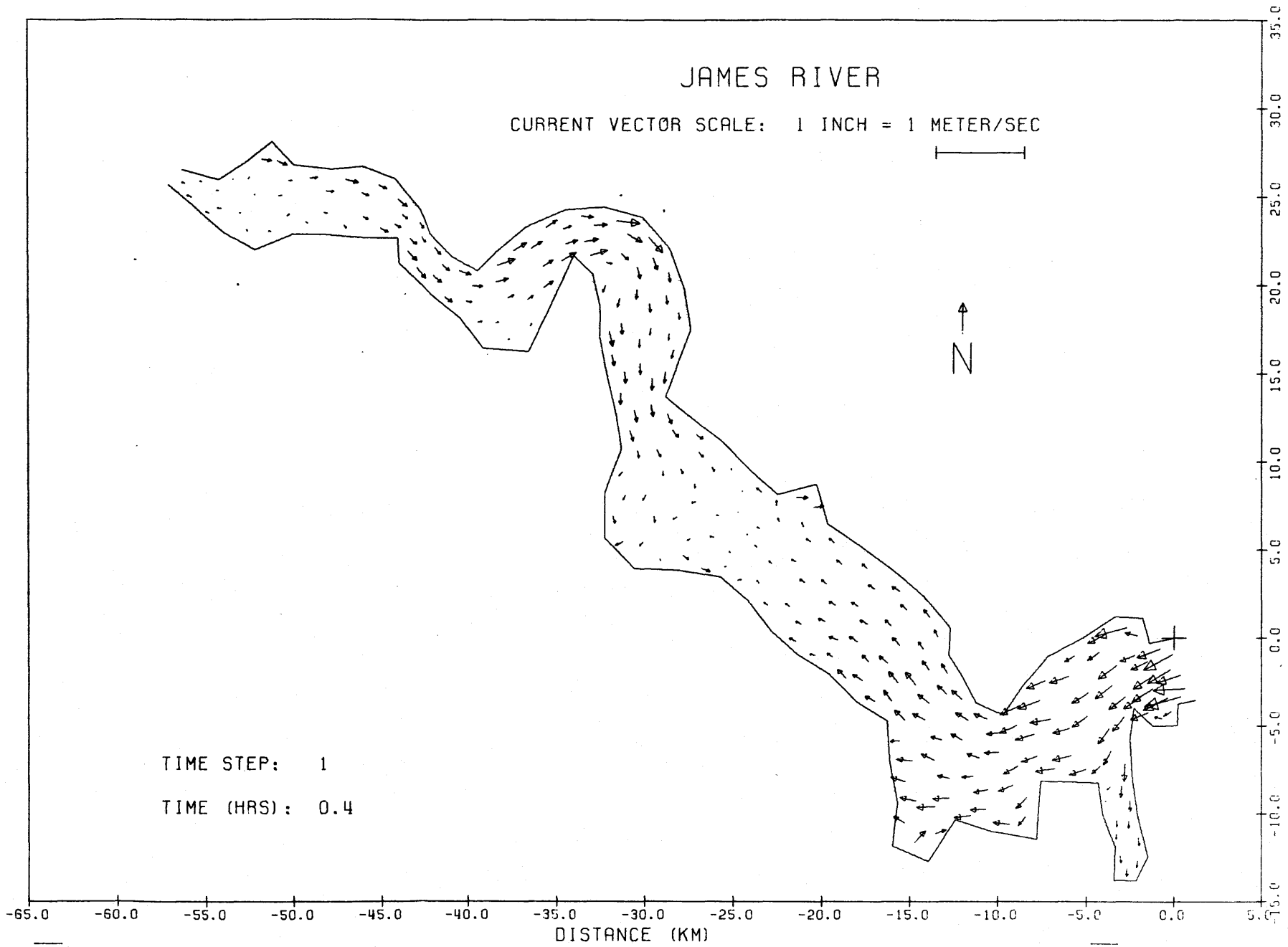


# JAMES RIVER

CURRENT VECTOR SCALE: 1 INCH = 1 METER/SEC



TIME STEP: 1  
TIME (HRS): 0.4

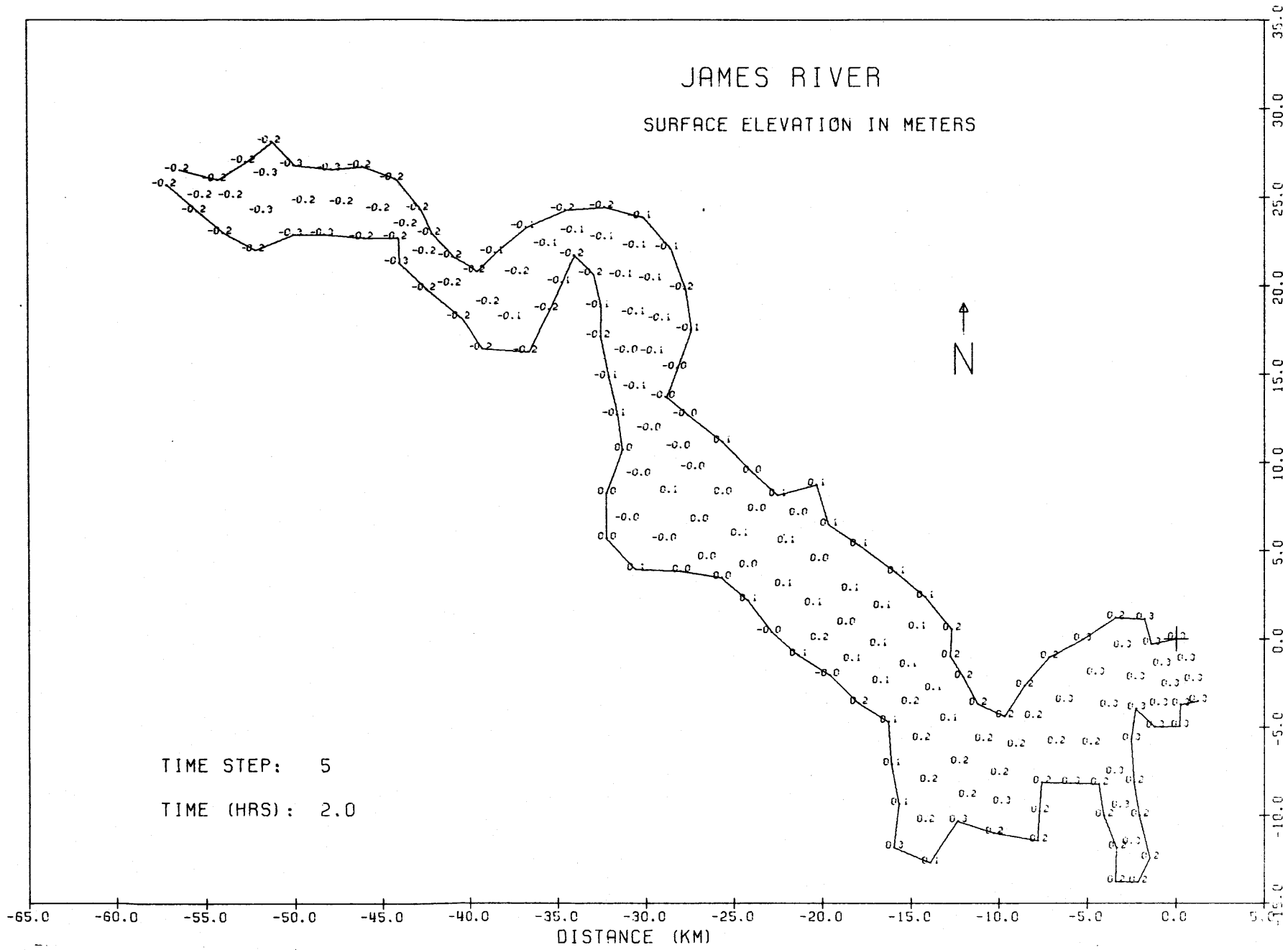


DISTANCE (KM)

SCALE (METERS/INCH) : 5000

# JAMES RIVER

SURFACE ELEVATION IN METERS



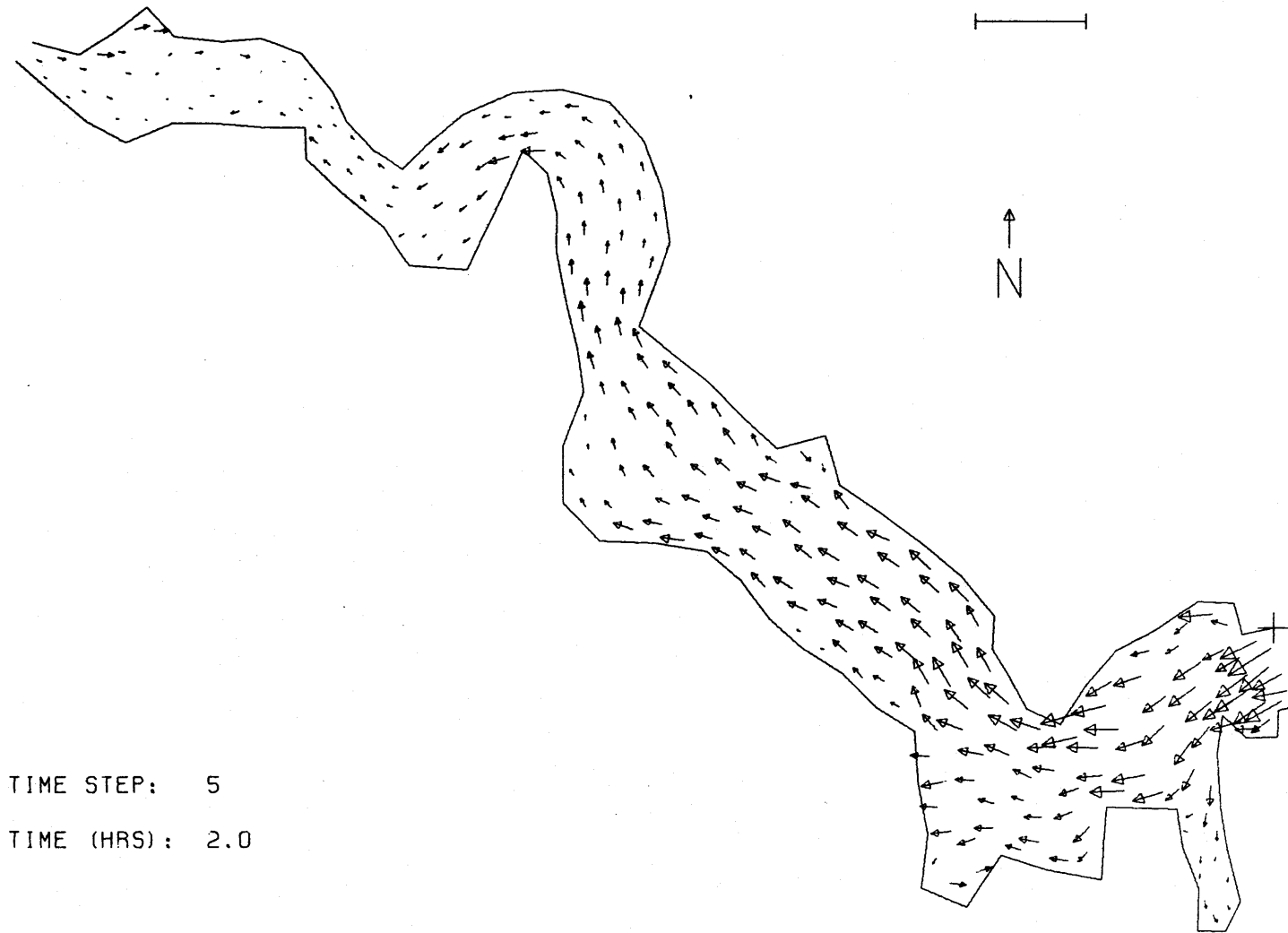
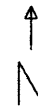
TIME STEP: 5

TIME (HRS): 2.0

DISTANCE (KM)  
SCALE (METERS/INCH): 5000  
06

# JAMES RIVER

CURRENT VECTOR SCALE: 1 INCH = 1 METER/SEC



TIME STEP: 5  
TIME (HRS): 2.0

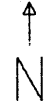
-65.0 -60.0 -55.0 -50.0 -45.0 -40.0 -35.0 -30.0 -25.0 -20.0 -15.0 -10.0 -5.0 0.0 5.0  
DISTANCE (KM)

35.0  
30.0  
25.0  
20.0  
15.0  
10.0  
5.0  
0.0  
-5.0  
-10.0  
-15.0  
DISTANCE (KM)

SCALE (METERS/INCH): 5000

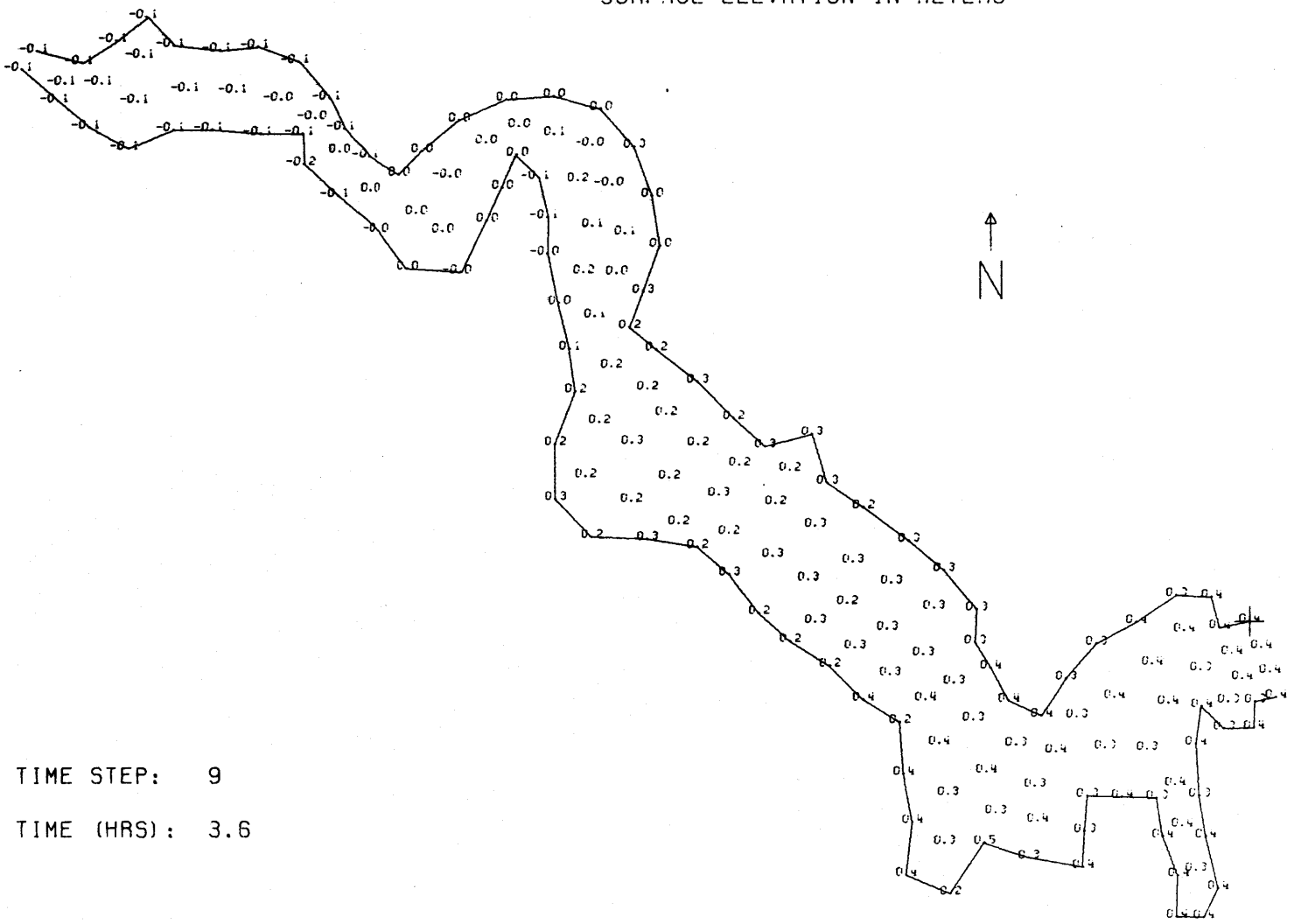
# JAMES RIVER

SURFACE ELEVATION IN METERS



DISTANCE (KM)

SCALE (METERS/INCH): 5000

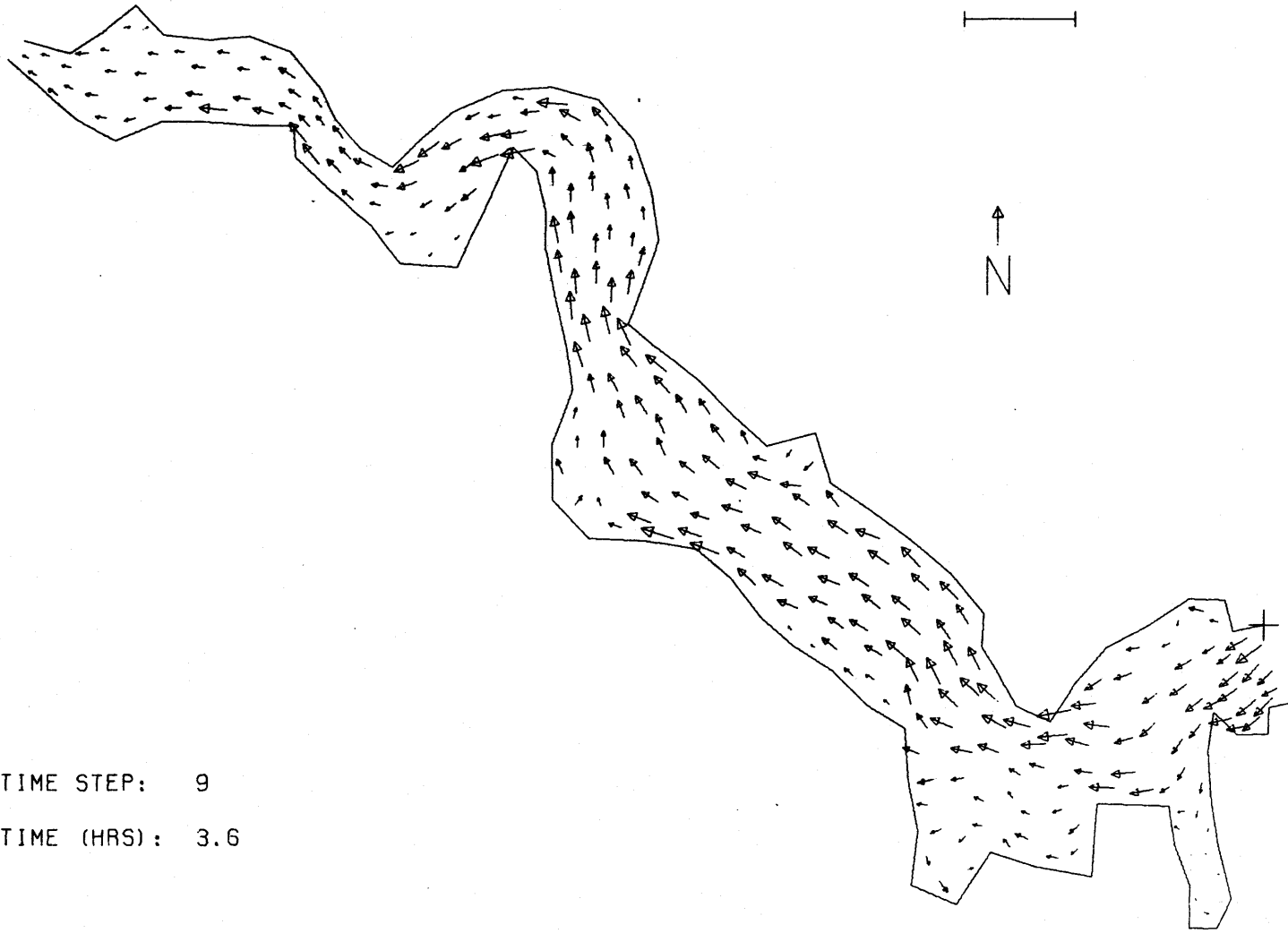
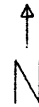
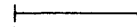


TIME STEP: 9  
TIME (HRS): 3.6

-65.0 -60.0 -55.0 -50.0 -45.0 -40.0 -35.0 -30.0 -25.0 -20.0 -15.0 -10.0 -5.0 0.0 5.0  
DISTANCE (KM)

# JAMES RIVER

CURRENT VECTOR SCALE: 1 INCH = 1 METER/SEC



TIME STEP: 9

TIME (HRS): 3.6

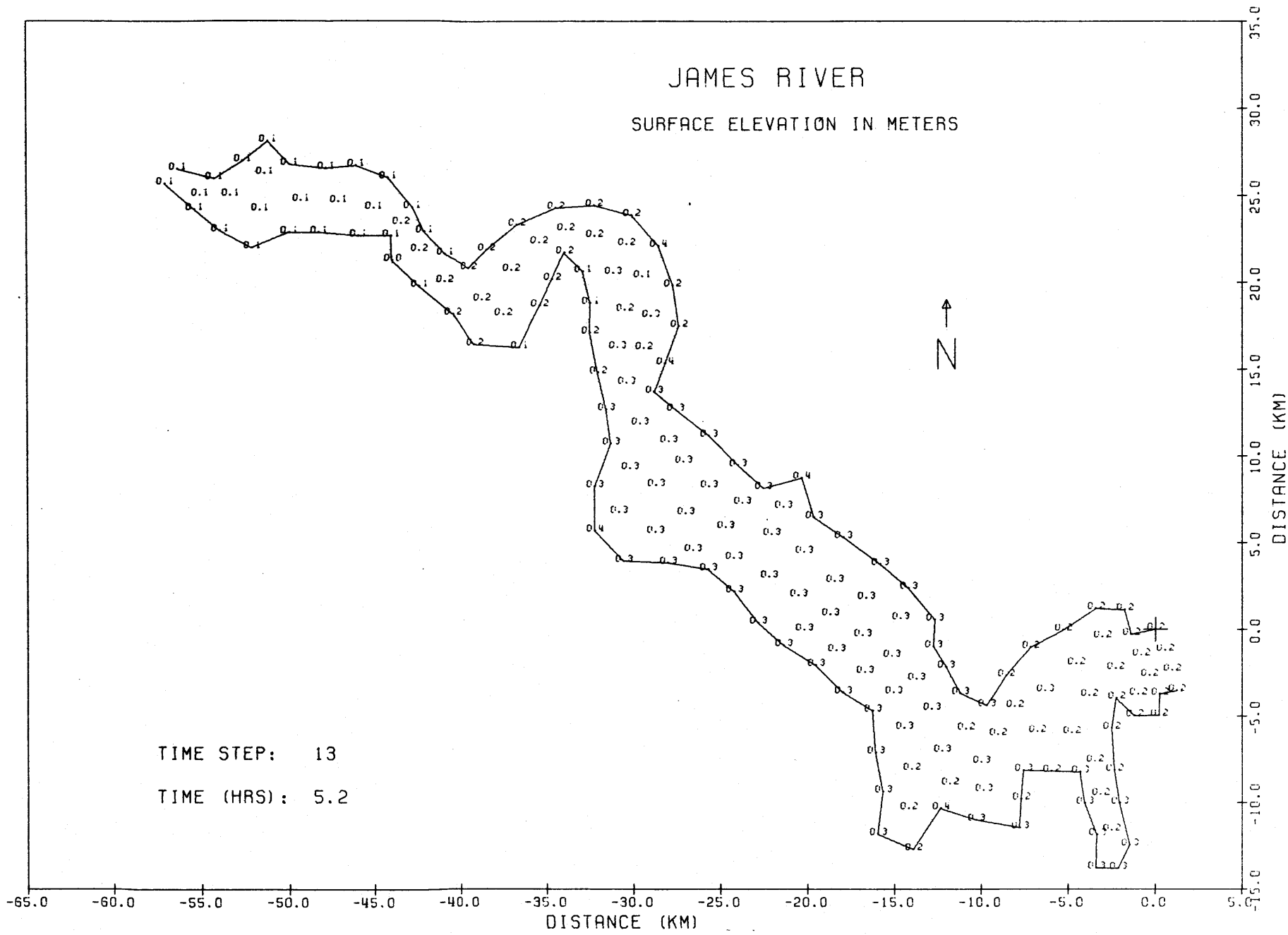
DISTANCE (KM)

SCALE (METERS/INCH): 5000

66

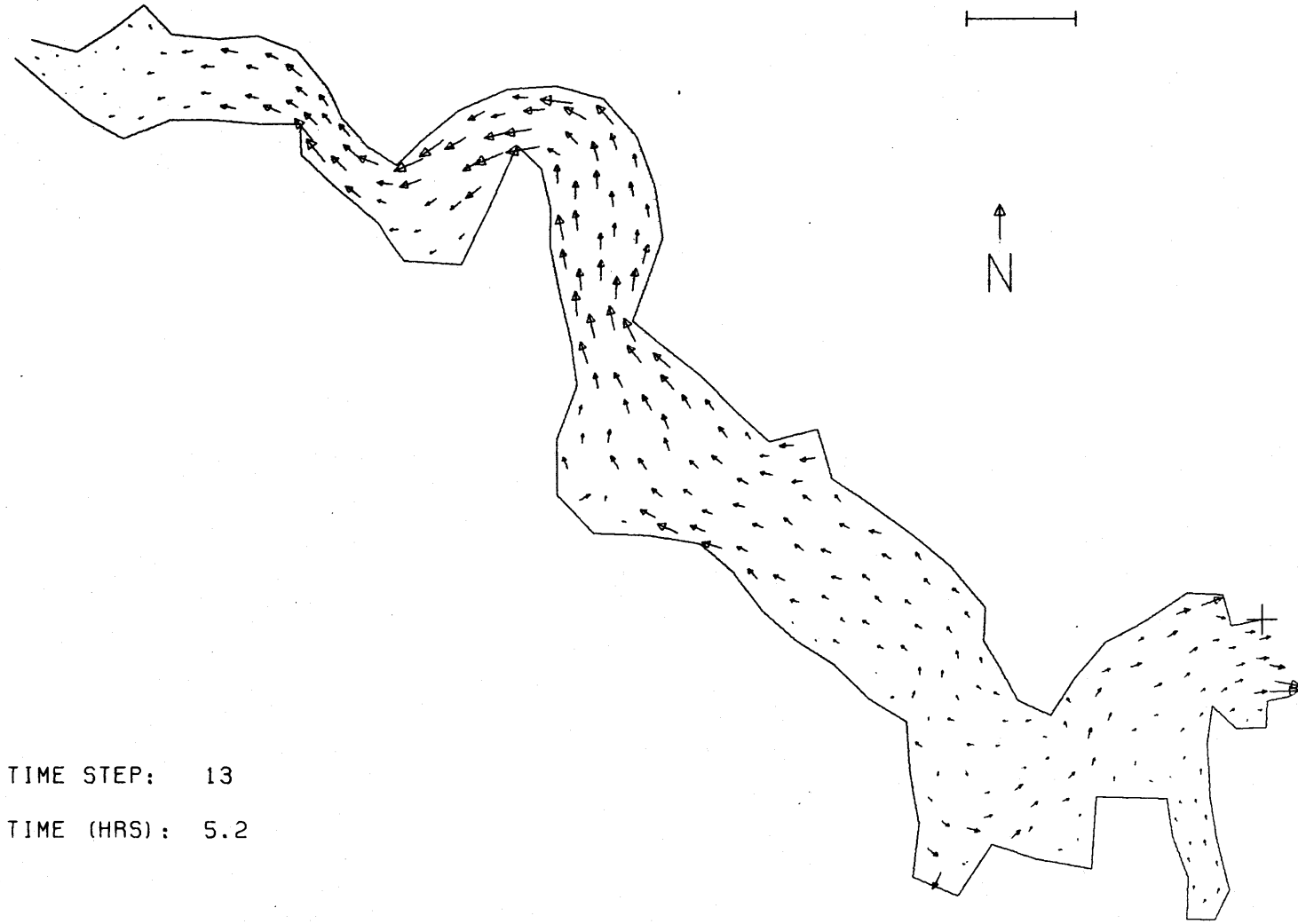
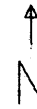
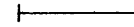
-65.0 -60.0 -55.0 -50.0 -45.0 -40.0 -35.0 -30.0 -25.0 -20.0 -15.0 -10.0 -5.0 0.0 5.0  
DISTANCE (KM)

35.0 30.0 25.0 20.0 15.0 10.0 5.0 0.0 -5.0 -10.0 -15.0



# JAMES RIVER

CURRENT VECTOR SCALE: 1 INCH = 1 METER/SEC



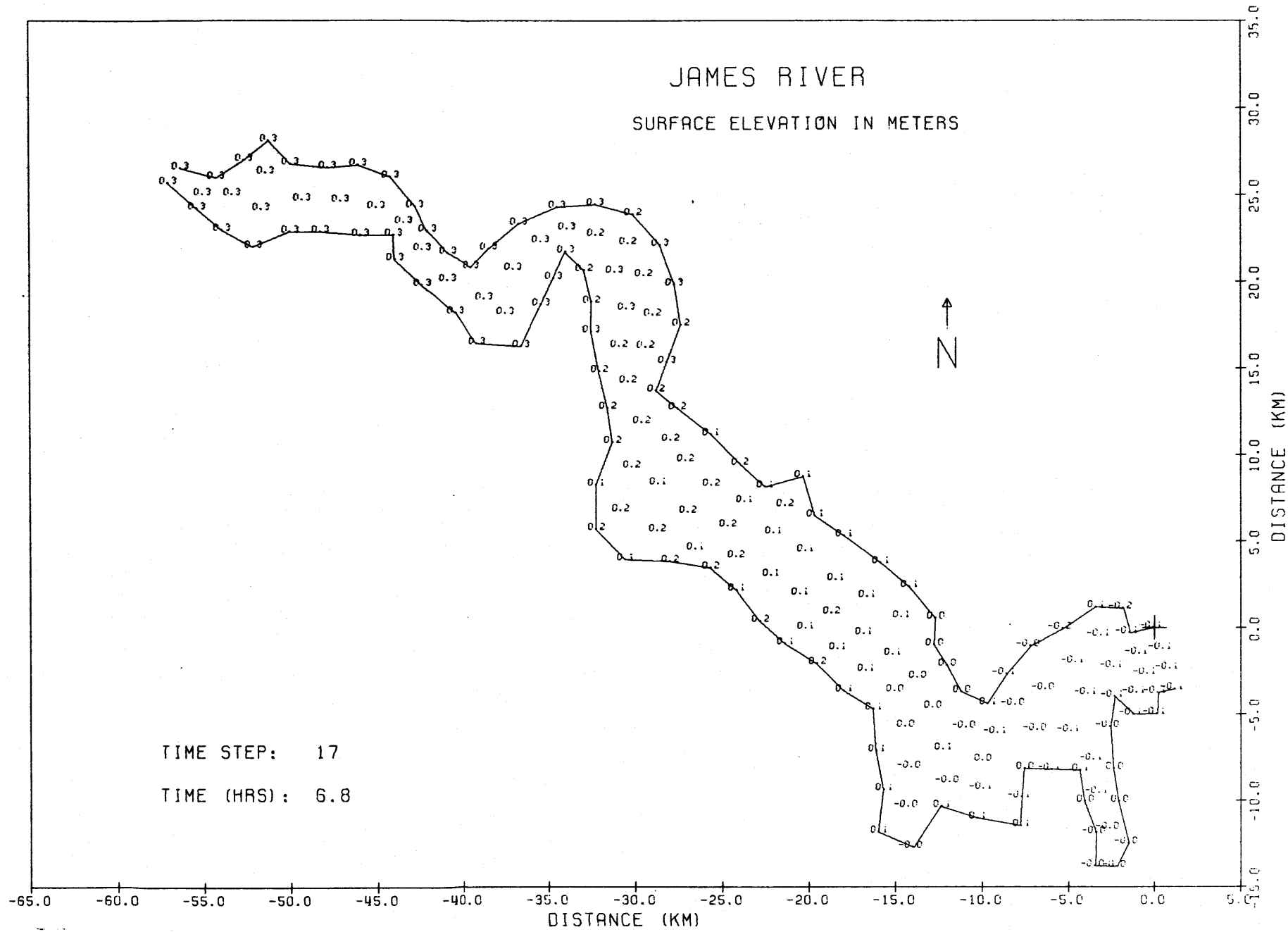
TIME STEP: 13

TIME (HRS): 5.2

-65.0 -60.0 -55.0 -50.0 -45.0 -40.0 -35.0 -30.0 -25.0 -20.0 -15.0 -10.0 -5.0 0.0 5.0  
DISTANCE (KM)

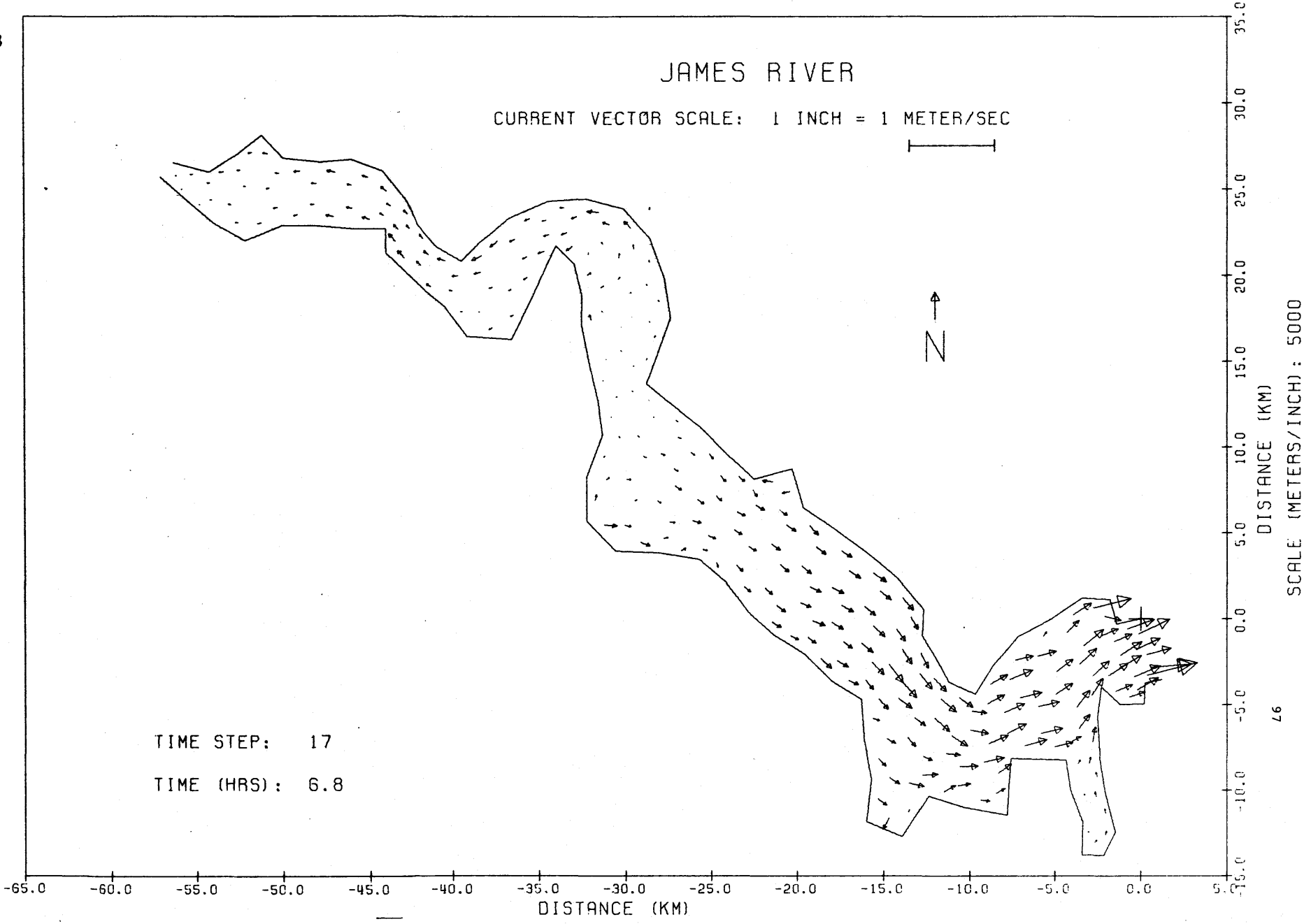
35.0 30.0 25.0 20.0 15.0 10.0 5.0 0.0 -5.0 -10.0 -15.0  
DISTANCE (KM)

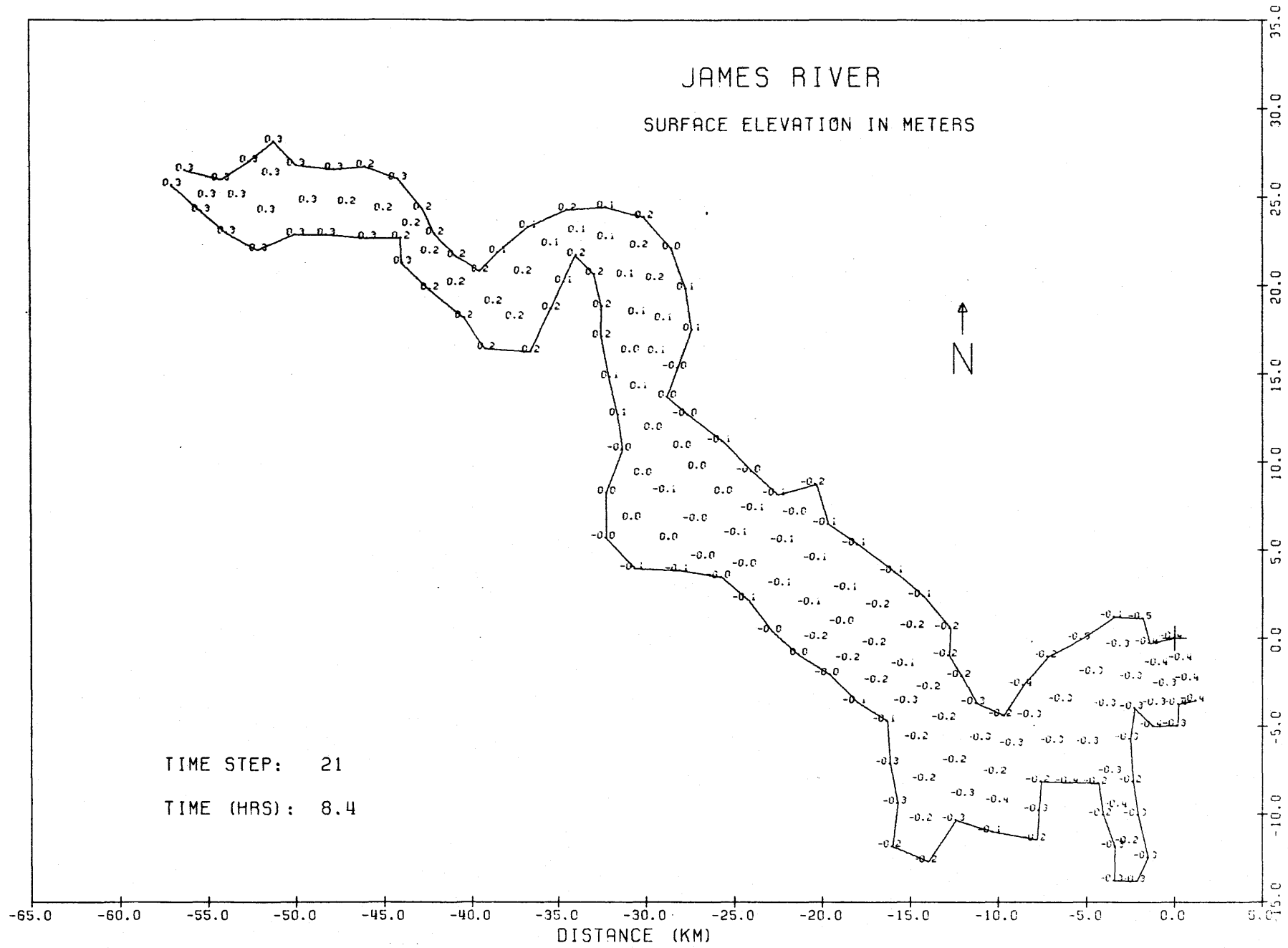
SCALE (METERS/INCH): 5000





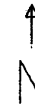
3



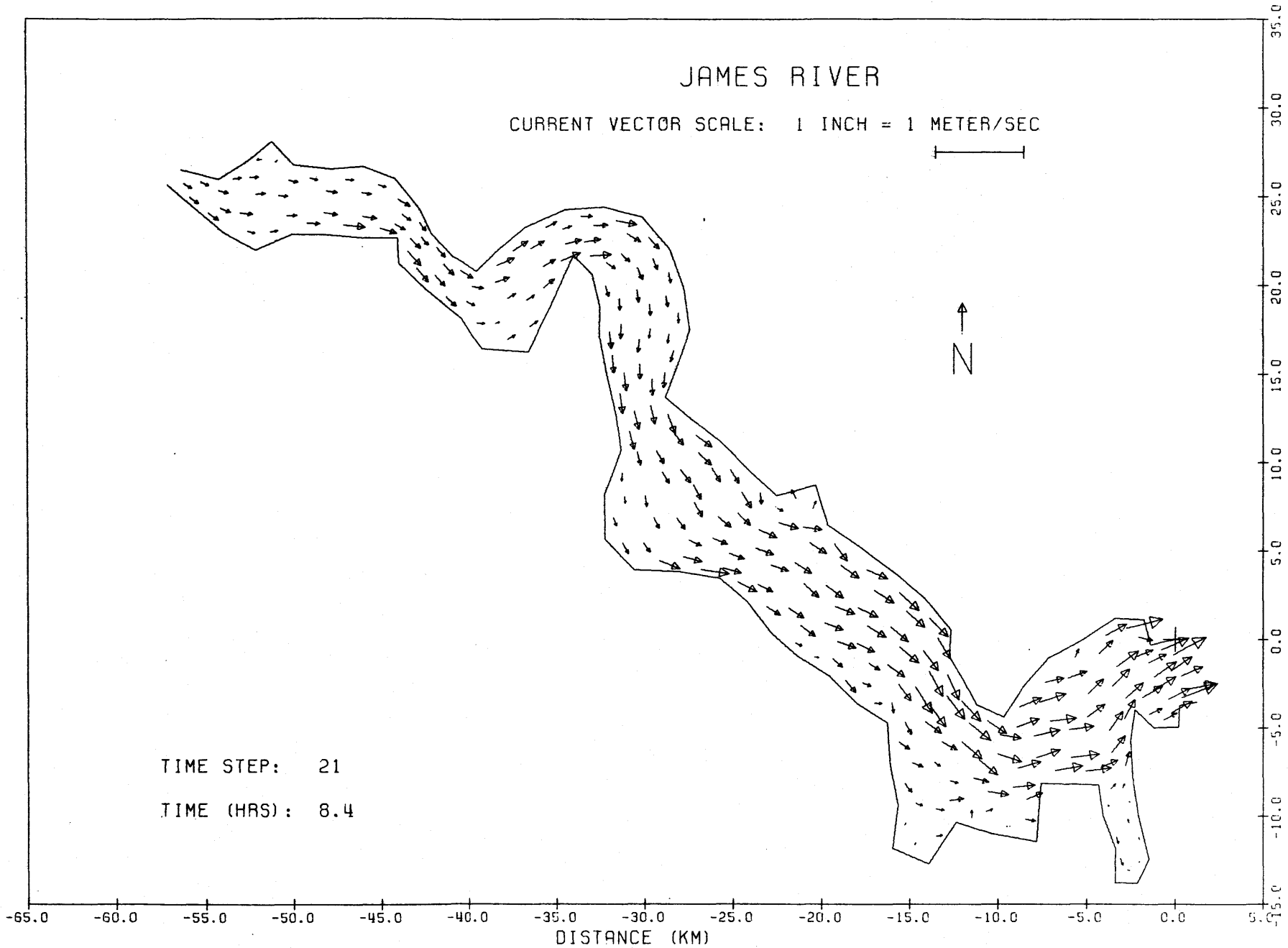


# JAMES RIVER

CURRENT VECTOR SCALE: 1 INCH = 1 METER/SEC



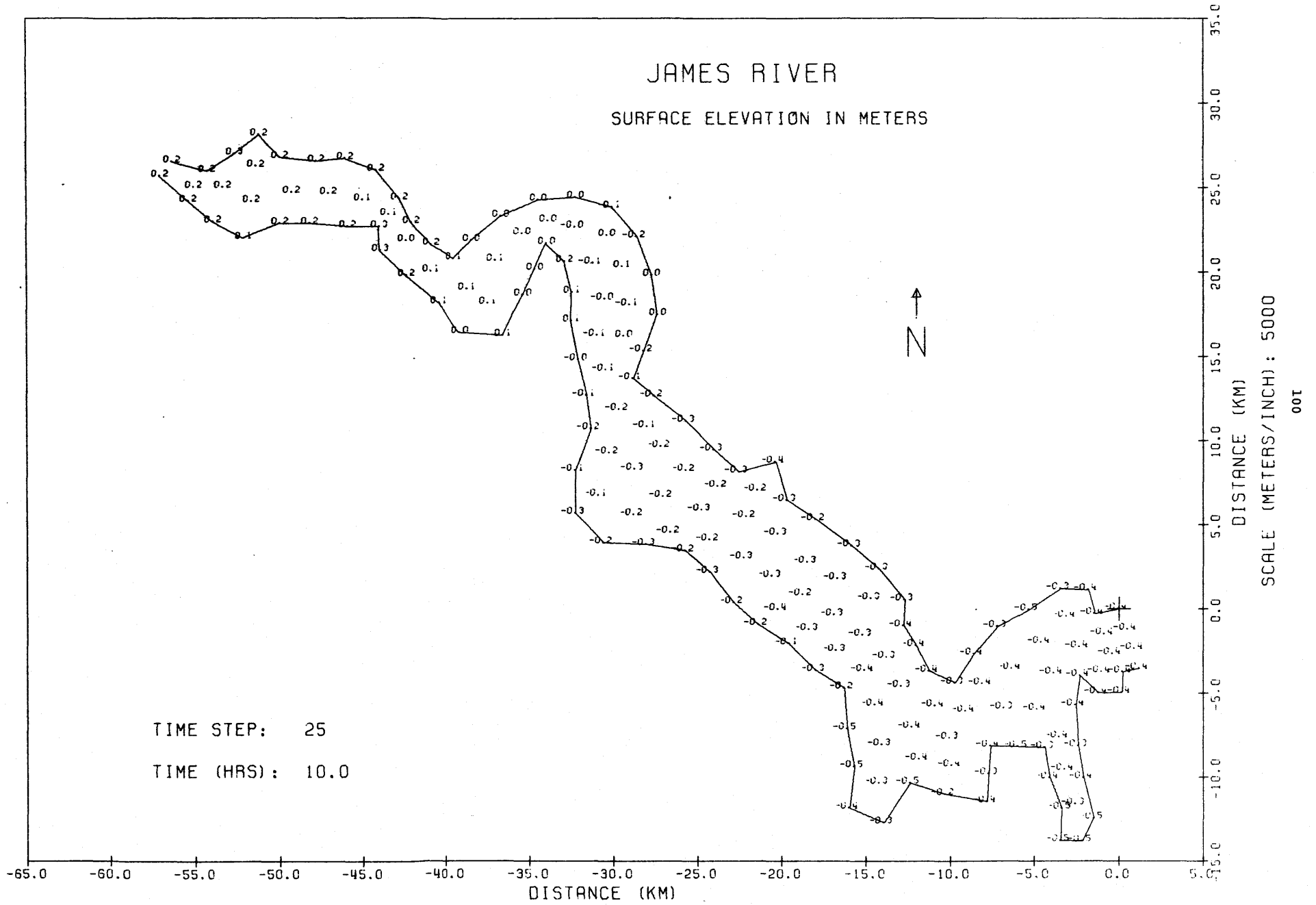
TIME STEP: 21  
TIME (HRS): 8.4

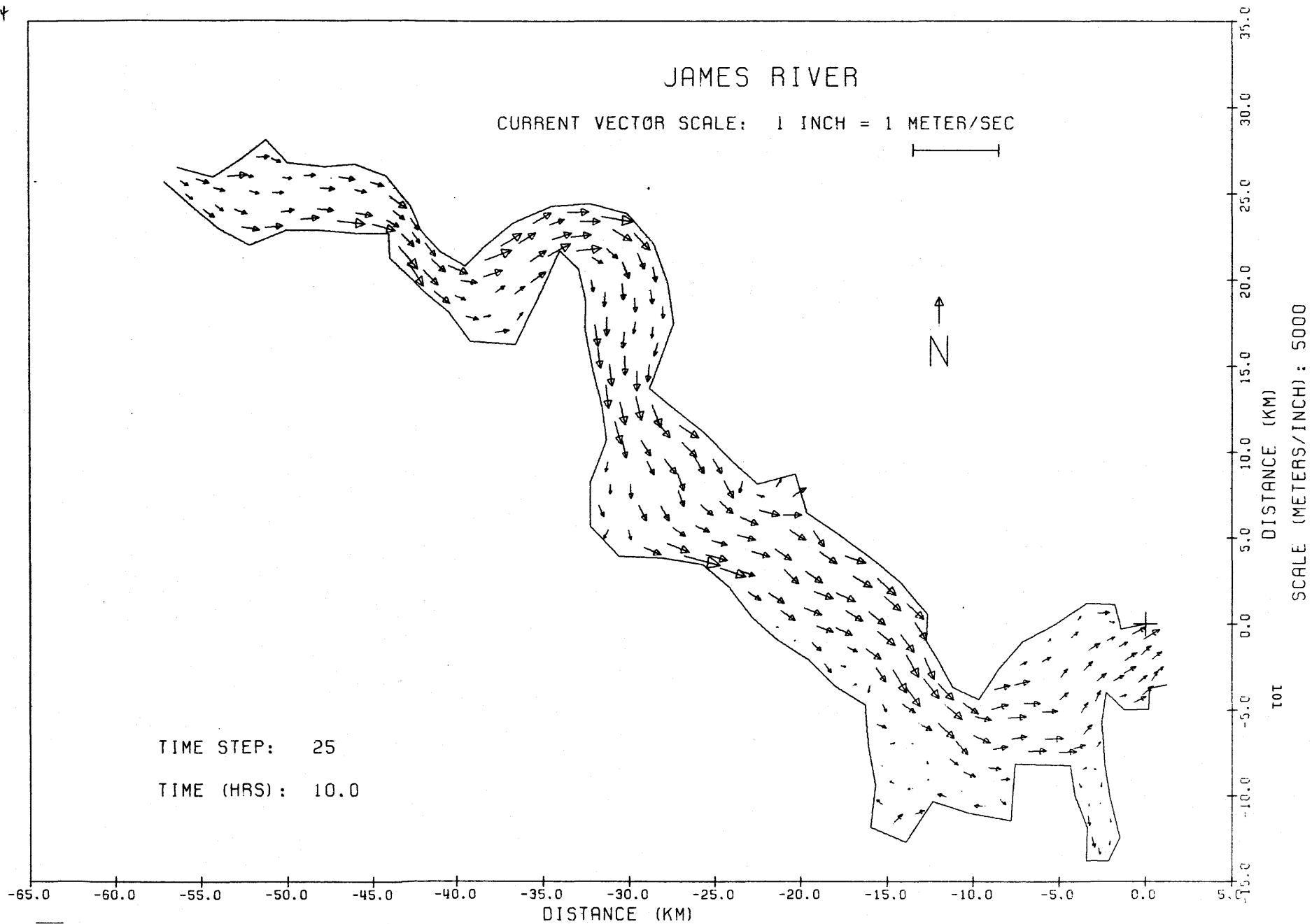


DISTANCE (KM)  
SCALE (METERS/INCH): 5000

# JAMES RIVER

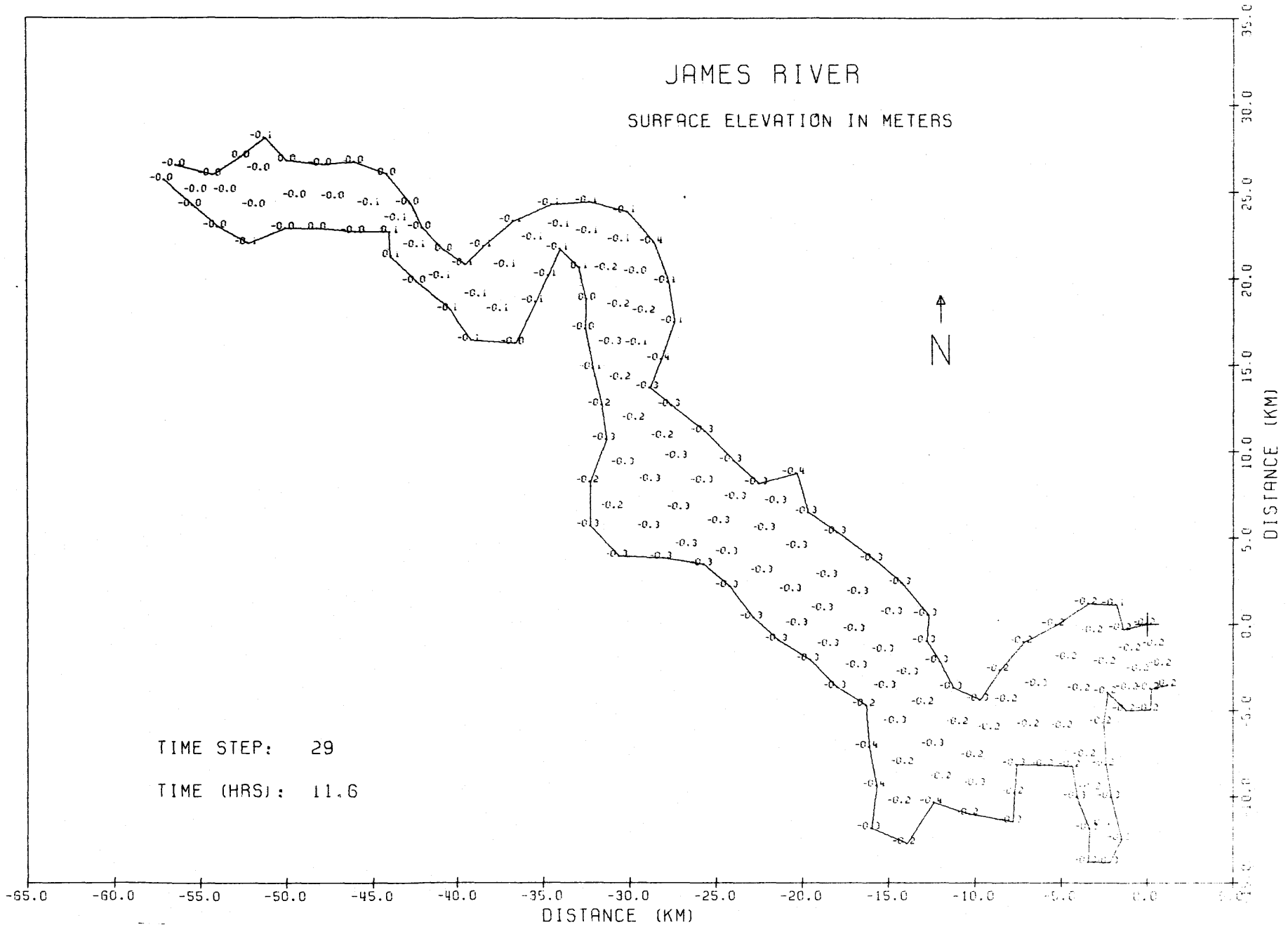
SURFACE ELEVATION IN METERS





# JAMES RIVER

SURFACE ELEVATION IN METERS

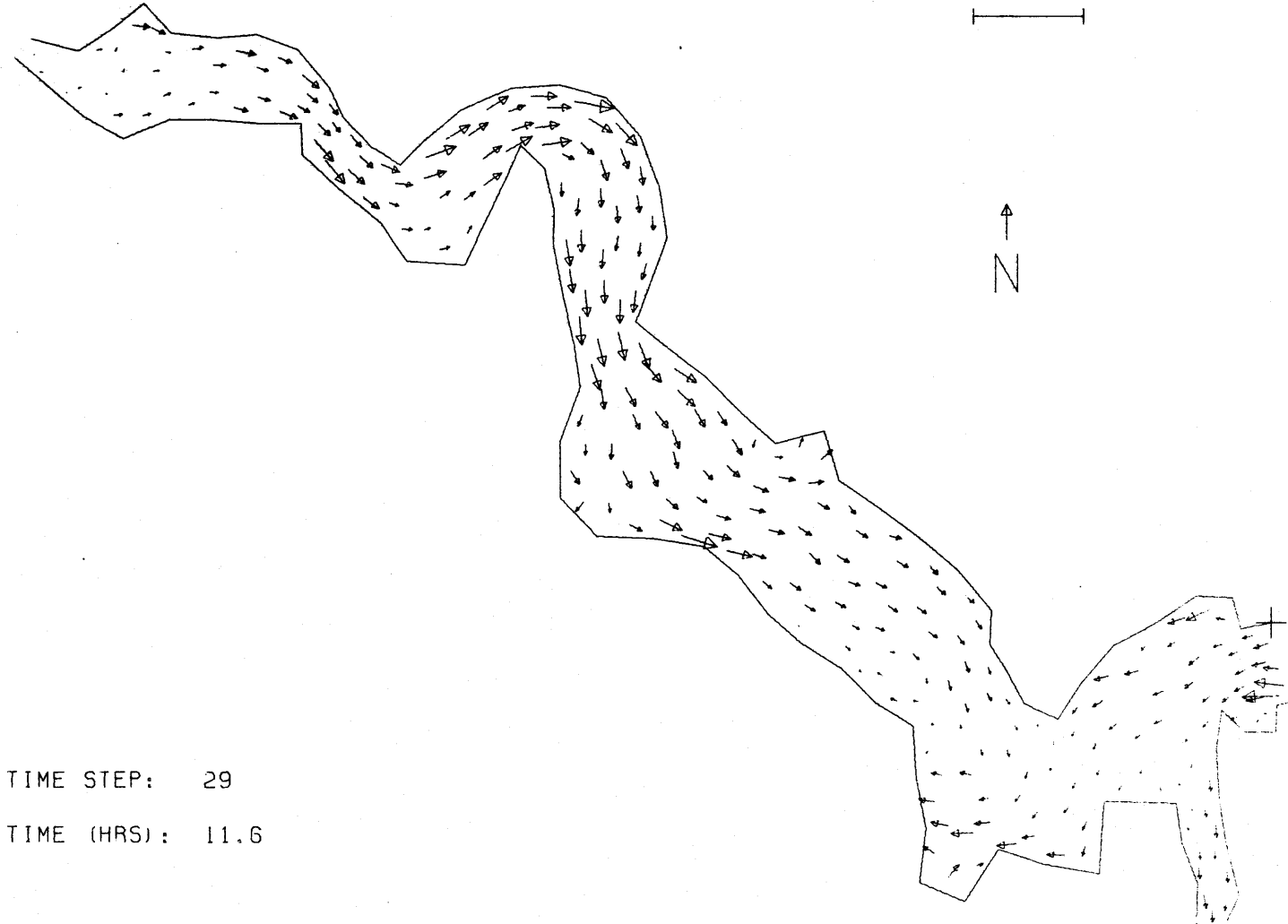
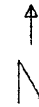


TIME STEP: 29  
TIME (HRS): 11.6

SCALE (METERS/INCH): 5000

# JAMES RIVER

CURRENT VECTOR SCALE: 1 INCH = 1 METER/SEC



TIME STEP: 29

TIME (HRS): 11.6

DISTANCE (KM)

SCALE (METERS/INCH): 5000

10T

-65.0 -60.0 -55.0 -50.0 -45.0 -40.0 -35.0 -30.0 -25.0 -20.0 -15.0 -10.0 -5.0 0.0

DISTANCE (KM)

0.0 5.0 10.0 15.0 20.0 25.0 30.0 35.0

## APPENDIX B

## SIMULATION OF TIDES IN THE CHESAPEAKE BAY

This appendix presents a sequence of the calculated results of water elevation and flow circulation within a tidal cycle in the Chesapeake Bay. The water elevation is referred to the NGVD (1929).

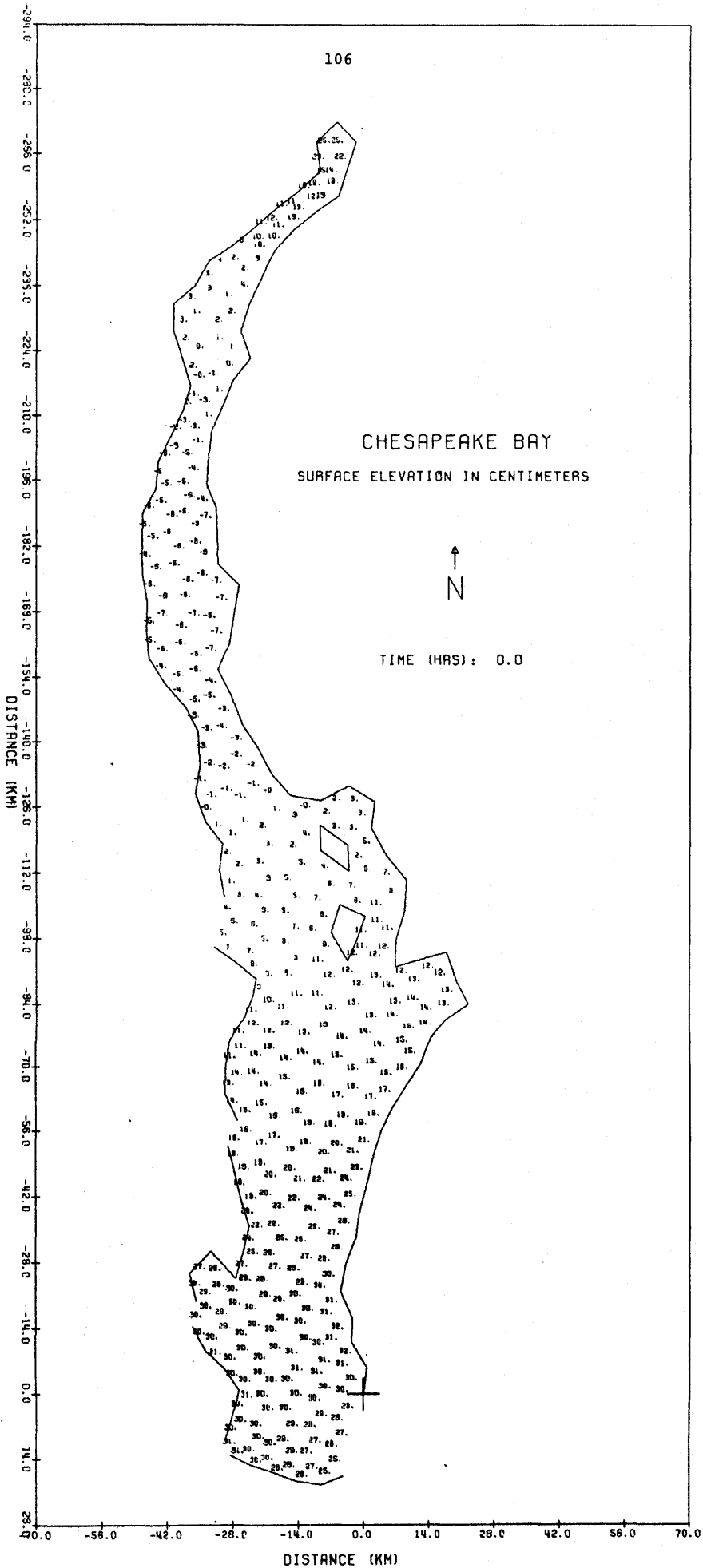


Figures B.1 - B.16. Water elevation and circulation of the Chesapeake Bay in a tidal cycle.

CHESAPEAKE BAY  
SURFACE ELEVATION IN CENTIMETERS




TIME (HRS): 0.0



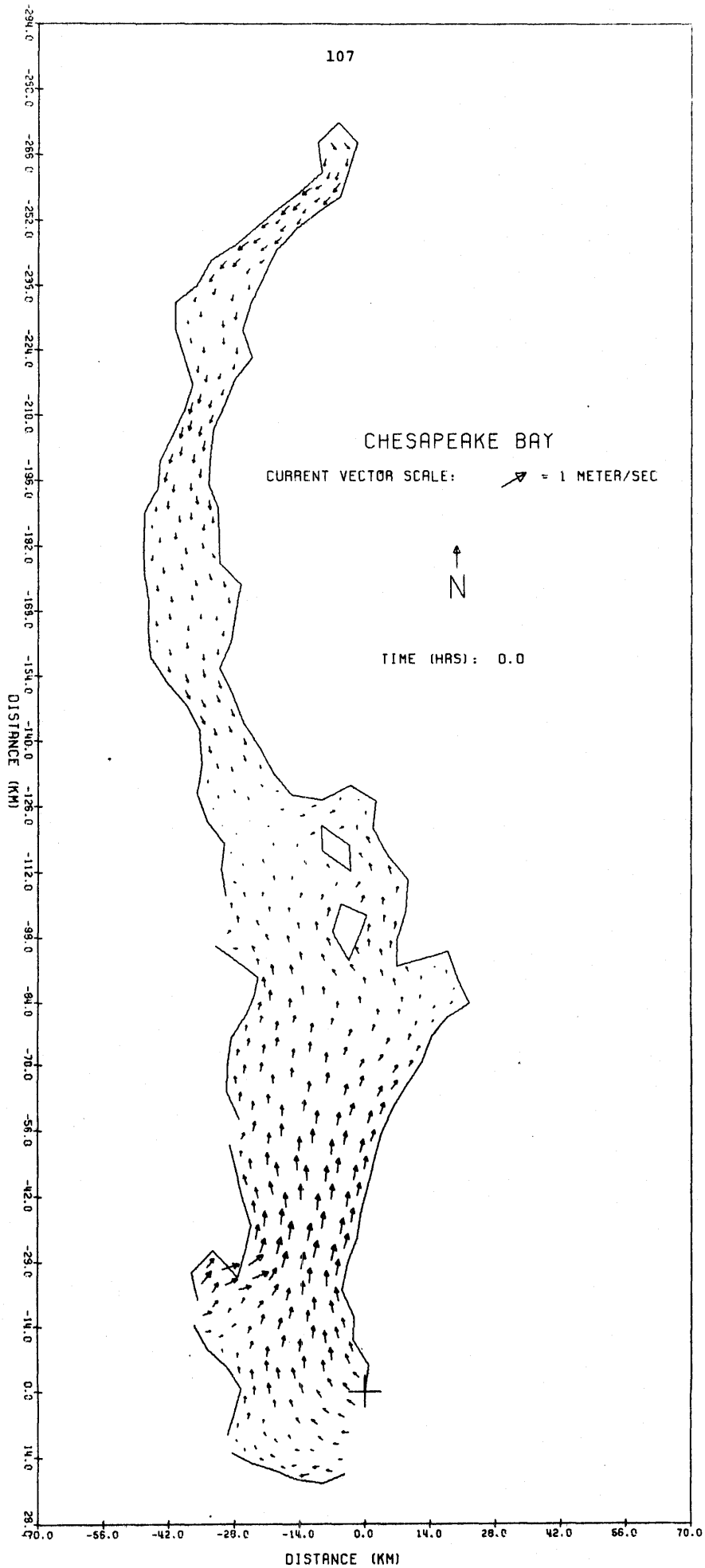
107

### CHESAPEAKE BAY

CURRENT VECTOR SCALE:  = 1 METER/SEC



TIME (HRS): 0.0

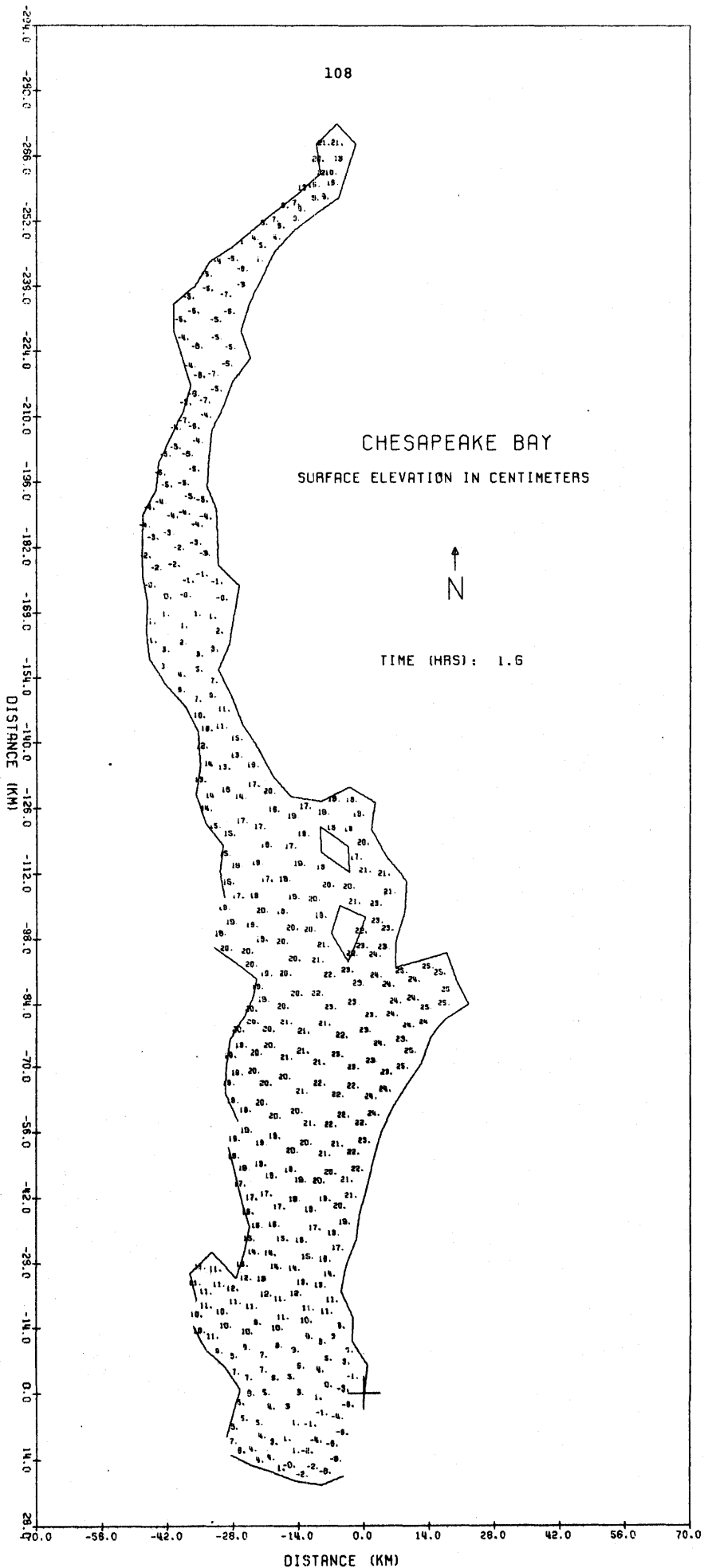


108

CHESAPEAKE BAY  
SURFACE ELEVATION IN CENTIMETERS




TIME (HRS): 1.6



109

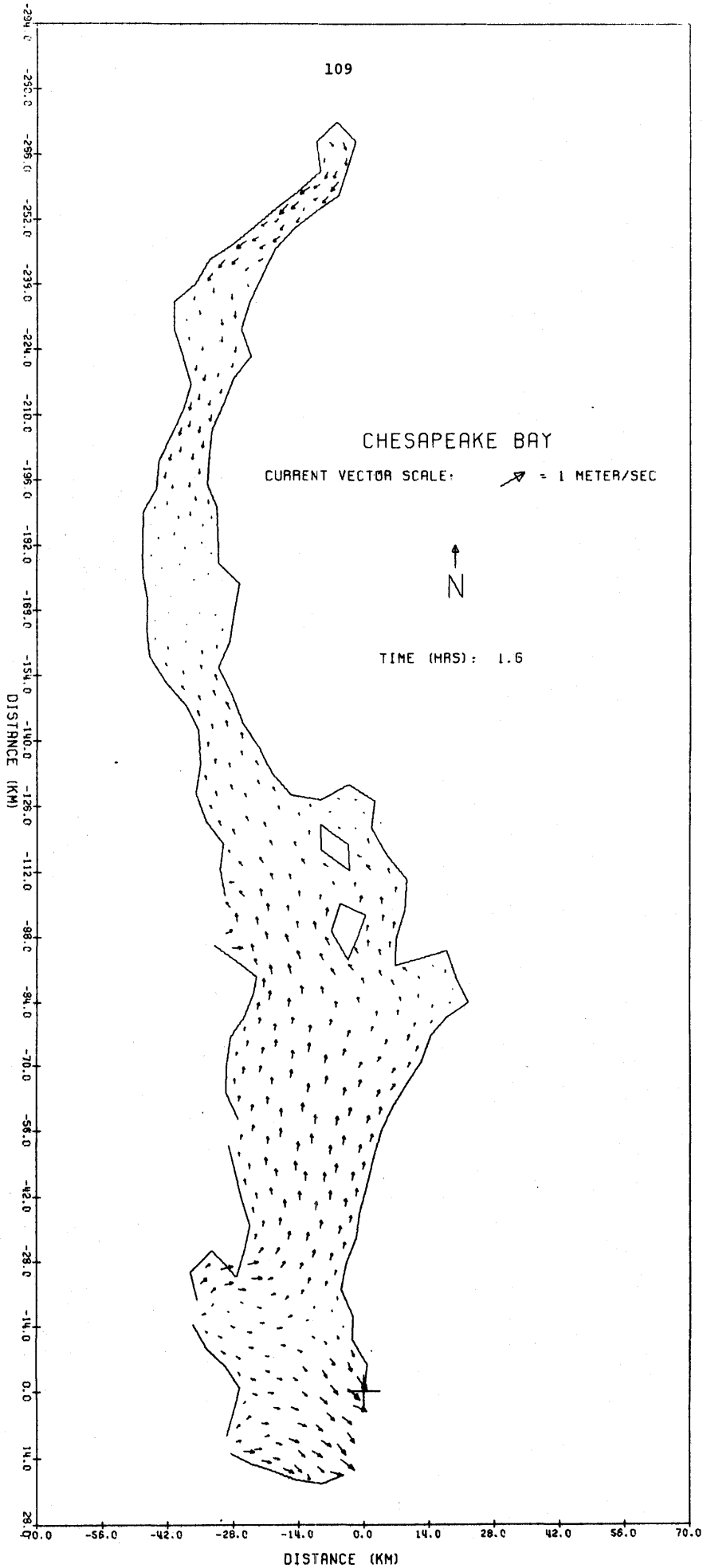
### CHESAPEAKE BAY

CURRENT VECTOR SCALE:  = 1 METER/SEC



TIME (HRS): 1.6

DISTANCE (KM)




DISTANCE (KM)



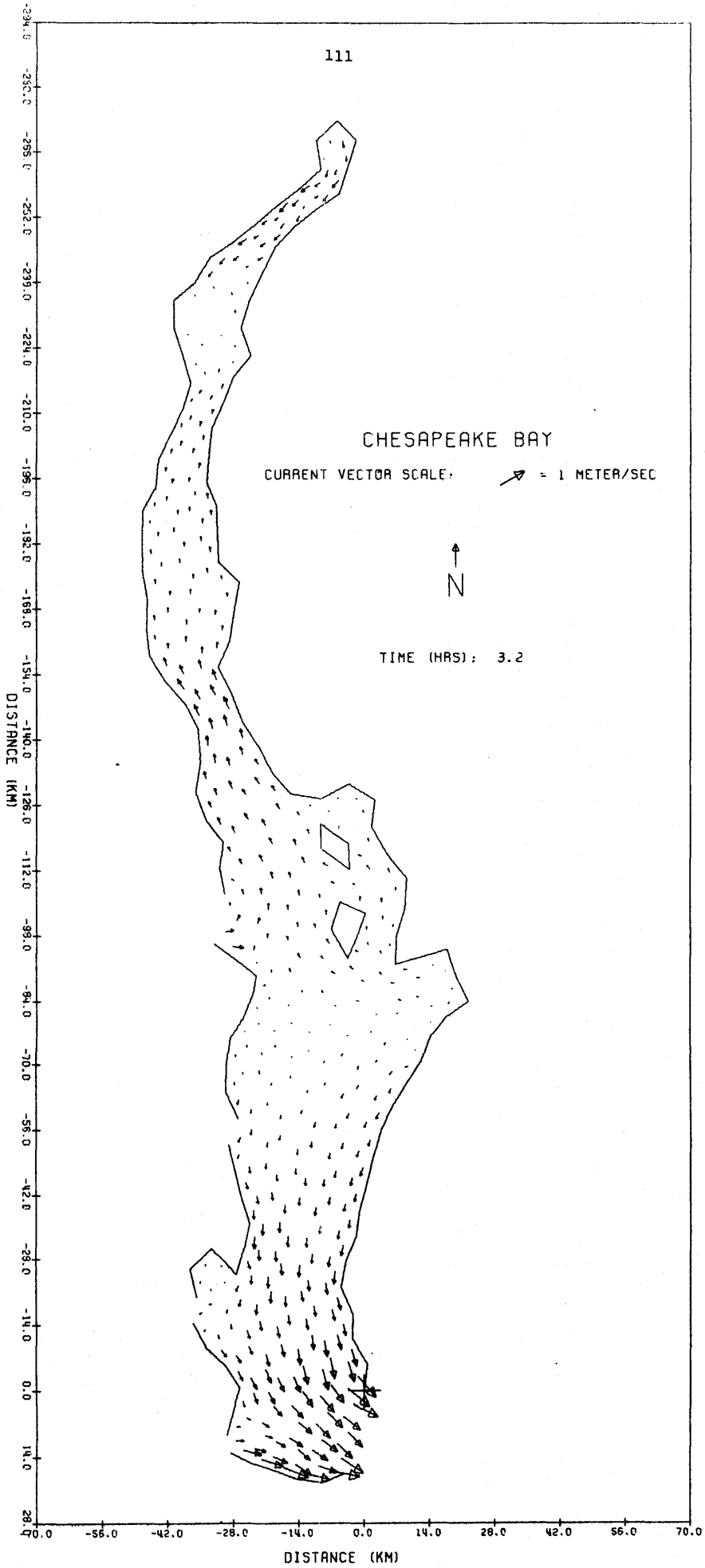
111

### CHESAPEAKE BAY

CURRENT VECTOR SCALE:  = 1 METER/SEC



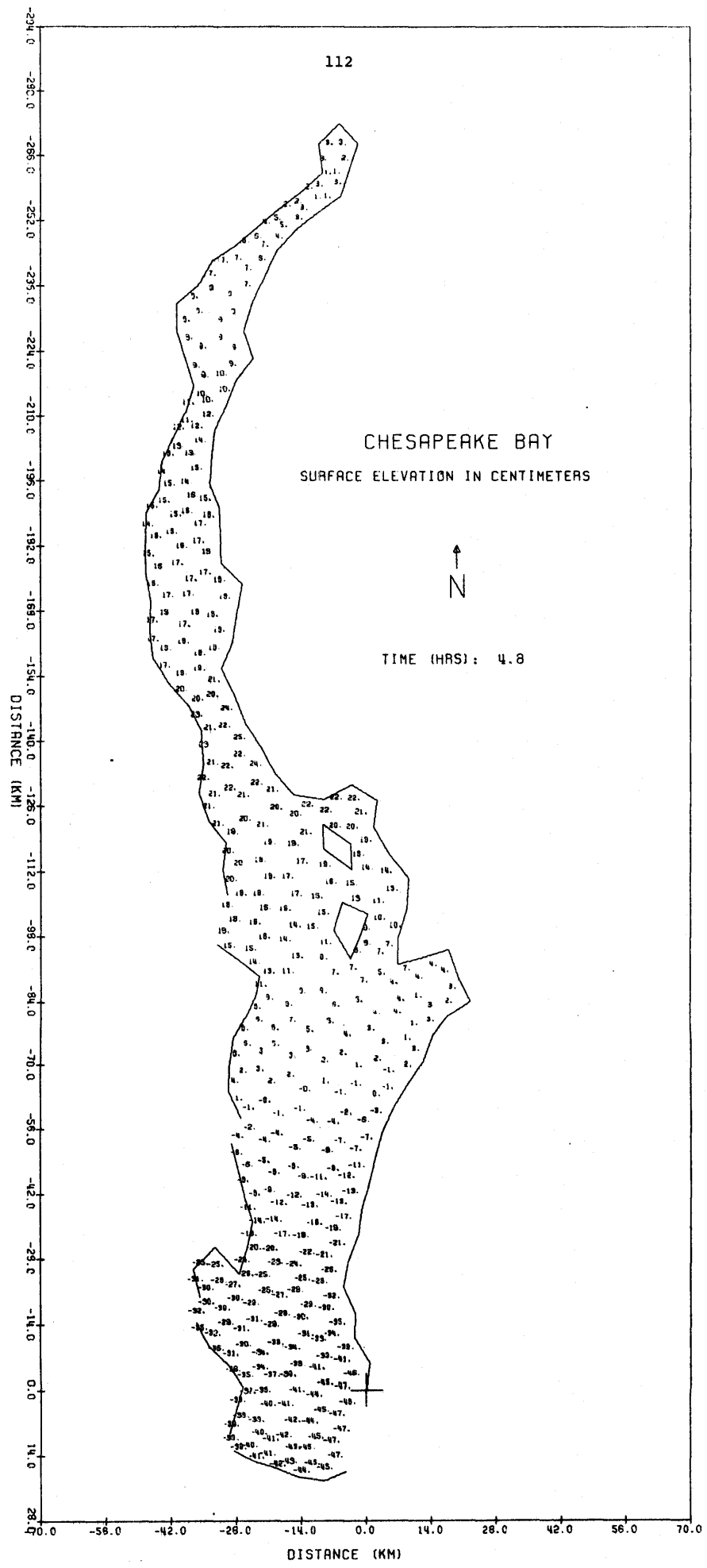
TIME (HRS): 3.2



CHESAPEAKE BAY  
SURFACE ELEVATION IN CENTIMETERS




TIME (HRS): 4.8





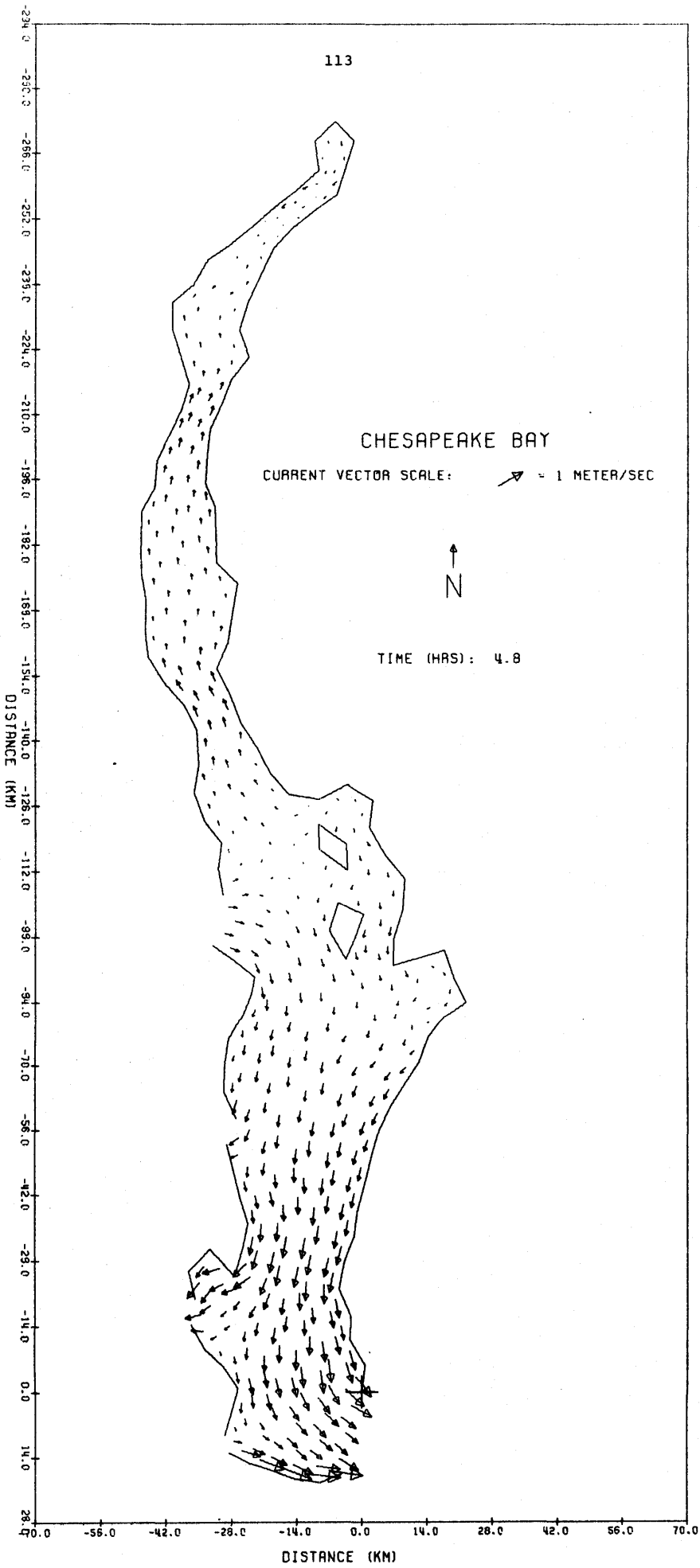
113

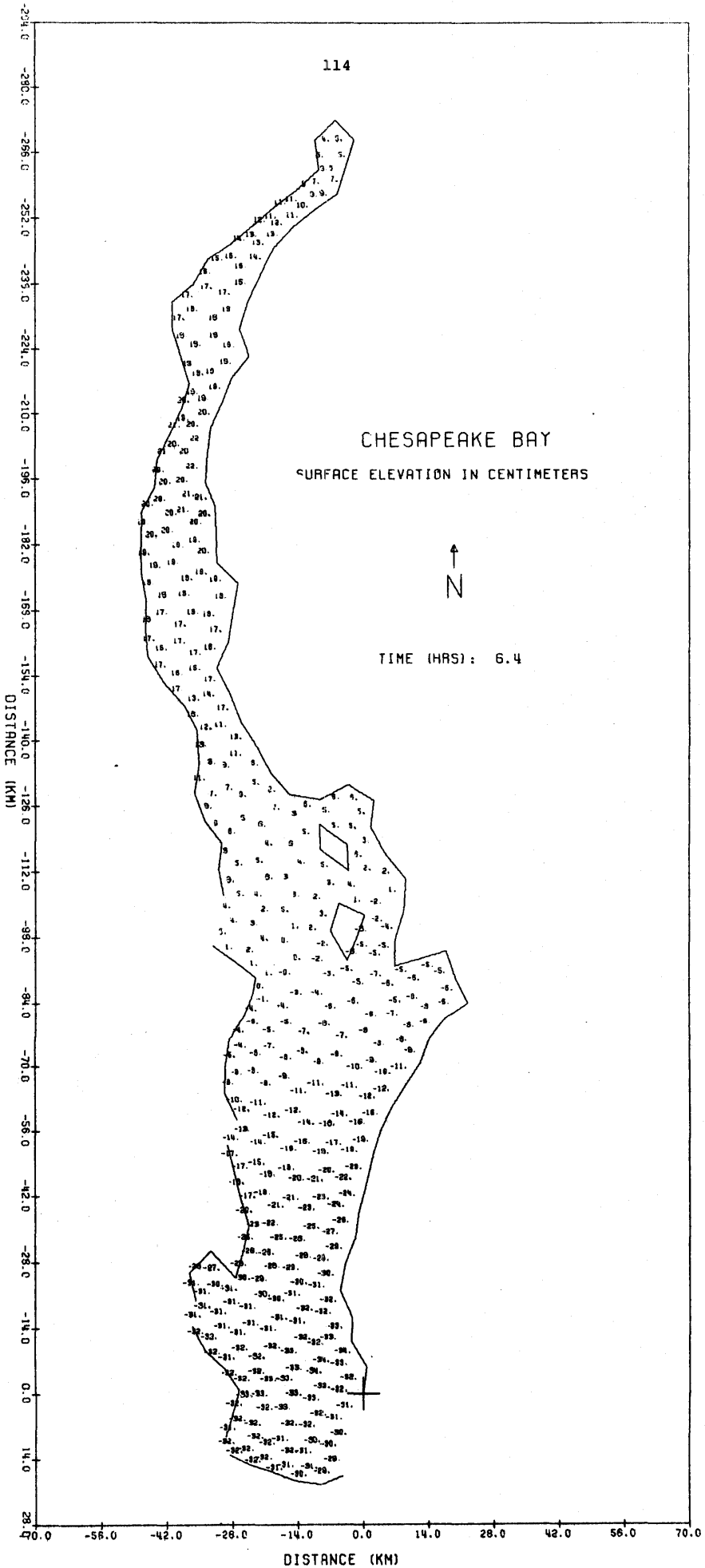
CHESAPEAKE BAY

CURRENT VECTOR SCALE:  = 1 METER/SEC




TIME (HRS): 4.8





115

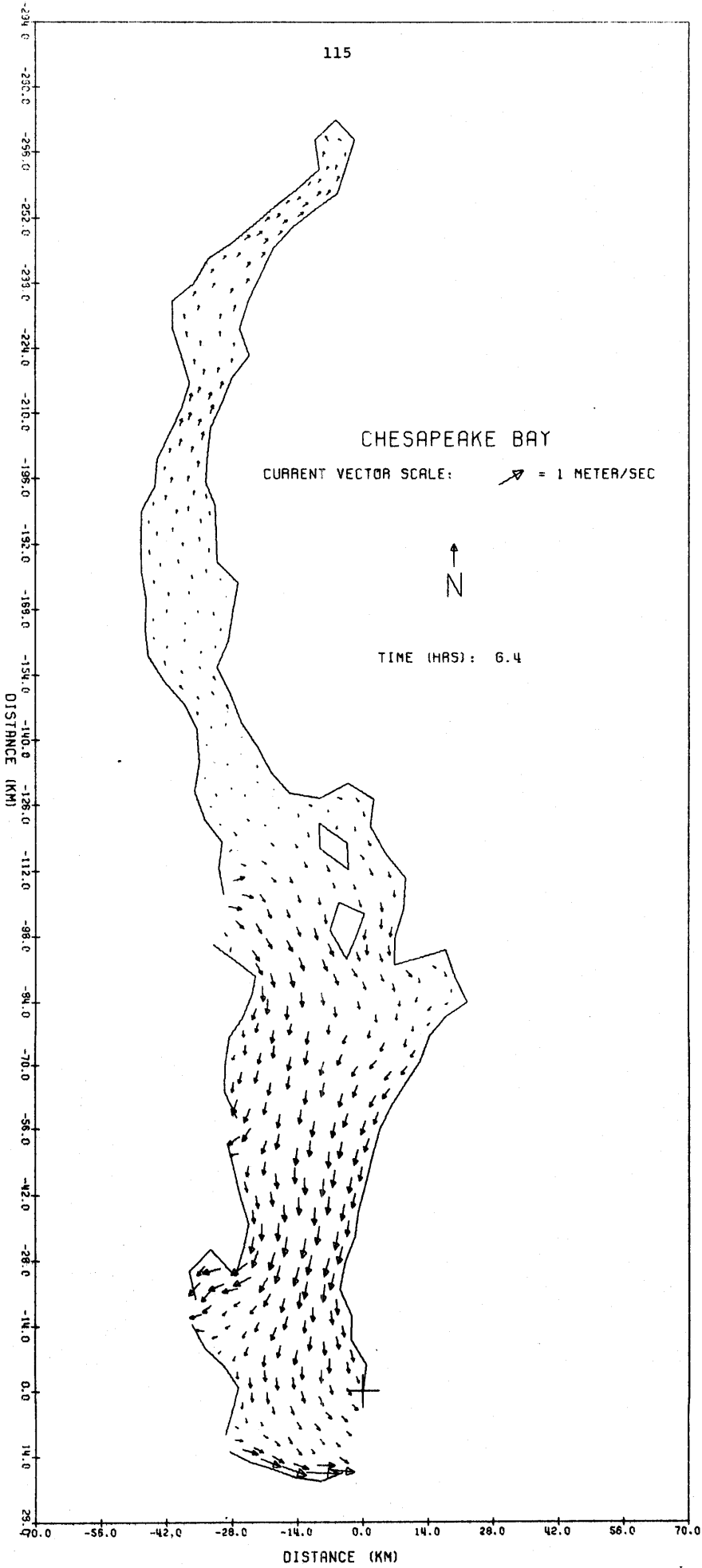
### CHESAPEAKE BAY

CURRENT VECTOR SCALE:  = 1 METER/SEC



TIME (HRS): 6.4

DISTANCE (KM)



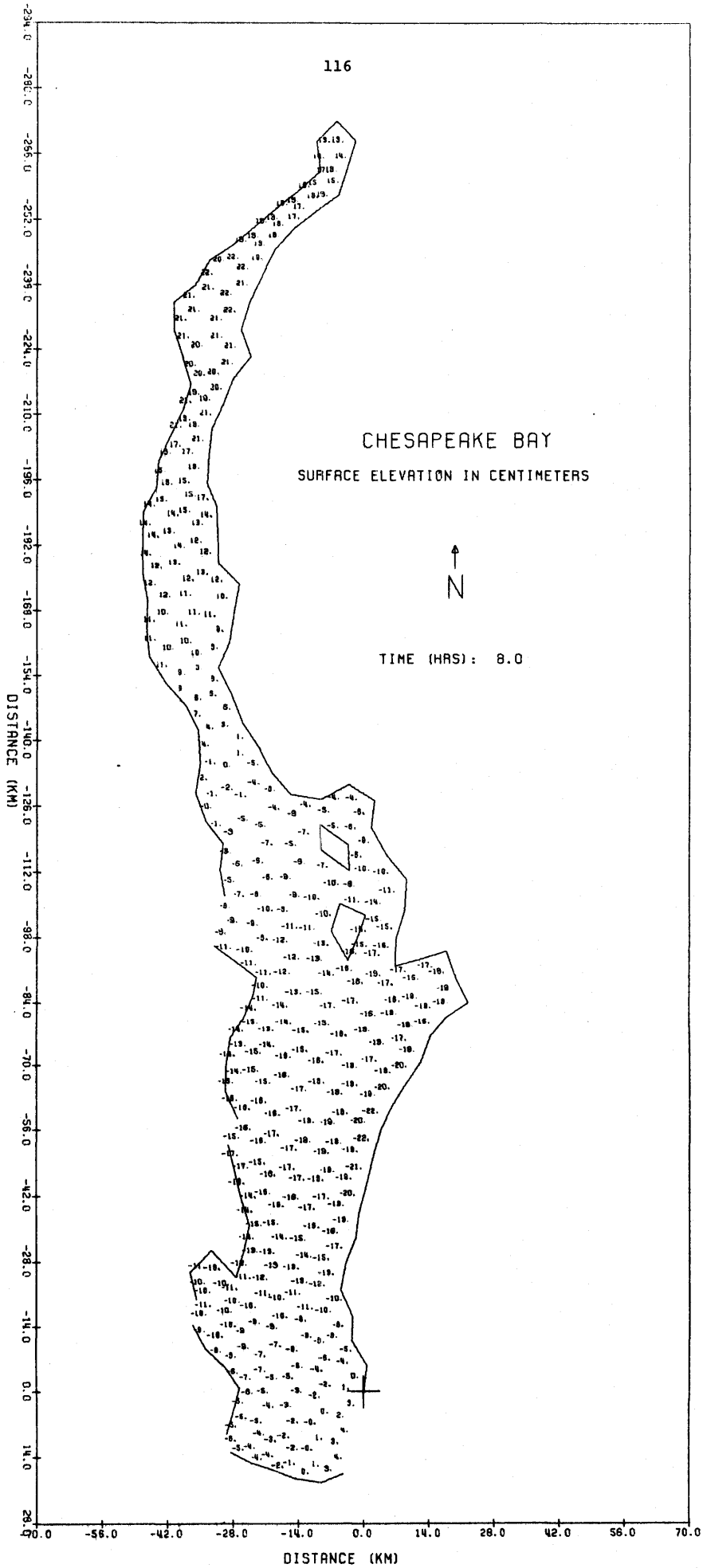
DISTANCE (KM)

116

CHESAPEAKE BAY  
SURFACE ELEVATION IN CENTIMETERS




TIME (HRS): 8.0



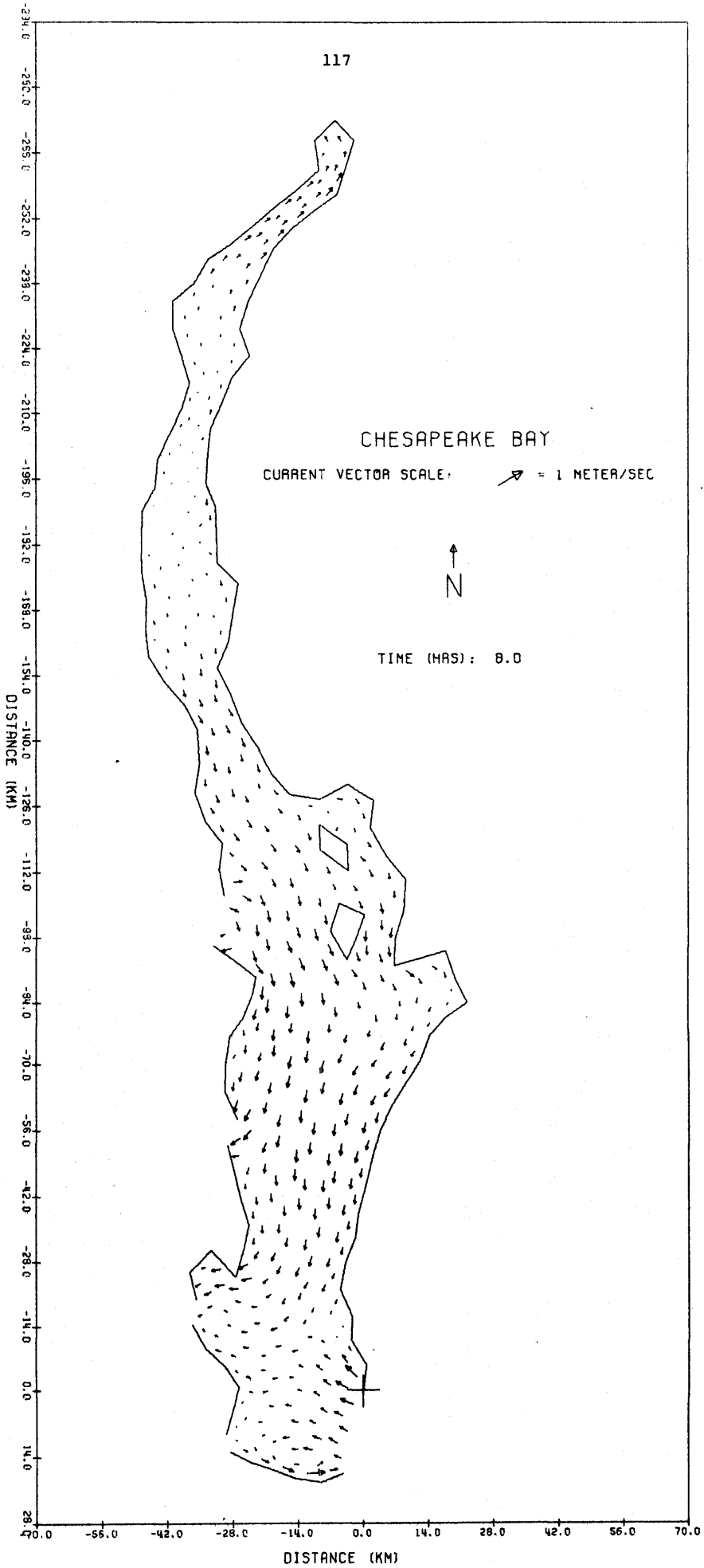
117

CHESAPEAKE BAY

CURRENT VECTOR SCALE:  = 1 METER/SEC



TIME (HRS): 8.0

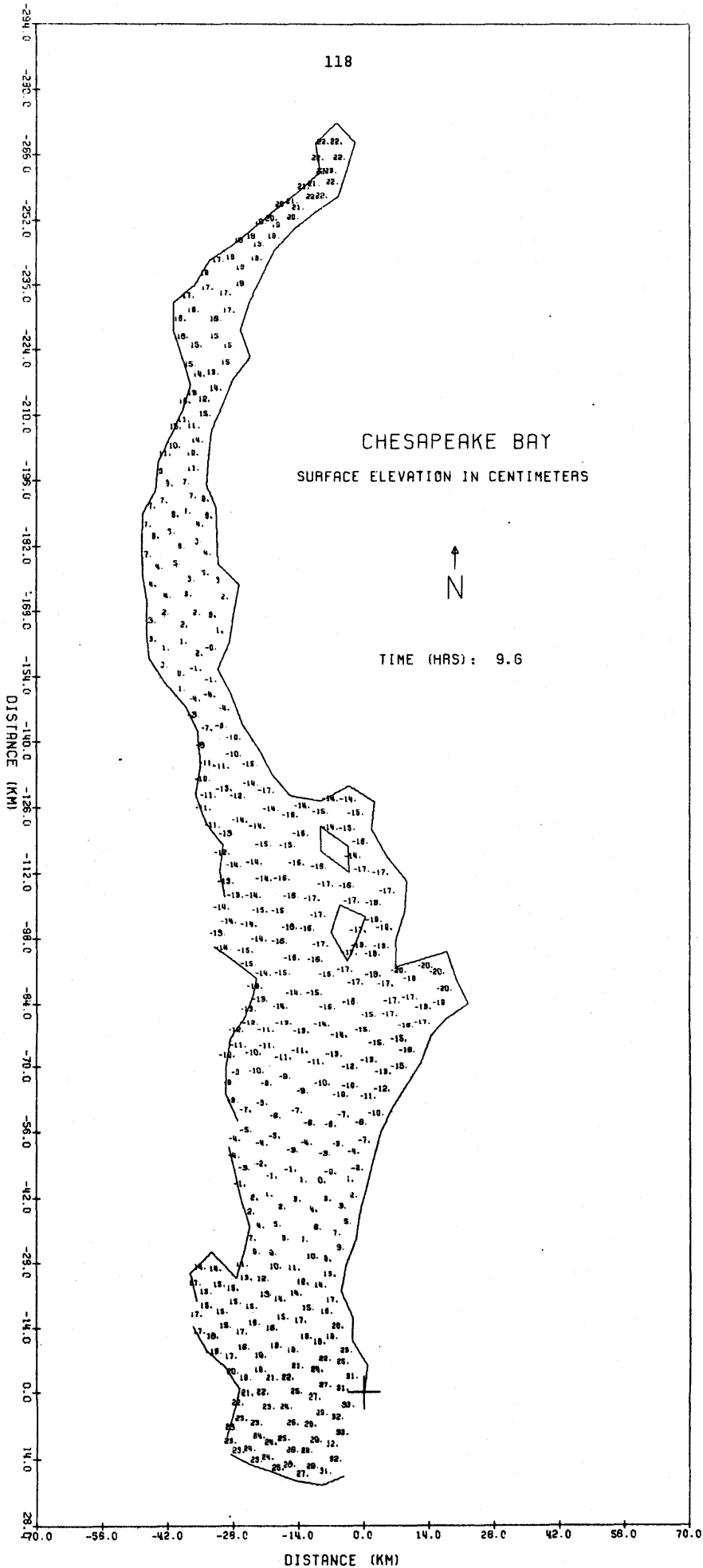


118

CHESAPEAKE BAY  
SURFACE ELEVATION IN CENTIMETERS




TIME (HRS): 9.6



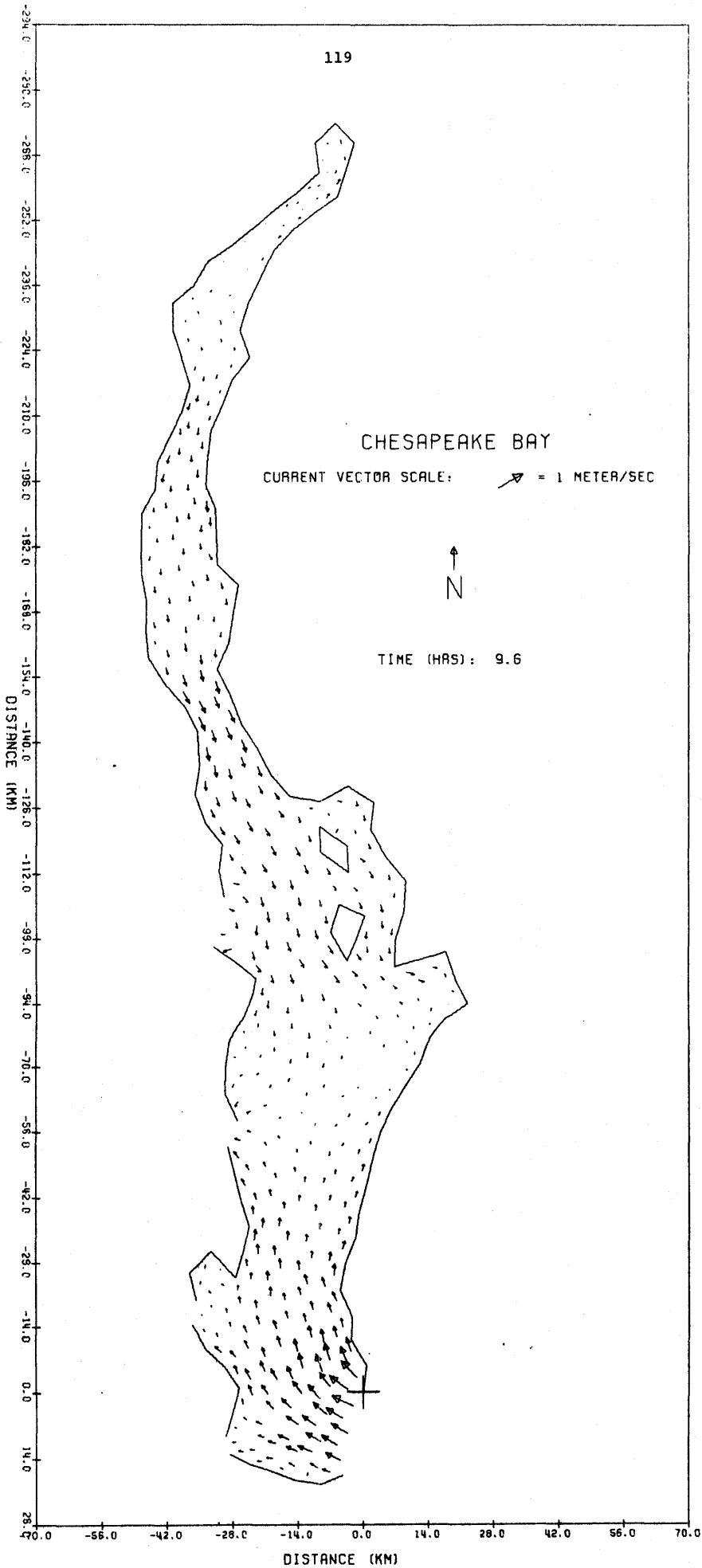
119

### CHESAPEAKE BAY

CURRENT VECTOR SCALE:  = 1 METER/SEC

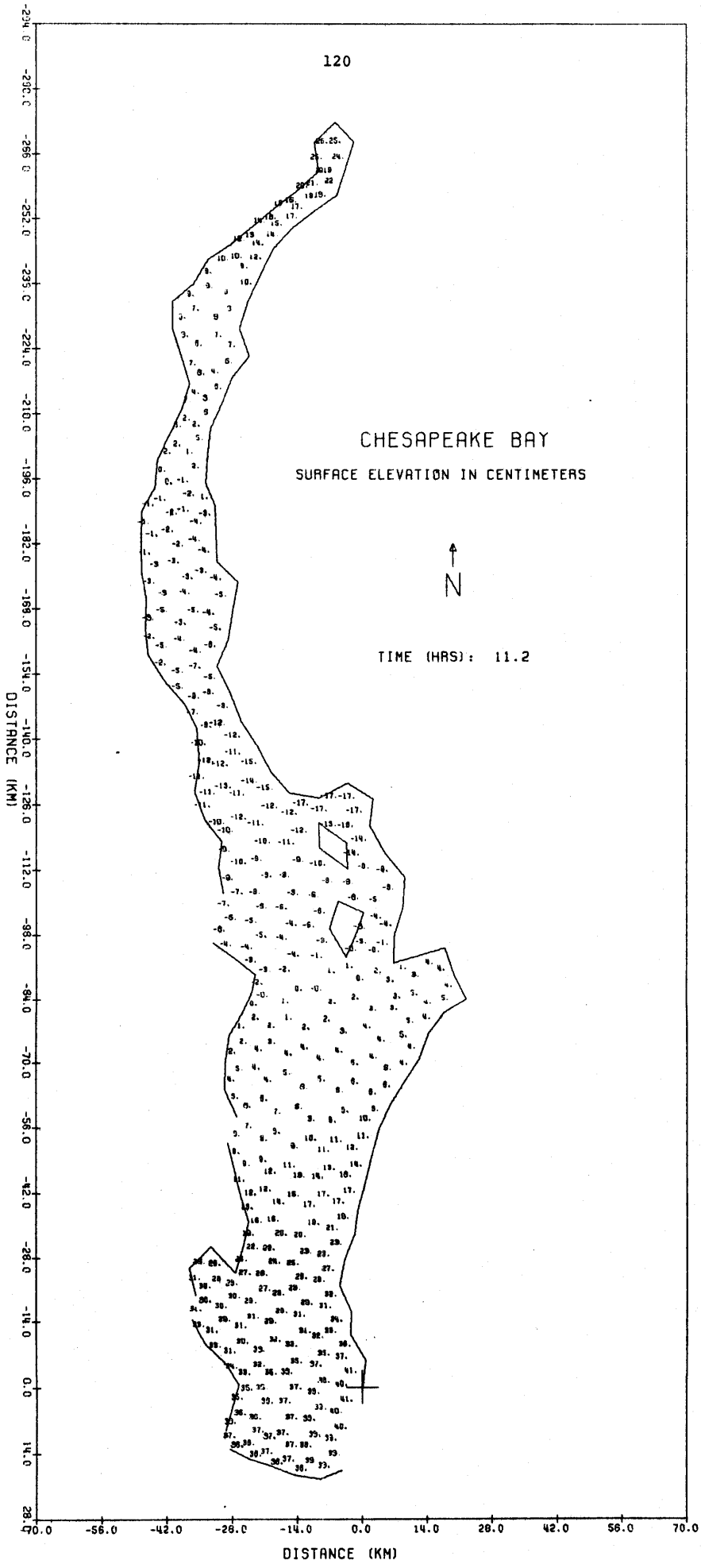


TIME (HRS): 9.6

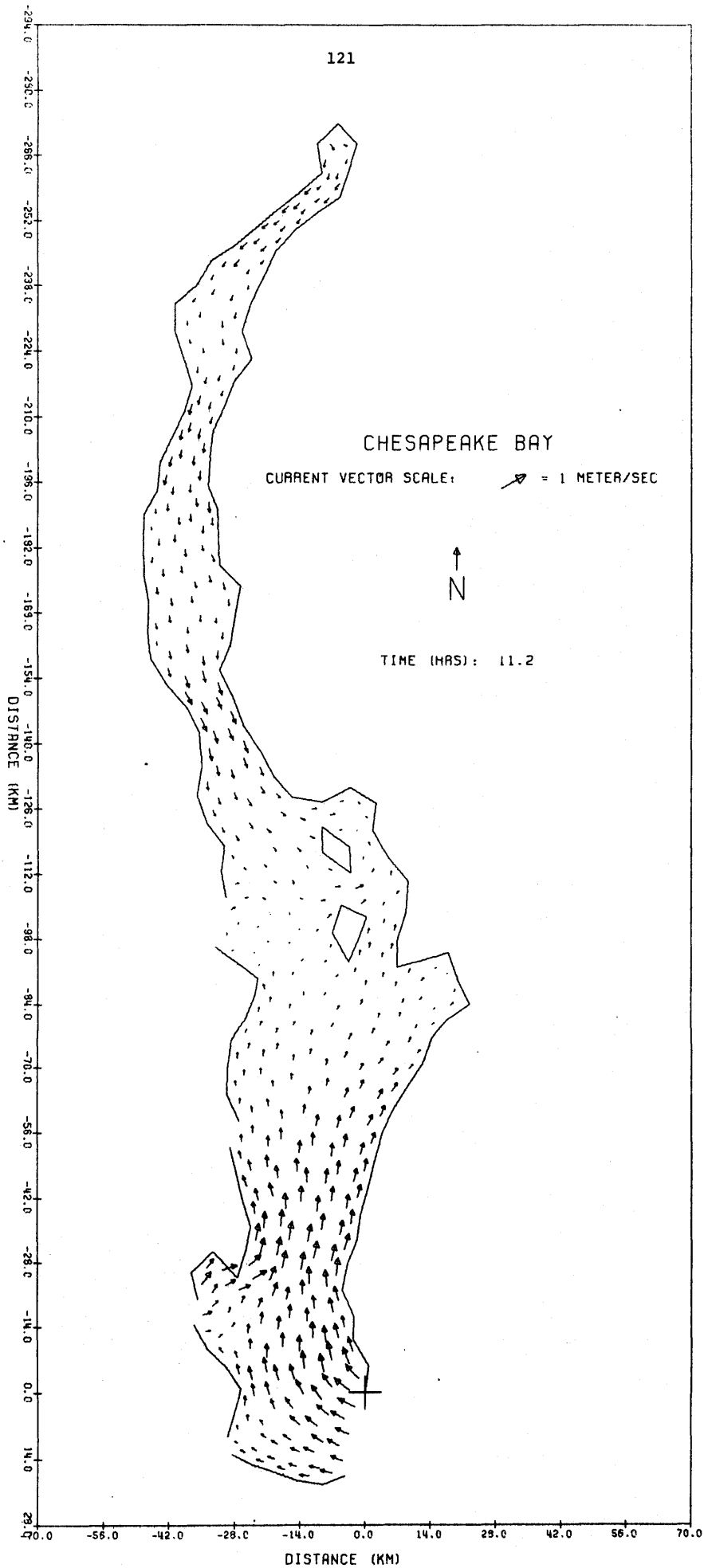


DISTANCE (KM)

DISTANCE (KM)







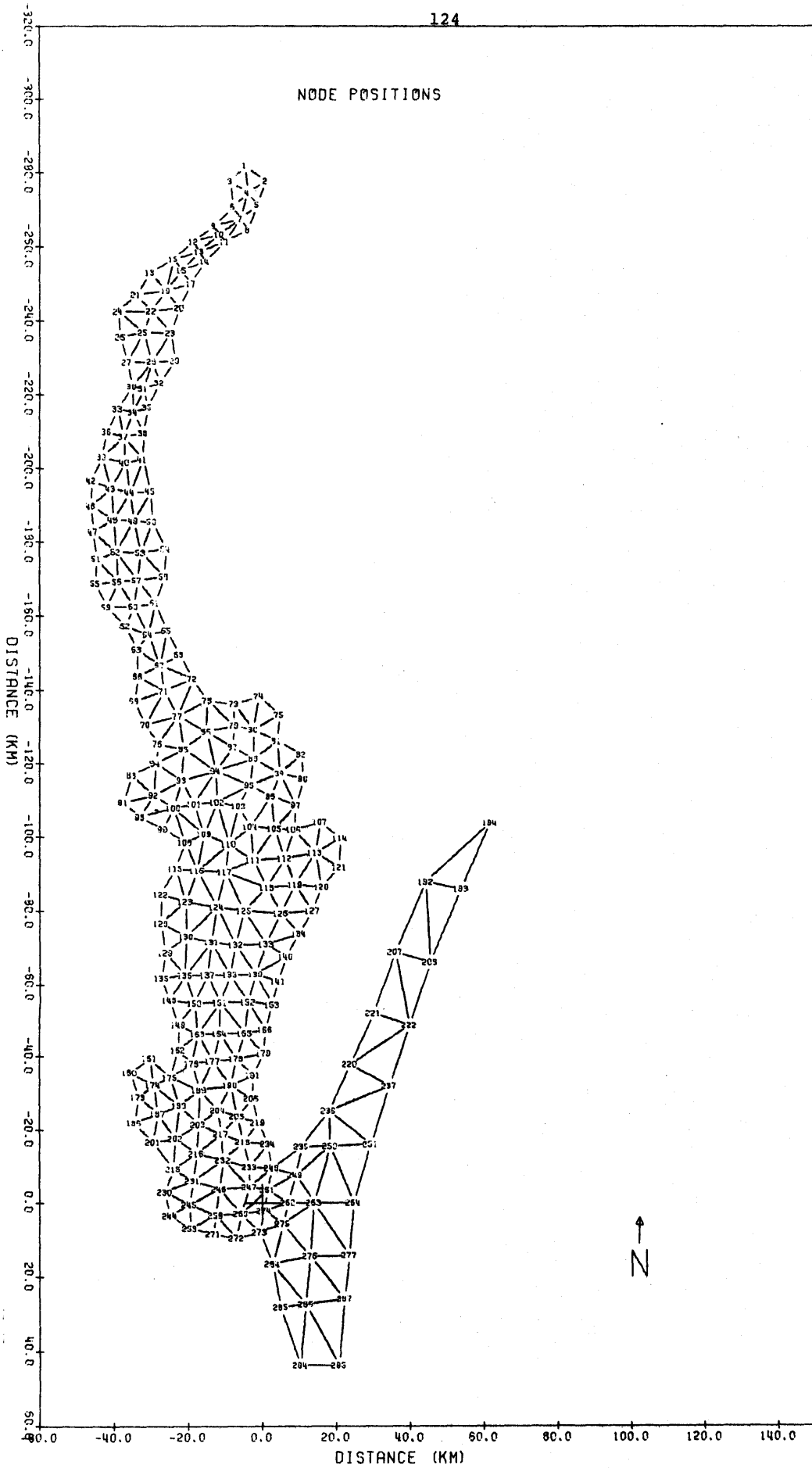
## APPENDIX C

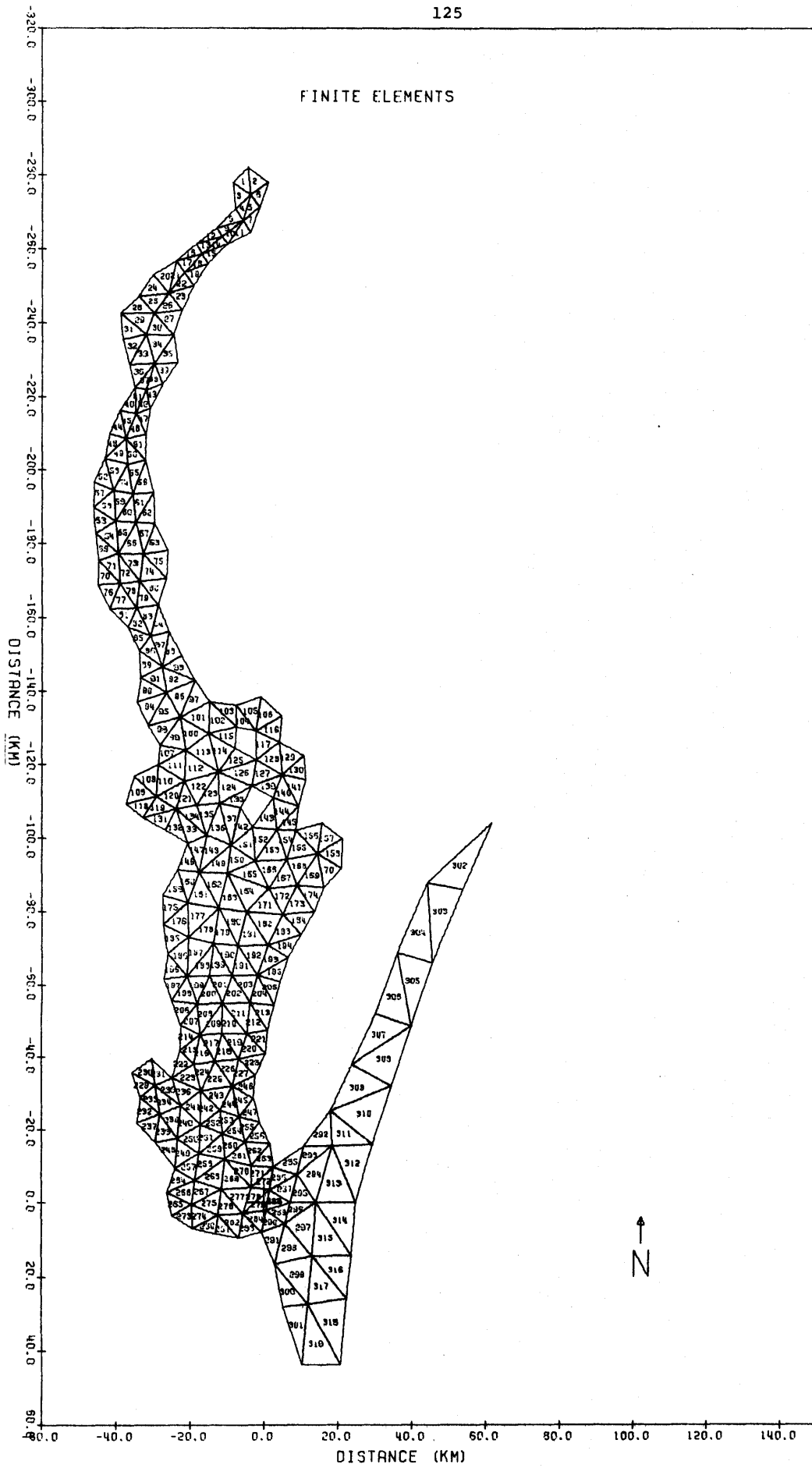
Storm Surge Hindcast in the Chesapeake Bay  
and its Virginia Atlantic Nearshore Ocean

This appendix presents a sequence of the calculated results of water elevation and flow circulation in the Chesapeake Bay and its Atlantic nearshore ocean due to the model hurricane Connie 1955. The water elevation is referred to the NGVD (1929). Included also are the enlarged finite element grid system for the bay, and the model hurricane track of Connie 1955, Figure 4.7, showing time history of position of the hurricane center.

Figures C.1 - C.25. Enlarged finite element network for the bay and the results of the storm surge hindcast of model hurricane Connie 1955.

NODE POSITIONS





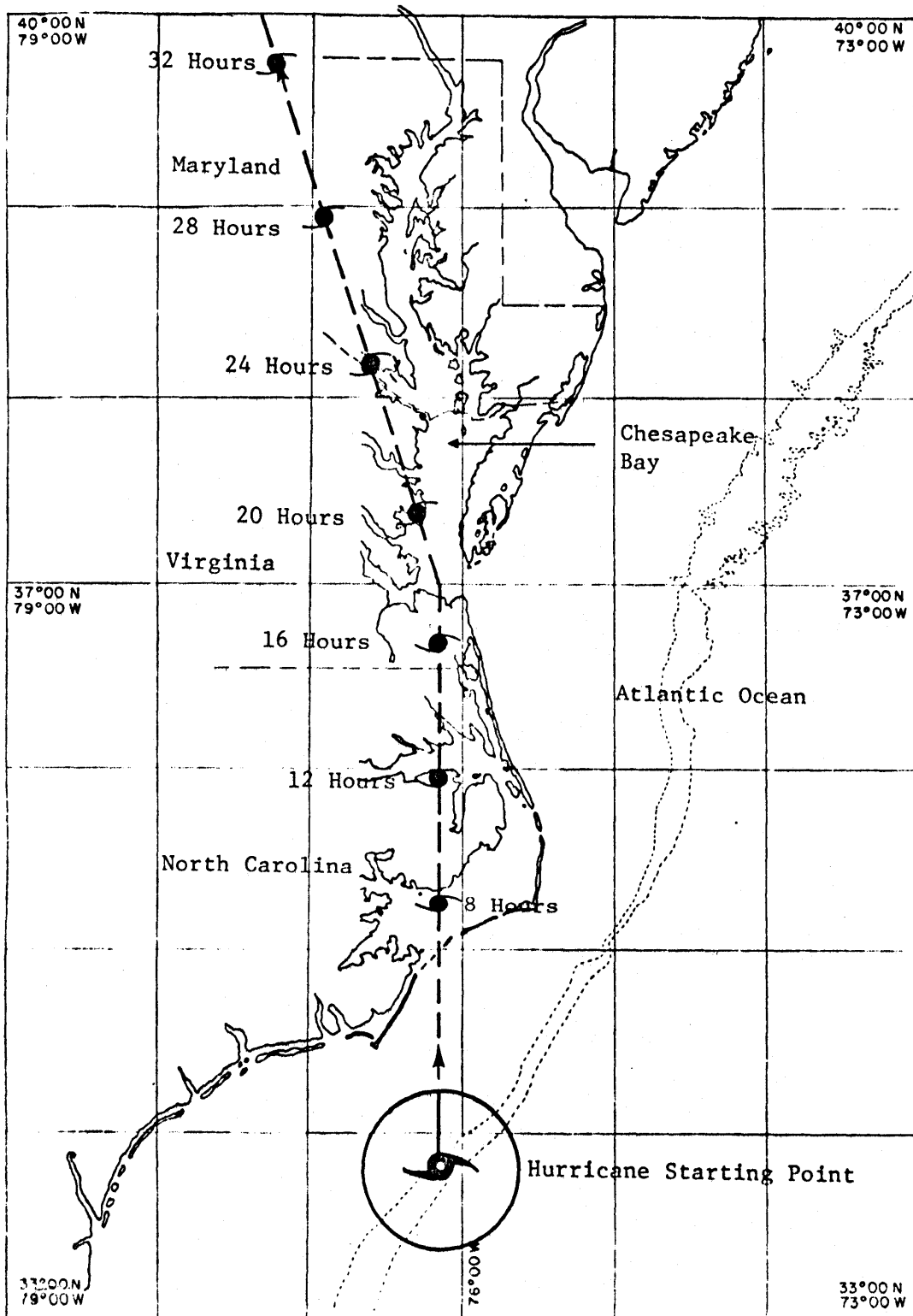
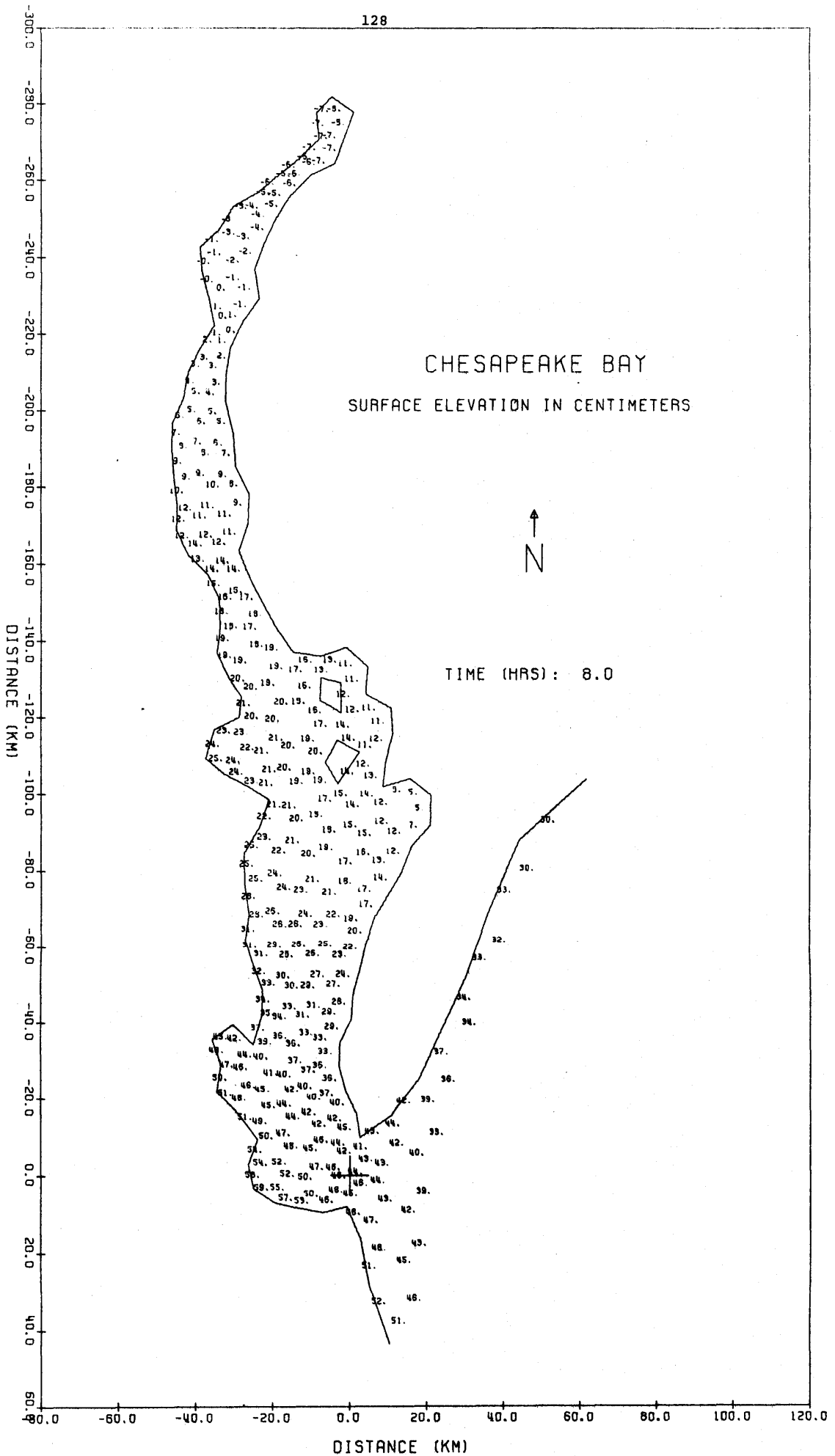
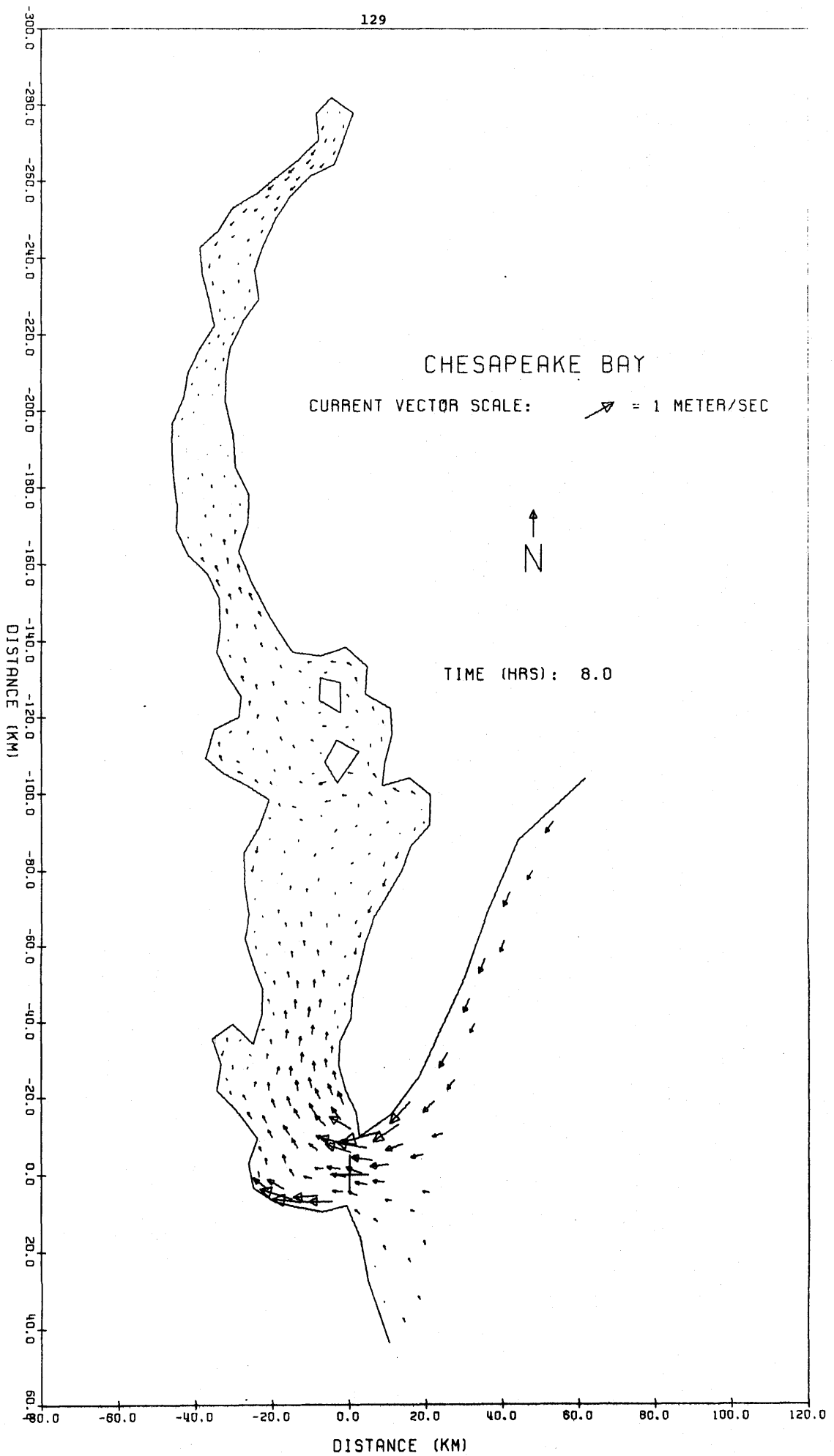


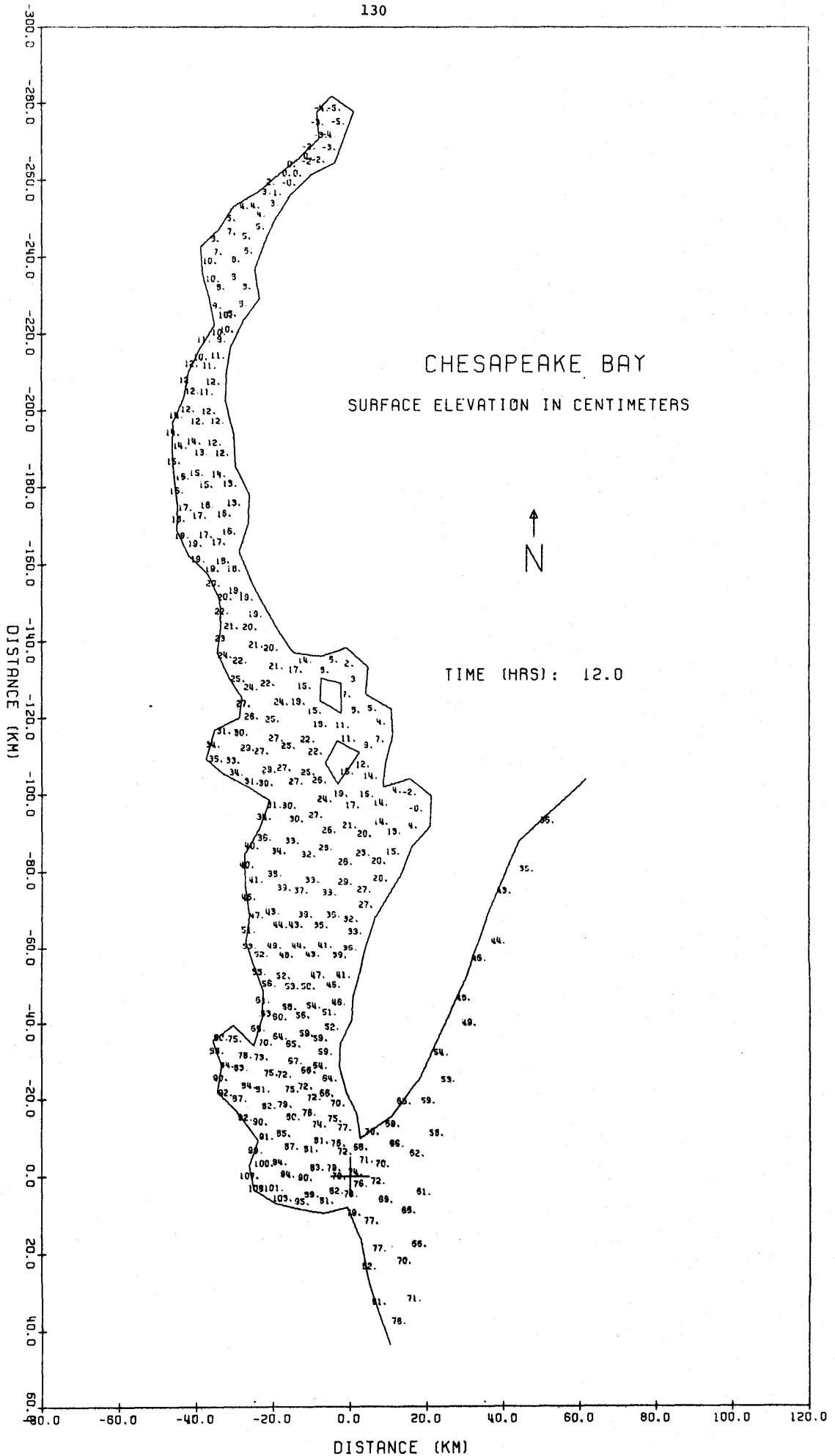
Figure 4.7. The model track of Hurricane Connie, 1955

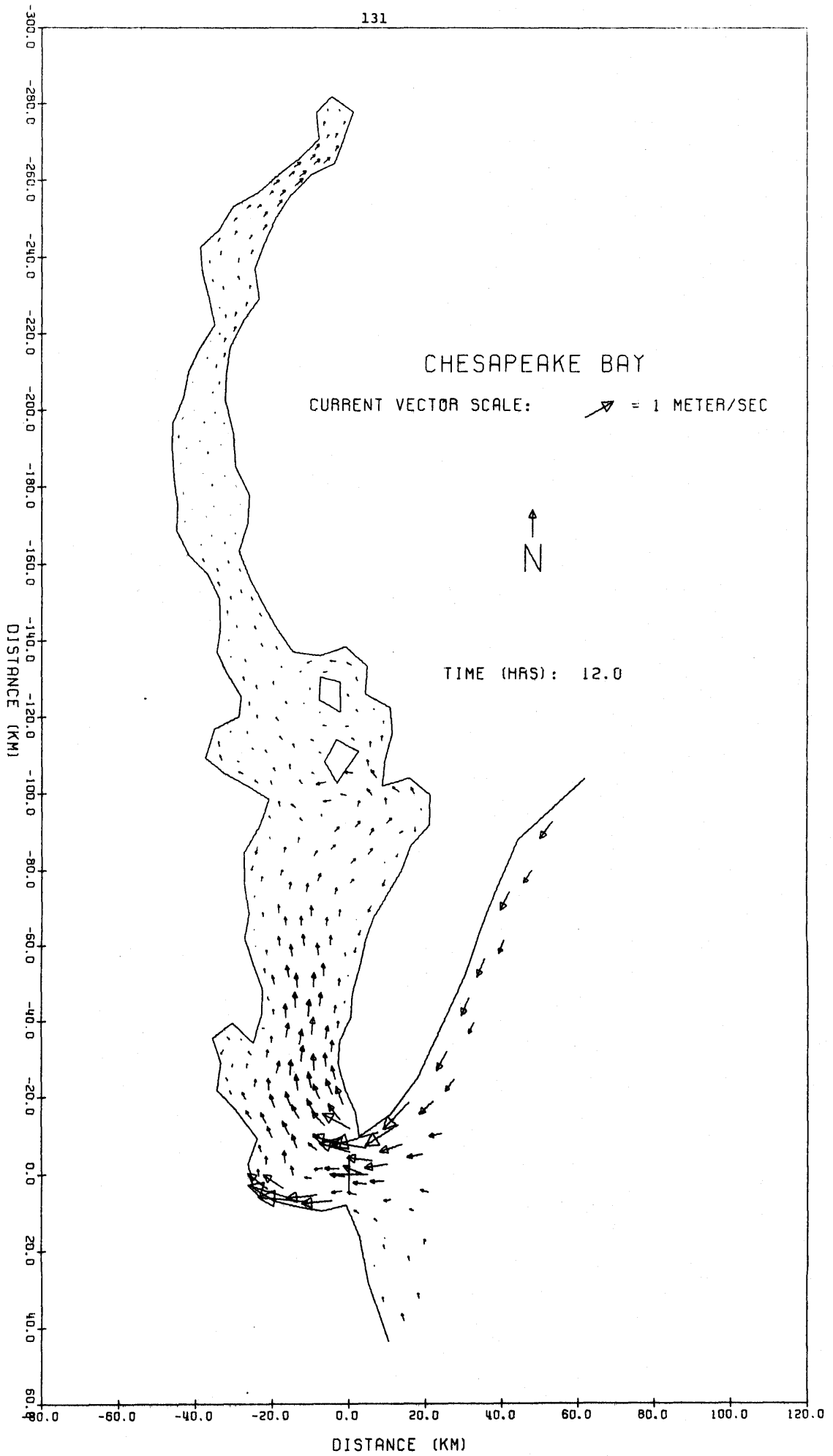


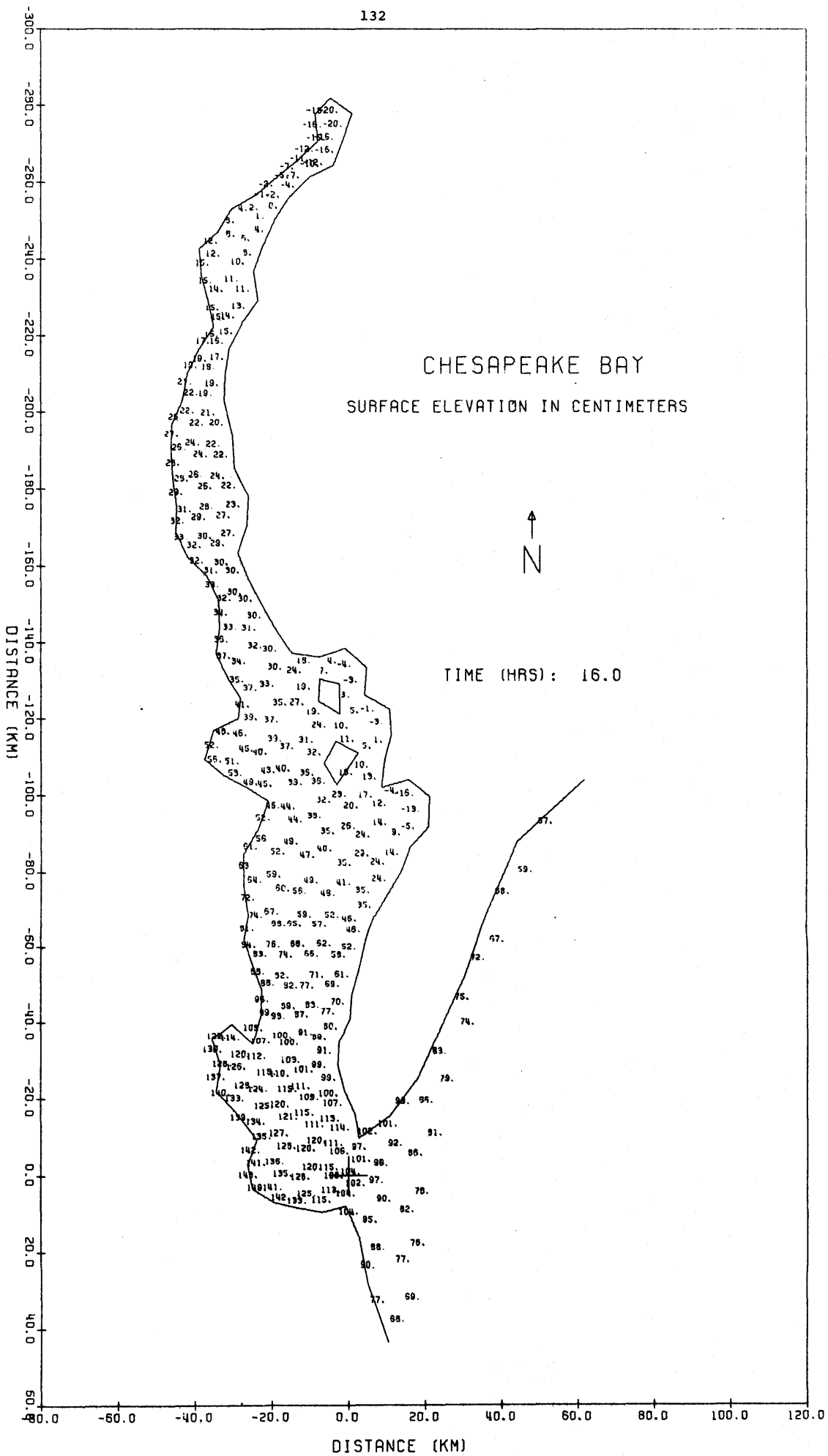


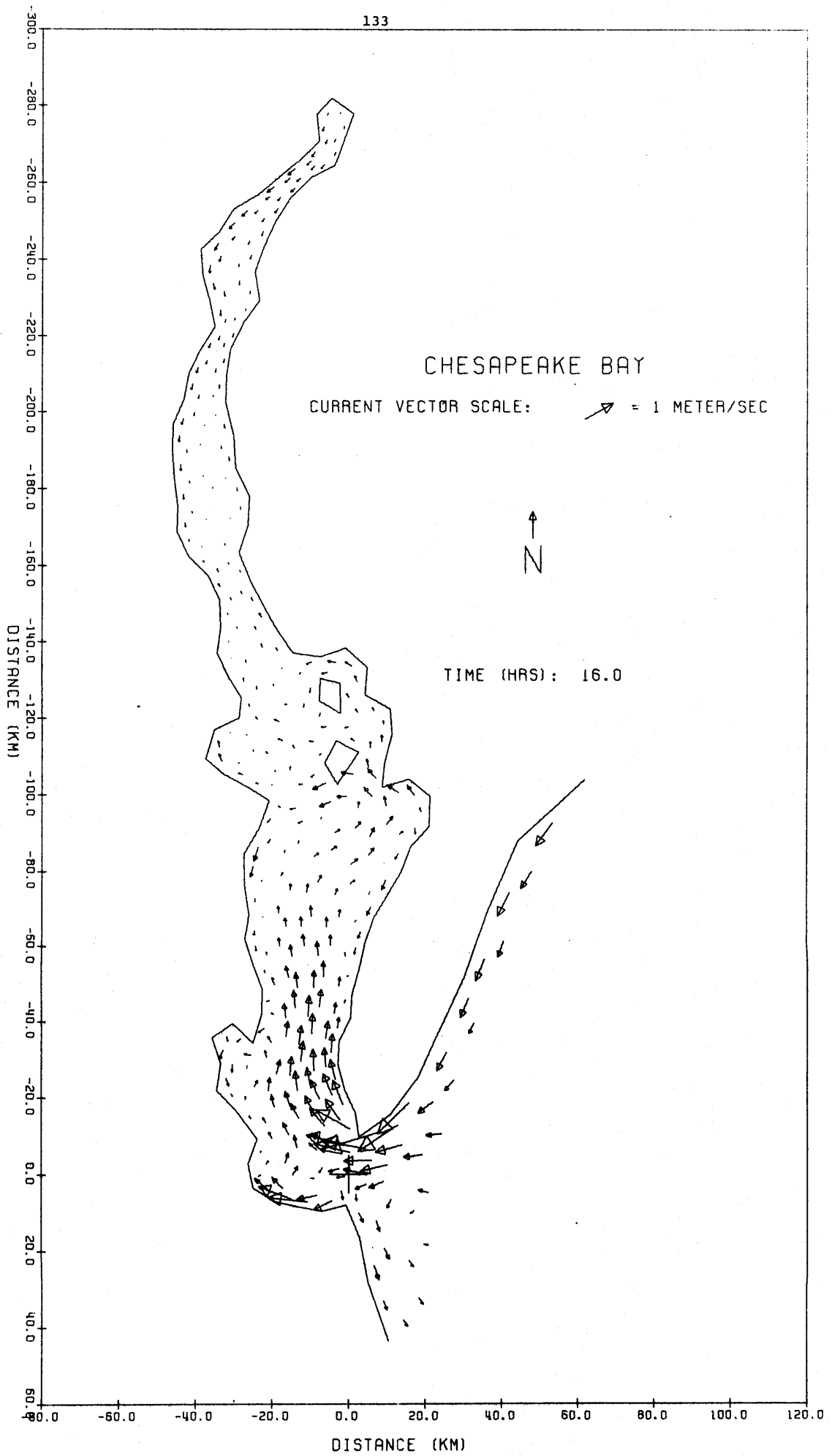


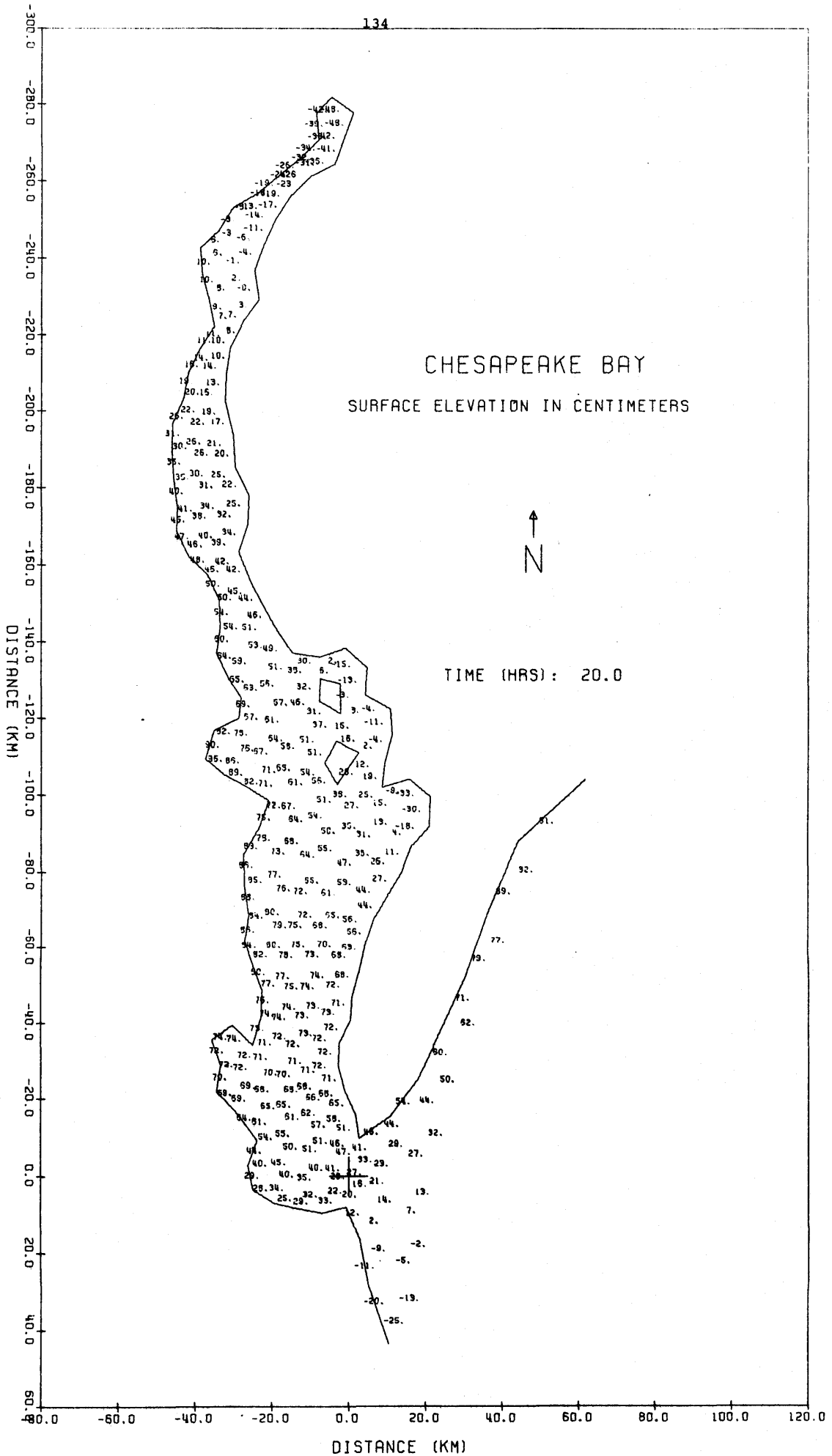


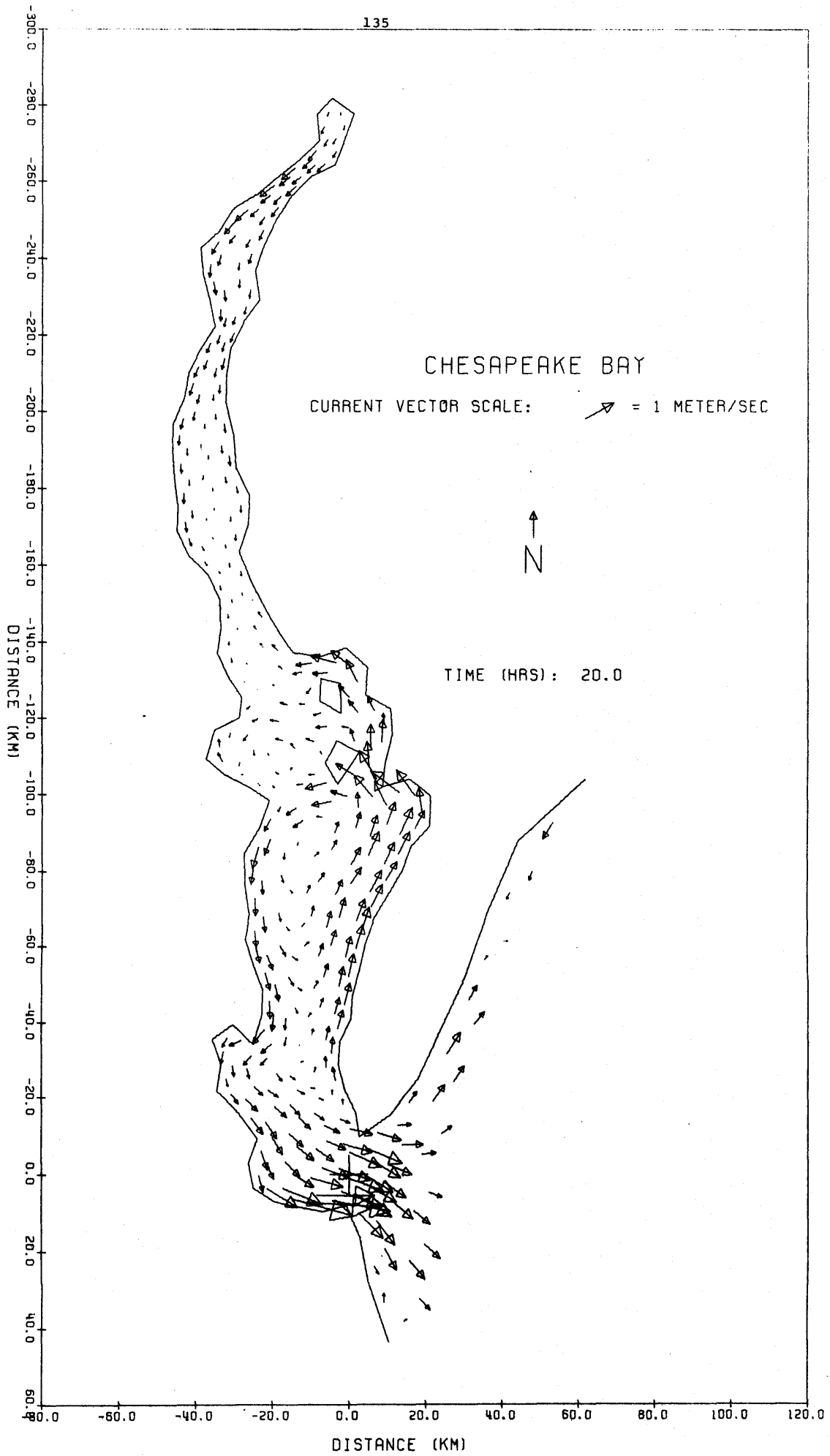


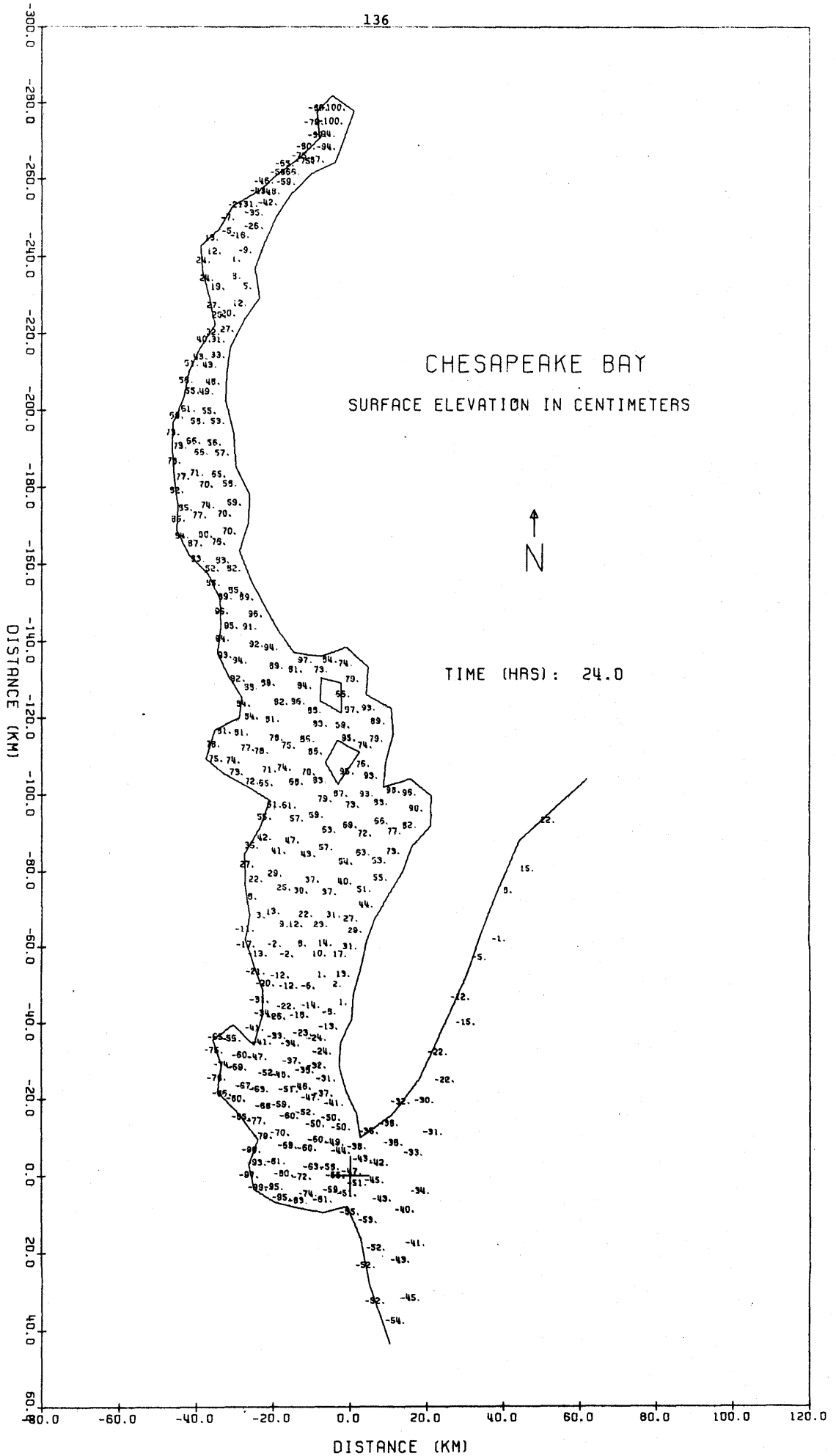




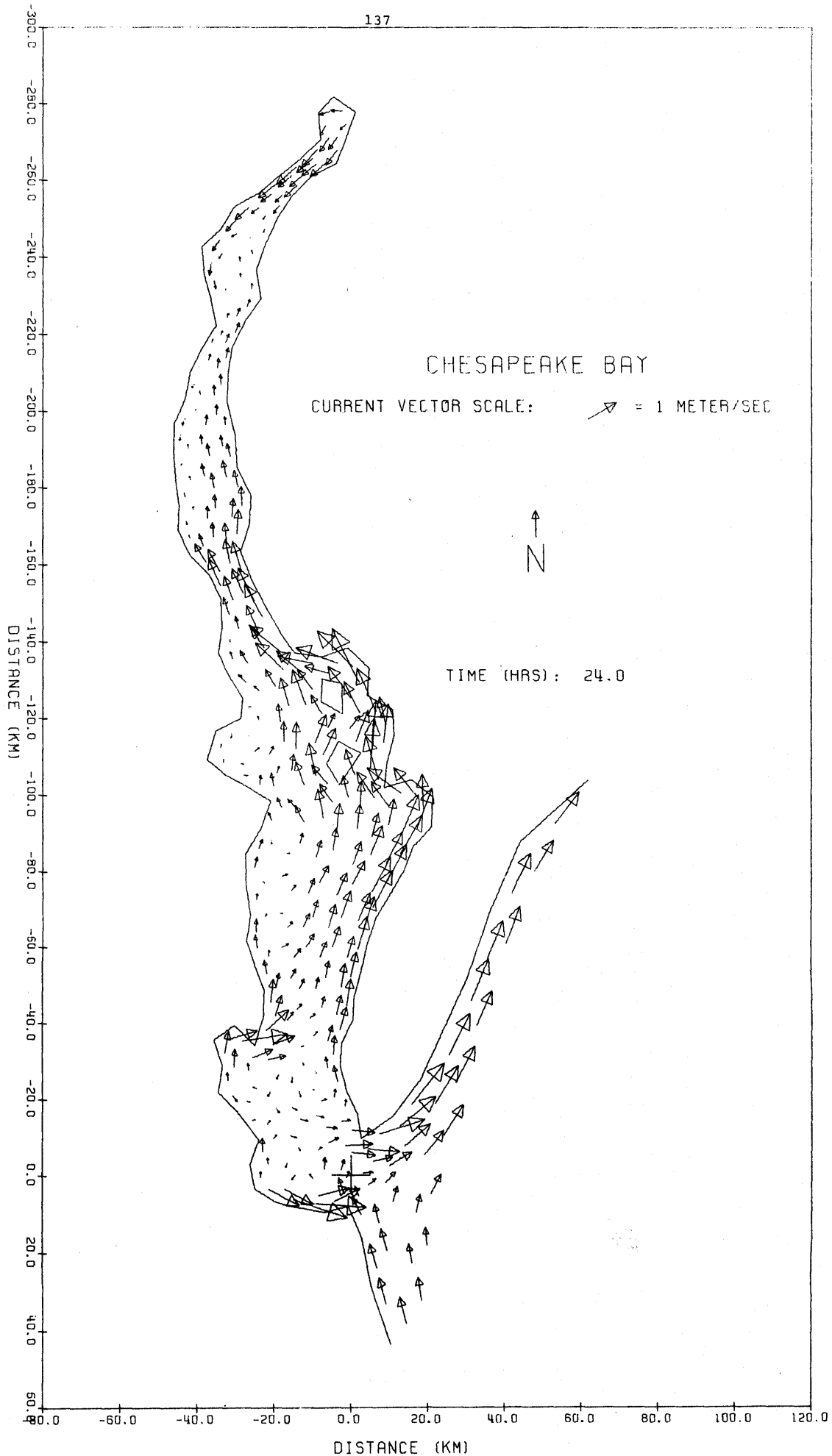


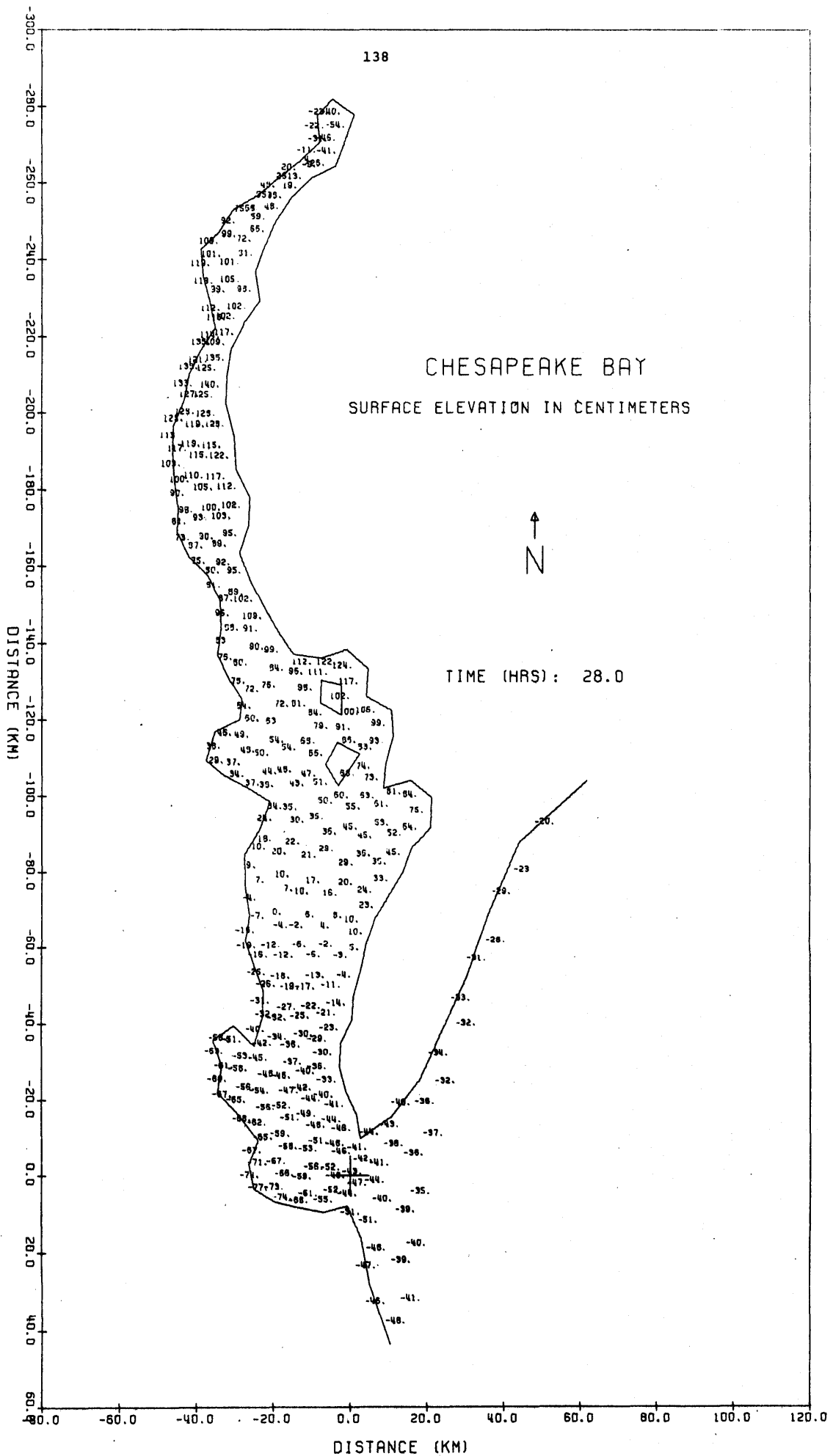


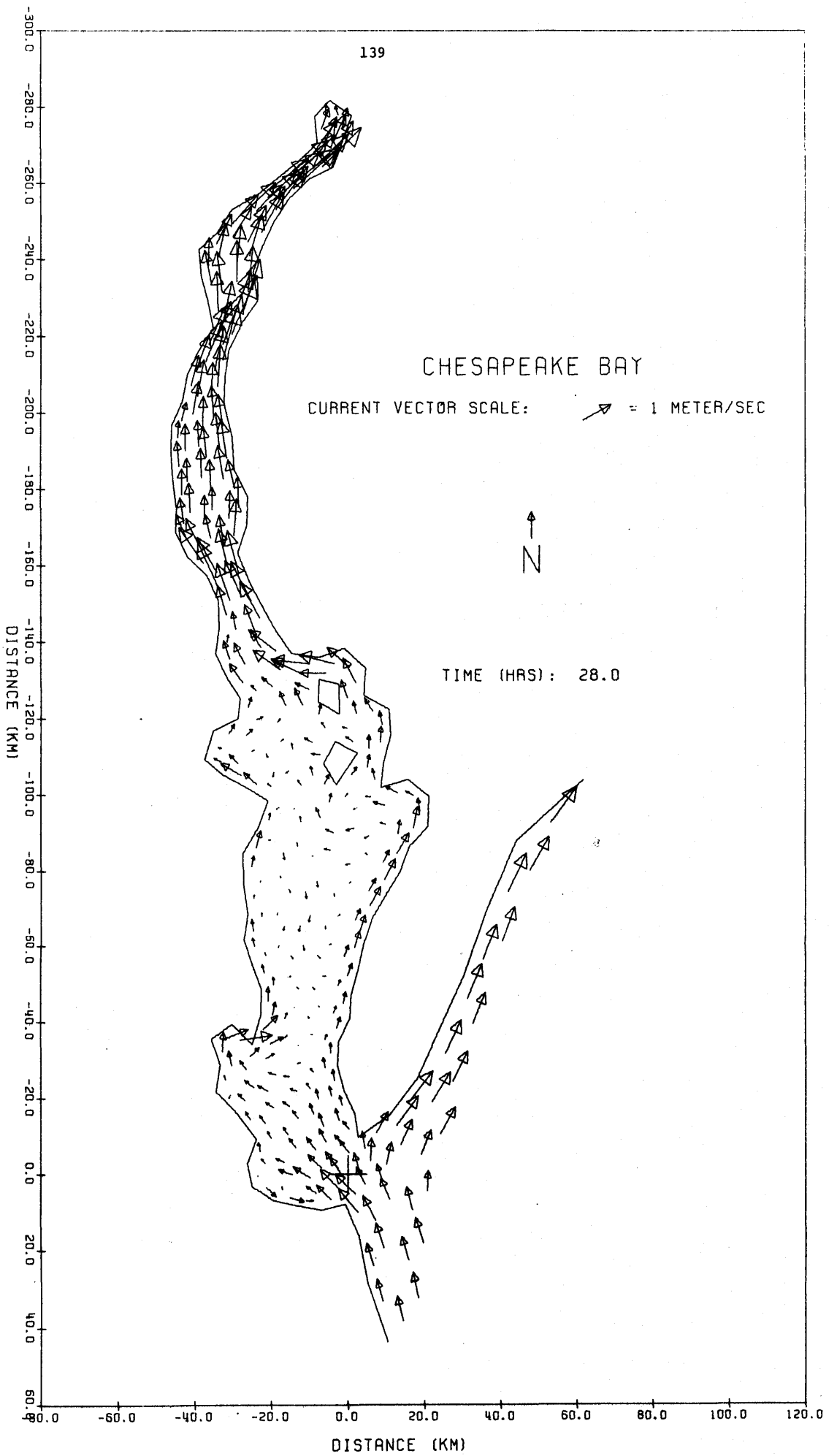


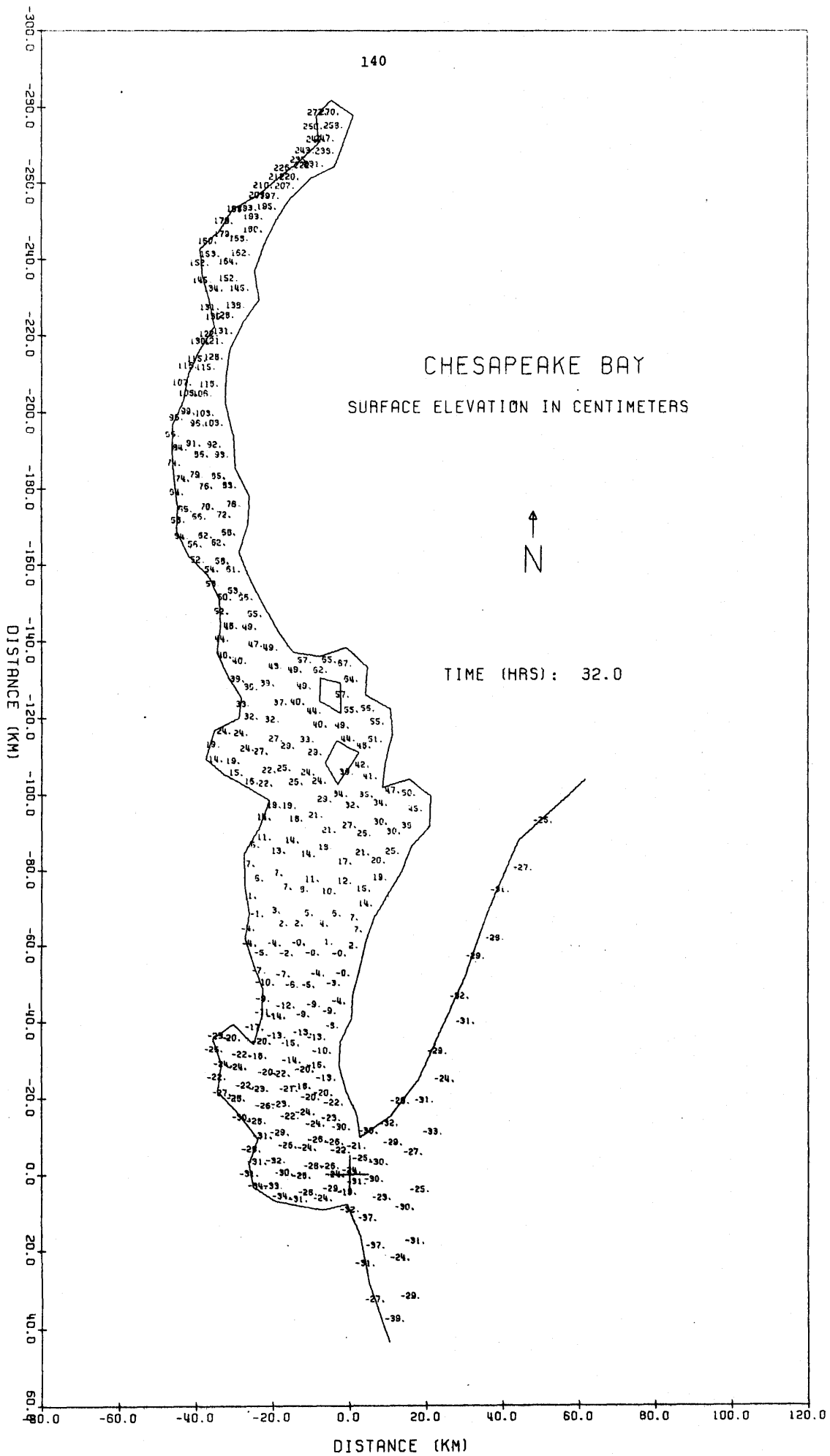


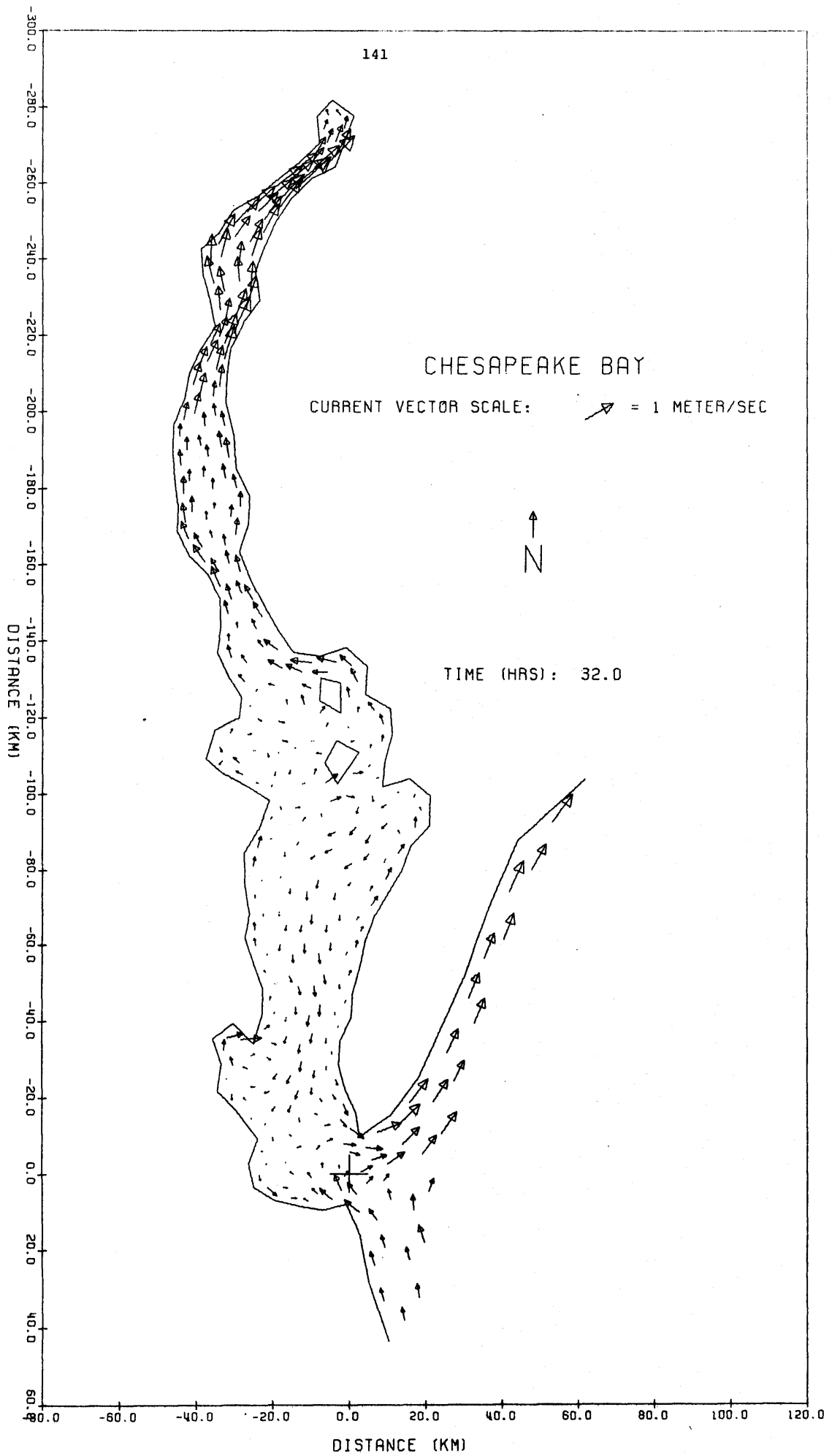












142

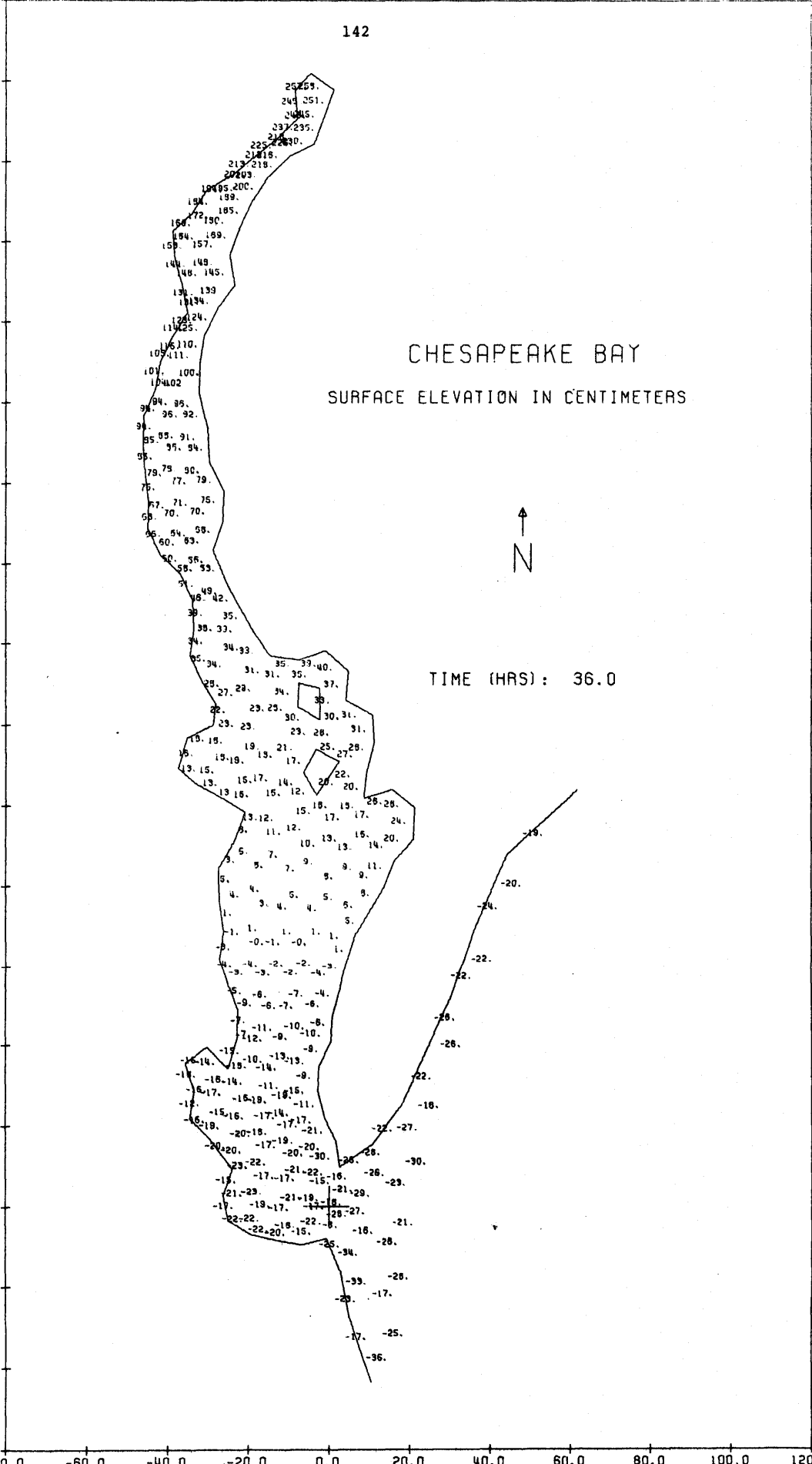
# CHESAPEAKE BAY

SURFACE ELEVATION IN CENTIMETERS

TIME (HRS): 36.0




-300.0  
-290.0  
-260.0  
-240.0  
-220.0  
-200.0  
-180.0  
-160.0  
-140.0  
-120.0  
-100.0  
-80.0  
-60.0  
-40.0  
-20.0  
0.0  
20.0  
40.0  
60.0  
DISTANCE (KM)



DISTANCE (KM)

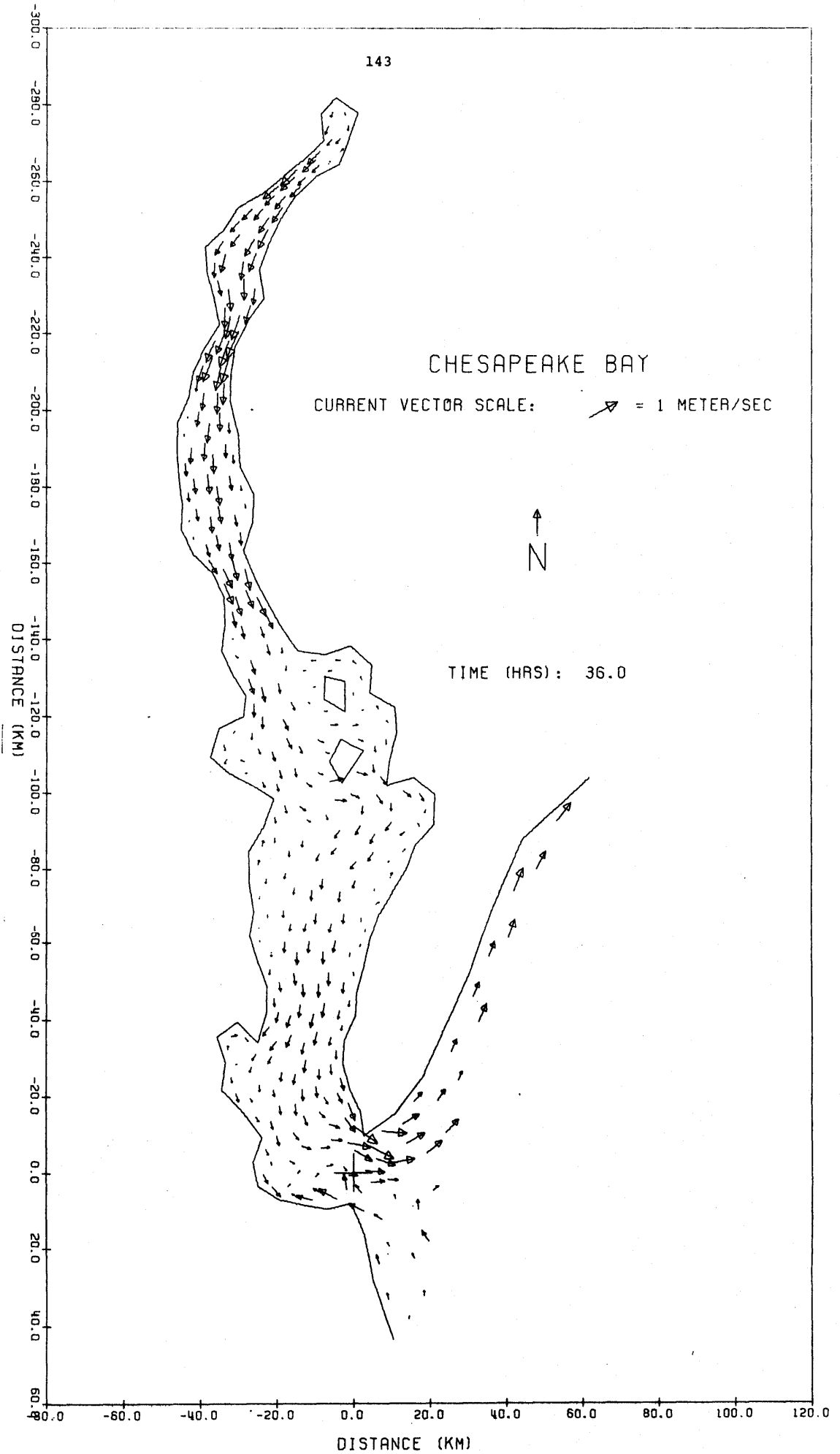
143

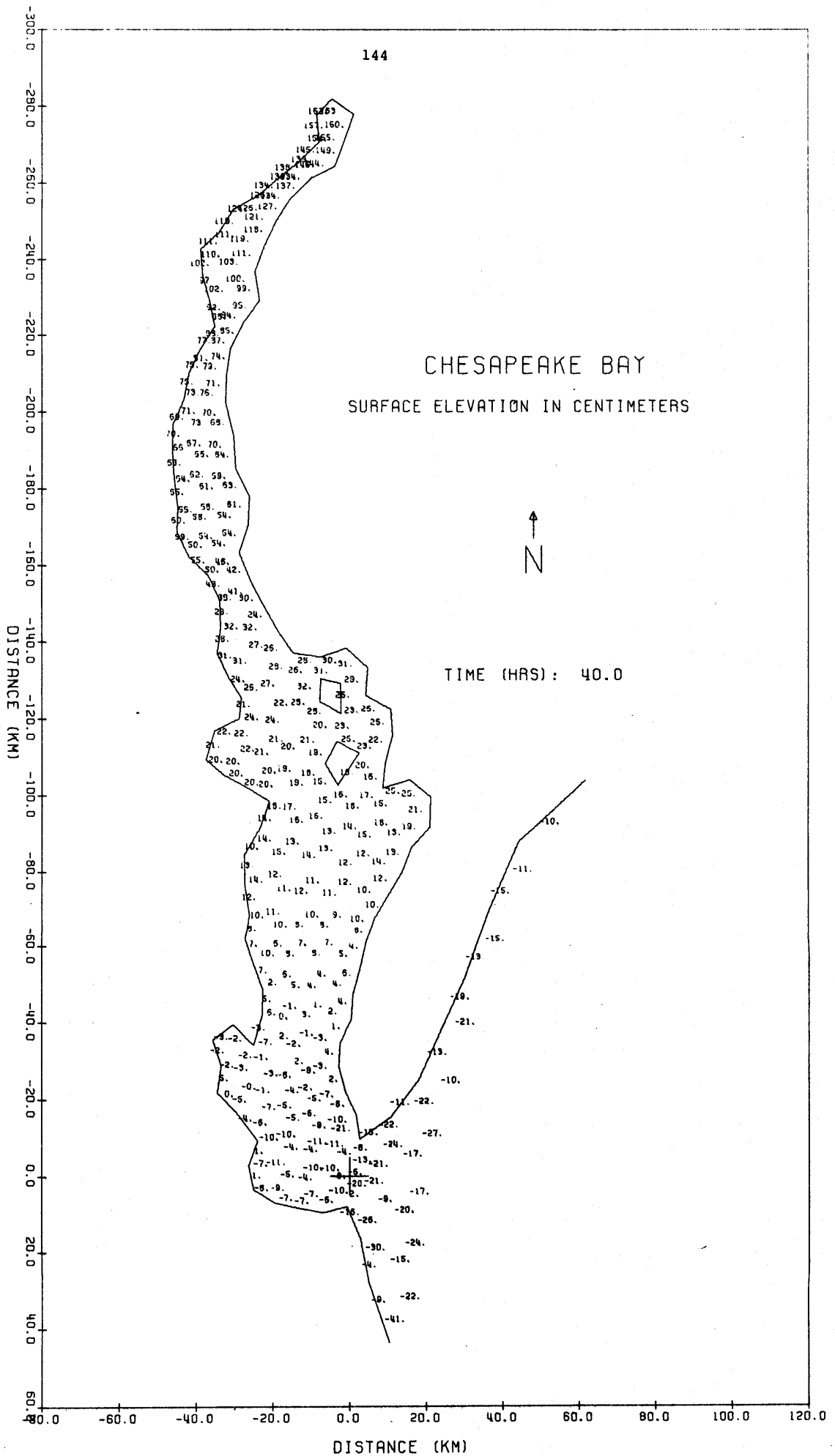
# CHESAPEAKE BAY

CURRENT VECTOR SCALE:  = 1 METER/SEC

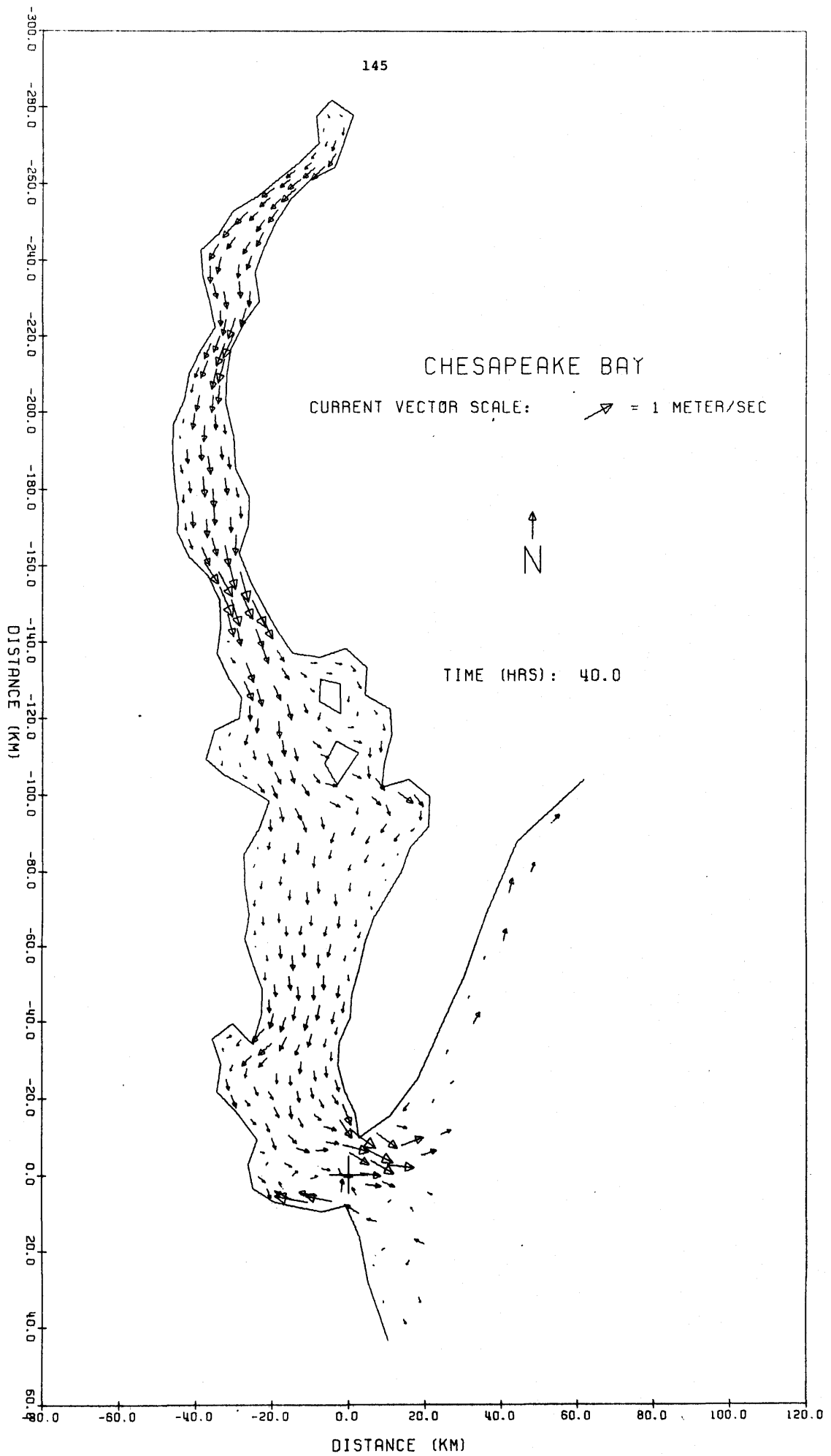


TIME (HRS): 36.0





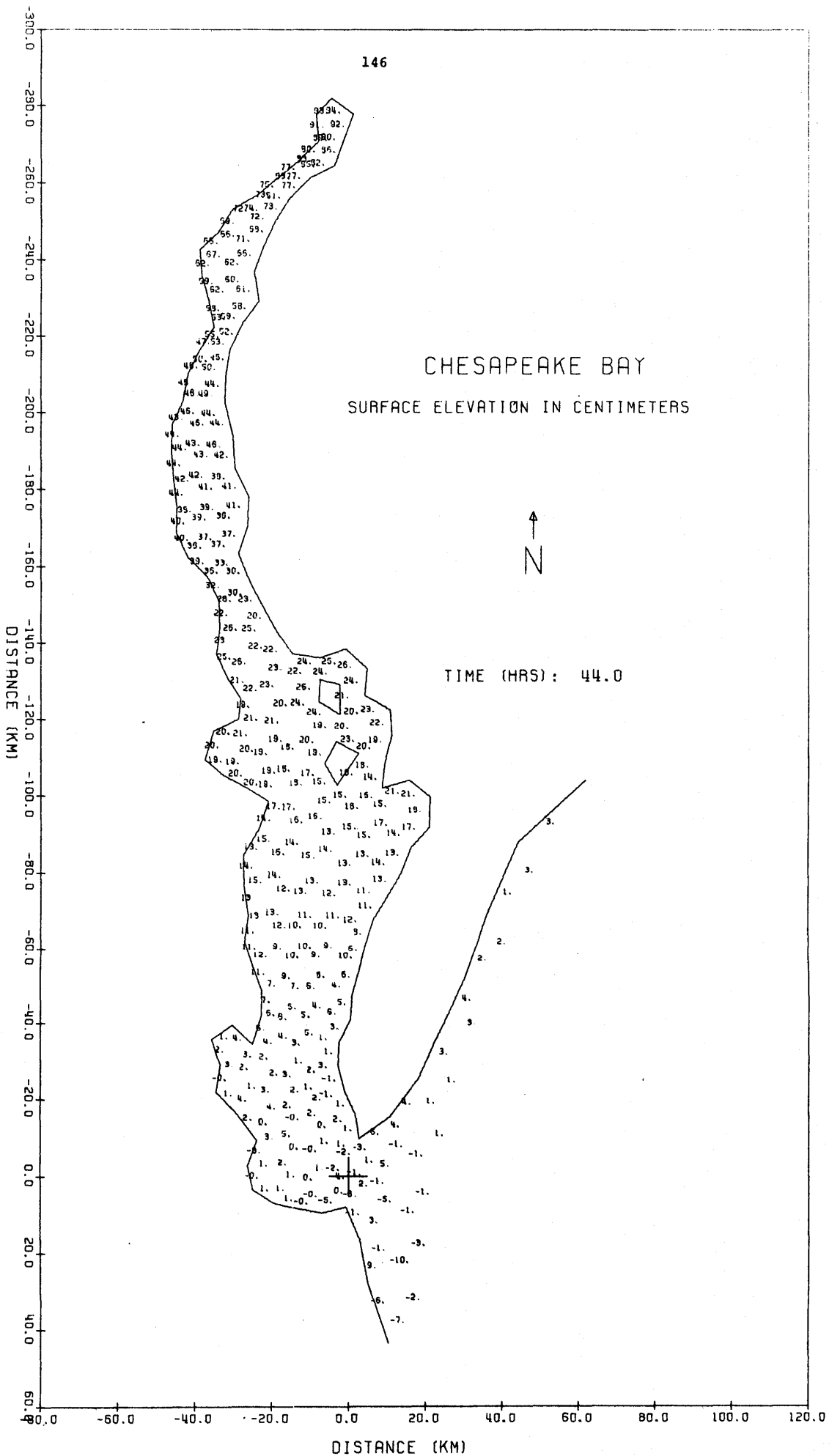




# CHESAPEAKE BAY


SURFACE ELEVATION IN CENTIMETERS

TIME (HRS): 44.0



147

# CHESAPEAKE BAY

CURRENT VECTOR SCALE:  = 1 METER/SEC

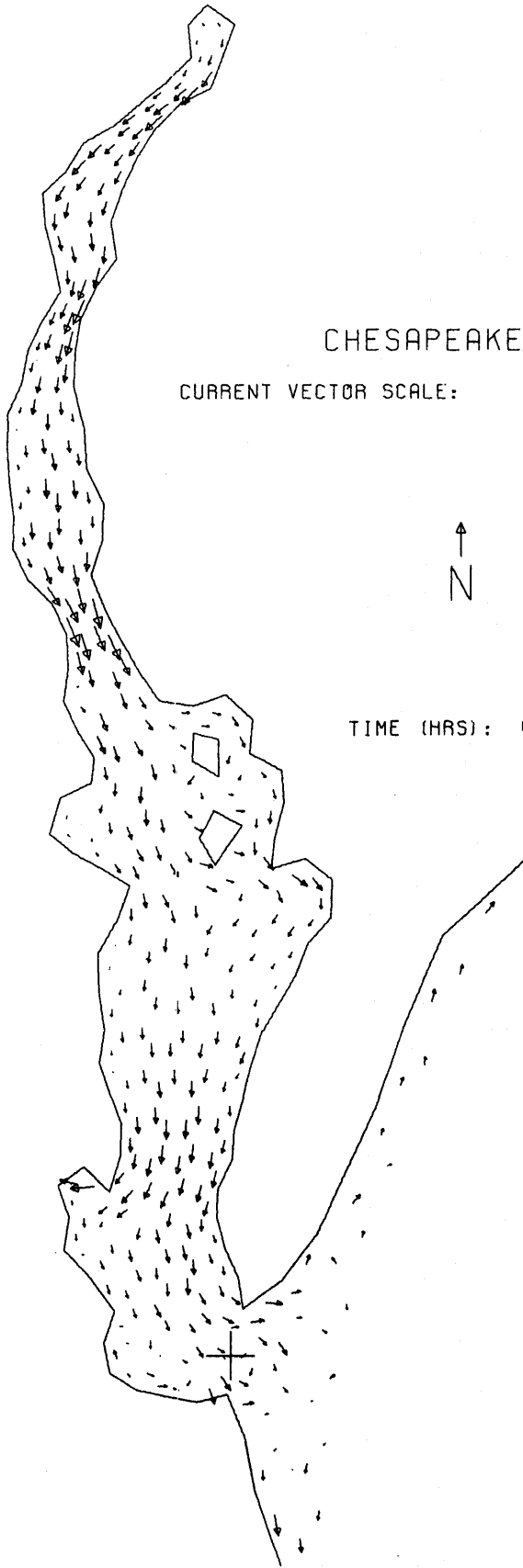


TIME (HRS): 44.0

DISTANCE (KM)

-300.0  
-280.0  
-260.0  
-240.0  
-220.0  
-200.0  
-180.0  
-160.0  
-140.0  
-120.0  
-100.0  
-80.0  
-60.0  
-40.0  
-20.0  
0.0  
20.0  
40.0  
60.0  
80.0  
100.0  
120.0

DISTANCE (KM)

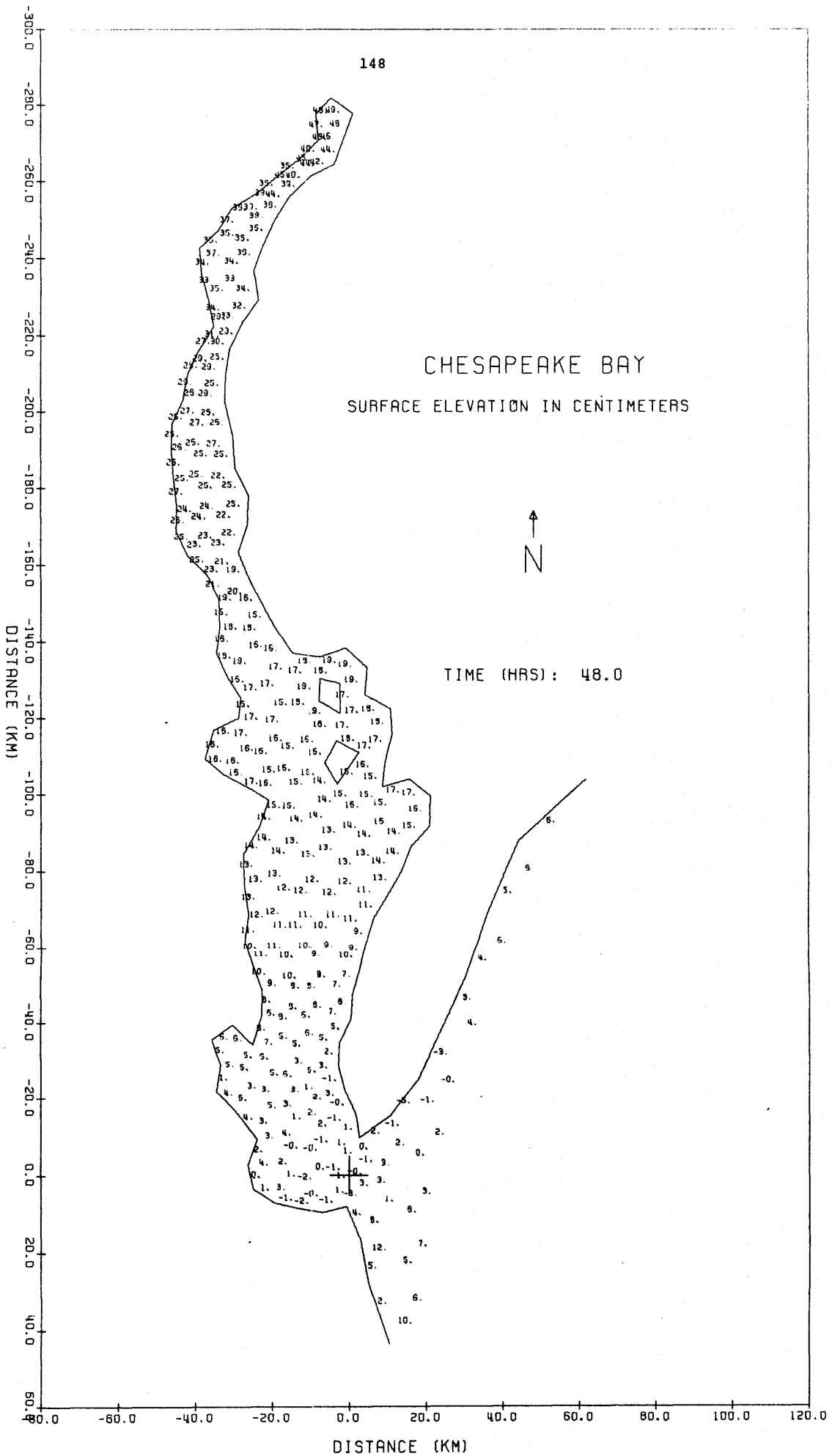


148

CHESAPEAKE BAY  
SURFACE ELEVATION IN CENTIMETERS




TIME (HRS): 48.0



149

# CHESAPEAKE BAY

CURRENT VECTOR SCALE:  = 1 METER/SEC



TIME (HRS): 48.0

